The Hong Kong Polytechnic University

Department of Building Services Engineering

Structure-borne sound transmission from vibratory equipment to coupling structures in buildings

Yun Yi

The dissertion submitted in partial fulfillment of the requirements for the Degree of Doctor of Philosophy

2010

CERTIFICATE OF ORIGINALITY

I hereby declare that this thesis is my own work and that, to the best of my knowledge and belief, it reproduces no material previously published or written, nor material that has been accepted for the award of any other degree or diploma, except where due acknowledgement has been made in the text.

I also declare that the intellectual content of this thesis is the product of my own work, even though I may have received assistance from others on style, presentation and language expression.

_____ (Signed)

_____Yun Yi_____ (Name of student)

Department of Building Services Engineering

The Hong Kong Polytechnic University

Hong Kong, China

November, 2009

ABSTRACT

This thesis addresses the problems of vibration-isolated machines and the structure-borne sound transmission in coupling building structures.

It first presents a study of the comprehensive assessment of the stability as well as the power transmissibility on the use of inertia blocks for vibration-isolated systems. The results indicate that the primary use of an inertia block does not affect the isolation performance, but it decreases the vibration velocity of the isolated vibratory machine and in turn increase the stability especially for a source machine of highly uneven mass distribution. An insight into the selection of the inertia block for the comprehensive performance of a vibration-isolated system is also provided.

Secondly, a theoretical research of the flexural and longitudinal wave motion in a semi-infinite coupling periodic dual-layered beam structure is presented. A new transfer matrix method is derived for the fully coupled flexural and longitudinal waves, and the numerical calculation is performed to investigate the propagation of characteristic wave types in the structure. It is found that three symmetric and three antisymmetric types of characteristic coupled wave motion in a periodic structure, and the energy contribution of the wave motion depends on both of the pass-forbidden band of the characteristic wave types and the combination of the excited wave types.

Thirdly, the experimental research for the flexural-longitudinal motions in a finite coupling dual-layered beam structure is conducted to validate the developed method. The results of measurement agree well with the numerical results from the developed method. The analysis using the validated method shows that the longitudinal energy transmitted in the cross-layer can be enhanced not only at the longitudinal resonant modes of the finite beam but also at the flexural resonant modes of the beam branches.

Moreover, a simulation of vibration control design implies that the cross-layer transmitted vibration can be decreased by the attached cantilevers with mass.

Fourthly, the power flow transmission through a finite coupling dual-layered beam structure with a boundary condition is studied. The model considering the mono-coupling of flexural wave only is compared with the model considering the multi-coupling of flexural and longitudinal waves. The simulation suggests that the transmission of power flow through the structure largely depends on the characteristic of the periodic coupling elements and the exciting position. The multi-coupling model is similar to the mono-coupling model mainly in the relatively low frequency.

Finally, the coupling effect on the vibration control of two coherent vibratory machines placed on a dual-layered floor plate is investigated. The total power of structure-borne sound transmitted from two coherent sources to a coupling floor structure is found to be different from that transmitted from the independent source on a plate without coupling, especially at some strong coupling modes. It is suggested that the power transmissibility method should consider the interactions of the mounting points of coherent machine sources on a coupling floor structure as well as the effective floor mobility for the independent machine source. The whole study promotes the fundamental understanding and prediction method of structure-borne sound control for vibratory machines on the coupling multi-layered structures.

Submitted by Yun Yi.
For the degree of: Doctor of Philosophy
at the Hong Kong Polytechnic University in November, 2009.

Keywords:

Structure-borne sound; Transmitted power; Vibration-isolated system, Vibratory source, Power transmissibility; Isolation performance; Coupling dual-layered structure; Periodic structure; Transfer matrix method; Propagation constant, Characteristic wave-type; Coherent sources.

PUBLICATIONS ARISING FROM PHD STUDY

Journal papers during PhD study:

Y. Yun and C. M. Mak, "A study of coupled flexural-longitudinal wave motion in a periodic dual-beam structure with transverse connection," *Journal of the Acoustical Society of America* 2009; **126**: 114-121.

Y, Yun and C.M. Mak, "Assessment of the stability of isolated vibratory building services systems and the use of inertia blocks", *Building and Environment* 2010; **45**: 758-765.

Y, Yun, C.M. Mak and S.K. Tang, "A study of the effect of inertia blocks on the stability of the vibratory system and the performance of vibration isolation," *Applied* Acoustics 2007; **68:** 1511-1524.

Conference papers during PhD study:

Y. Yun and C.M. Mak, "Finite periodic structure of beam for low frequency structure-borne sound attenuation", *Proceedings of 14th International Congress on Sound and vibration, Cairns, Australia* (July 2007).

Papers under review:

Y. Yun and C.M. Mak, "Coupled wave transmission through a finite periodic dual-layer structure with transverse connection", submitted to *Journal of Vibration and Acoustics, ASME journal* (2009).
Y. Yun and C.M. Mak, "A study of power transmission through a finite periodic dual-layer beam structure with transverse connection", (2008), Submitted to *Applied* Acoustics.

ACKNOWLEDGEMENTS

This thesis is a hard-won trophy of four years of research work whereby I have been supported and accompanied by many people during this period. It is a pleasant aspect that I herein have the opportunity to express my gratitude for all of them.

First and foremost, I sincerely offer the most gratitude to my chief-supervisor, Dr. Mak Cheuk-ming, who has supported me throughout my PhD study with his outright enthusiasm, inspiration and comprehensive view on the academic work whilst encouraging me to choose the approach in my own way.

My PhD study would not have been completed without the support and encouragement from my co-supervisor, Prof. Tang Shiu-keung. I would also like to thank the technician Mr. Stephen Chan, who often gave some advices and help on my experiment in the lab when needed. Furthermore, I would like to thank all the members in our research group for their help, especially Mr. Ou Da-yi for his helpful discussion on the skills of finite element simulation.

I cannot end without thanking my dear parents, family members and my intimate friends on whose constant supports with friendship, affection and love I have relied throughout my study and personal life during the past years.

The road of PhD was not always smooth as an ideal condition, but the living attitude from the fluctuation in these years is really an achievement of life. “Stay hungry. Stay foolish.” It was a maxim for some of the greatest creators of the information time. Now, as graduate to begin a brand new road, I wish to keep that for myself in future.

TABLE OF CONTENTS

LIST OF FIGURES

LIST OF TABLES AND NOMENCLATURE

CHAPTER 1. LITERATURE REVIEW

1.1 RESEARCH WORK CONTRIBUTED TO THE SOURCE-RECEIVER CHARACTERIZATION

The problems of machine-induced noise or vibration are of increasing concern in modern buildings. They are generally divided into two categories as airborne sound transmission and structure-borne sound transmission. The problems mainly due to airborne noise are generally well understood, and a series of methods and procedures have been established for the measurement, analysis, prediction, rating and control of airborne sound in building engineering [1, 2]. Therefore for acoustics engineers, a problem of airborne noise such as the mechanical noise of a chiller or pump radiated from a plant room into a building usually is not difficult to be worked out. However, the noise re-radiated from the vibration of building structures (floor, wall, ceiling, etc) often results in a number of serious problems that are difficult to be resolved, because commonly structure-borne sound transmission from a vibrating machine to the building structure is more difficult to be estimated and controlled properly. In view of this difficulty, the methods for the prediction of structure-borne sound transmission and vibration isolation effect are of importance in the research field of noise control in building engineering.

To meet the requirement for control of structure-borne noise, a suitable definition of a source-receiver system is needed for the analysis of its ability to impart vibrational energy into the passive structure with connection (including path). One essential difficulty for working out the problems about structure-borne sound is that the transmission of structure-borne sound is dependent on both of vibratory sources and receiver structures. The assumption for air-borne sound that a source is constant in its

strength and the impedance of a receiver is insensitive to its relative location to source does not apply for structure-borne sound. It has taken time for researchers to build reasonable characterization of sources independent of receivers, so as to develop effective prediction methods of structure-borne sound transmission in case of the complex interactions between a given source machine and varied supporting structures. So far in engineering, the assumption has been of a simple source as a single mass point and a translational excitation and motion in a single degree of freedom [1-4]. However such an ideal case scarcely happens. There are six components corresponding to six degrees of freedom required for the general description of actions and motions at each contact point Apart from the direct interaction on same components at each point, an interaction may take place between different components at the same point and between different components at different points. All factors of the interactions involved in the transmission process can be characterized by two 6N×6N matrices of source mobility and receiver mobility for a source with N contact points [5, 6]. The elements of complex matrix commonly are complicated functions of frequency but the formulation does not often provide a distinct characterization of source in practice. In order to simplify the situation practically, the concept of effective mobility is introduced which is defined as the ratio of the actual velocity at a point and in one direction, to the contributions of the excitations from all components and points [6-8].

For structure-borne sound sources, a number of possible characterizations were suggested by some researchers. Wolde and Gadefelt [9] sought to be able to characterize the source's ability to deliver structure-borne sound power as an independent property so that the power transmission could be estimated directly. The term “free velocity” used is independent as a characteristic of the source activity. However, it cannot often be concluded to a significant single value for different vibratory sources. Because their motions in different dimensions would be

incompatible if multiple translational and rotational velocities are present. The development of the source descriptor, and the associated coupling function proposed by Mondot and Petersson [5] was possible as a result of two postulates. The first is that structure-borne sound and vibration transmission is properly described in terms of energy flow between sources and receivers rather than acting force or response velocity. Secondly, a liner network theory can be invoked in describing the transmission process. The source descriptor requires knowledge of source characteristics only but allows subsequent estimates of emission when additional information on the characteristics of receiver is available. It has the units of power and can be interpreted as that requires to achieve the free velocity at the contact point as being fed to the source structure. An advantage of the source descriptor concept is that the excitation components, including translational and rotational forces, usually become dimensionally compatible. The influence of multiple contact points and multiple components of excitation and motion on the structure-borne sound source descriptor was experimentally studied by Petersson and Gibbs [10]. The influence of point cross-coupling is different from that of transfer and transfer-cross coupling on the transmission of power. For a source, the moment can be expressed as a product of a force and a 'lever' that is inversely proportional to wave number, and moment-induced rotations can be no less or even more important than the translational components for structure-borne sound power transmission. As a result of the relevant studies for different types of structure [11,12], understanding of the significant role of moment excitation has been improved. Whilst, it is pointed that rotational excitations and responses will likely be more difficult to handle experimentally than forces. A comparison between a force and a moment of excitation directly is meaningless, but their relative importance in exciting a structure can be properly compared on a power basis. The characterization approach for various types of sources was developed in a series of studies [13-15] to include multi-point connected

vibratory systems. Owing to insufficient information available in practical installation conditions, simplifying assumptions are necessary for force distribution. Simple estimates of force ratios were conducted by Fulford and Gibbs to calculate the transmitted power into beam structures in comparison with the exact transmitted power [13]. It was suggested that, in regard to the source descriptor and coupling function formulation, a view of generalizing their forms, the mobilities of sources and supporting structures together with the free velocities of sources should be considered. Latterly it was undertaken in an attempt to establish generalized relationships amongst the parameters for each of the mass, stiffness, and resonant-controlled regions that can be expected for a structure [14]. The sequent methods of estimating the force ratios in multi-point connected source-receiver systems were analytically studied and followed by a statistical study [15]. Through the developed methodology, statistical estimates of the force ratios in multi-point connected source-receiver systems can be obtained for different controlled regions of source with different types of, e.g., plate-like or frame-like bases. A dimensionless form of the mobility matrix was developed by Moorhouse [16], of which the off-diagonal elements can quantify the coupling between two excitations of whatever dimensions (forces and moments).

The source descriptor is based on the knowledge of source characteristics, but for available estimates of power transmission quite a lot of additional information on the characteristics of receiver is required [17]. In the light of the usefulness of knowing the overall level of structure-borne sound power, an alternative approach often may be more appropriate for the real application of methodologies based on characterization of source. The way to approximate the main properties of dynamic behavior of a vibratory system (simplified mobility formulations of sources and structures) for frequency average power is more convenient in engineering. Some methods have been developed to approximate the power transmitted from machines to flexible receivers [18-20]. The

dynamic range of the structure-borne sound power transmission may be estimated by representing the mobility matrix of a receiver structure as a single upper and lower bounds in combination with the source descriptor [19]. The power mode approach suggested in [19] was further extended and approximations are developed for the maximum and minimum possible values and the mean value of the transmitted power [20]. The concept of characteristic power was presented as a development of the source descriptor [21]. It provides an equivalent single-point model for multiple-point connected sources and receivers, which makes it possible to superimpose the coupling factor for realistic source-receiver combinations on the frame for single point contact. Moreover, a reception plate method was introduced as a practical structure-borne sound source characterization for mechanical installations in buildings [22]. According to this method, laboratory data of source activity and mobility over all contact points are yielded in the forms of single equivalent magnitudes. Such quantities of machines can be applied for the estimation of installed structure-borne power in various structural mounts, by reference to a high source mobility, a low source mobility condition, or to a matched mobility condition. These studies provide a series of steps towards overcoming the practical problem of source descriptor and coupling function formulation for vibratory systems in engineering.

For an effective prediction of structure-borne sound transmission that is based on the characterization of sources and receivers of vibratory systems, the measurements of free velocity of sources and mobilities at contacts are of importance in engineering. The development has been the introduction of a standard for measurement of the velocity of resiliently mounted machines [23], which in practice can be taken as equal to their free velocity. However, direct measurement of free velocity and other source characteristics usually requires the source to be removed from the installation while operating in normal conditions. The methods based on the reciprocity principle have been in

application on measurements for acoustic and mechanical systems for a long time [24]. An indirect method, including the use of laser velocimetry together with the reciprocity principle, can give a reasonable estimation of the transfer functions and strength (velocity) of an tructure-borne sound source in situ [25]. For structural vibration, the model function was shown to be not contradictory to the reciprocity principle, based on which a vibro-acoustical modal analysis can be carried out with combined frequency response function measurements [26]. Recently reciprocal methods were also used to indirectly obtain the contact forces at the interface of a single and multi-point source-receiver system such as a fan base on a concrete floor [27], and the power transmission induced by force and moment was acquired from the reciprocity principle [28]. Moments may be less important than perpendicular forces as the source is away from structural discontinuities such as floor edges, but they tend to be more important in the proximity of structural discontinuities and have an increasing contribution with increased frequency irrespective of excitation location [28]. Although rotational excitations and responses often may likely be more difficult to handle experimentally than forces, the rotational components, e.g., moment mobility is required as well as translational components. A special moment exciter made of magneto-strictive rods initially was used by Petersson [29] for acquiring moment mobility in use of a large moment excitation. A twin shaker moment exciter was constructed by Sanderson et al. [30, 31] to measure beam moment mobility. Recently more studies have been conducted by Su, Mak and Gibbs [32, 33] on the measurement in case of considering cross mobility. Besides, the measurements based on modal test methods are applied to acquire the characteristics of vibration modes of structures as beams or thin plates in different boundary conditions [34-36]. By analyzing the coupled modes from the data in approximation with noise, it is possible to predict the dynamic characteristics of a structure such as a beam or plate in a real condition with a reasonable accuracy. The

method of state-space models for frequency response function data was used to handle arbitrary input signals and transients in frequency domain without introducing systematic errors [37]. The measurements can reduce both the data set and the noise levels without introducing bias errors caused by leakage. The developed modal test method improves the parameter estimates such as the damping ratio of a structure in practice. Concerning test methods for mechanical installations in heavyweight buildings, the approach proposed stems from recent work based on the reception plate method [38]. Moreover, the consideration was given to the application of reception plate method for source test method [39]. According to such method, a machine under test is attached to a simple plate, then under otherwise normal operating conditions, the total structure-borne power transmitted can be obtained from the spatial average of the mean square plate velocity.

There are still few reliable practical methodologies for engineers to accurately predict the real radiation of structure-borne sound in connected space that is resulted from vibratory machines. Regardless of this problem, commonly in building services engineering resilient isolators are widely used for mounting machines, and most isolators can effectively reduce the structure-borne sound that is transmitted from machines e.g. pumps, standby generators and chillers into building structures [1-4]. The "force transmissibility" method is commonly adopted in industry to assess the performance of vibration isolation [1-4]. In such an assessment, "isolation efficiency" is the criterion commonly obtained to estimate the function of selected isolators in a vibratory system. However, its accuracy has been criticized, since it is based on the vibratory force transmitted through a single contact point of a simple vibratory system, usually the dynamic actions and interactions between the supporting points of a multi-point vibratory equipment and the flexible floor are neglected. The active power (the real part of the complex power transmission) is included mostly as an indicator of

structure-borne sound considering that most excitations from vibrating machines will involve dissipation of power. Whilst the reactive power (imaginary part) is by definition stored during one half of an oscillation, and fully returned to the exciting source in the other half of the cycle [40]. In many situations such temporary exchanges are of no interest since they play no part in far field radiation from the structure, or transmission to the far field. Methods based on total active power to evaluate the performance of vibration isolation appear to be more reasonable because the interactions between different sources and receivers including magnitude and phase difference can be compared by single values.

A method based on the estimation of active power was therefore proposed to assess the performance of vibration isolation system [41], in which the models of a multi-point rectangular machine and a cylindrical machine were used for simulation. In another parallel study the “power transmissibility” method was proposed for an isolated multi-point vibratory system on a movable foundation [42]. This criterion can singly evaluate the performance of an isolated vibration system by use of the ratio of the totally transmitted active powers of a vibratory system with and without isolators. The extended research on the damping effect on power transmissibility was later conducted [43]. As theoretically increasing the damping of isolators would reduce the vibration level of vibratory machines, normally the low damping isolators as metal springs are preferred for large building services equipments. Despite the advantage in terms of reducing the structure-borne sound, the use of vibration isolators may lead to excessive rocking motions of the vibratory equipment in some region so that influence the running of machines. In this sense, the “vibratory velocity level” is taken as an indicator of the vibration status of a machine and is used to compare the stability of different mounting systems with isolators [44]. Such criterion is defined for general purpose that a machine is always excited by frequency-independent forces, the largest

amplitude of vibration motion at the natural frequency of mounted machine is used for reference to evaluate the intensity of a isolated vibratory system. It is clarified that increasing the damping of isolators also decreases the vibration intensity of a isolated source. As a result of comprehensive consideration, in some conditions the viscoelastic structural elements are used to design frequency-dependent damping of springs for vibration isolation system [45], of which the high damping can limit the vibration amplitude in low frequencies near resonances and the decreased damping values at high frequencies can achieve effective isolation.

1.2 RESEARCH WORK CONTRIBUTED TO THE CHARACTERISTICS OF STRUCTURES IN BUILDINGS

Apart from the source characteristics, the dynamic characteristics of connecting structures also play an essential role in the estimation of structure-borne sound transmission. In building engineering a lot of structures such as multi-storey buildings, multi-support beams, stiffened plates and other layered composite structures can be treated as periodic coupling structures. The vibration motions and transmitted structure-borne sound power in the structures should be estimated accurately by taking account of the coupling of wave motions. A coupling structure in buildings usually is treated as a combined group of identical or similar fundamental elements, which are spatially joined together regularly to form the whole structure. From the early time of 20th century, a group of mathematical techniques were increasingly developed for analyzing the electromagnetic waves in complicated crystal lattice structures and periodic electrical circuits, and the studies of such periodic waveguides as crystal solids [46] were largely enhanced. Many of these valuable techniques have been utilized in subsequent studies of the acoustic waves in periodic structures. Firstly the studies were conducted for a single type wave motion along a one-dimensional periodic beam either with simple supports or with point masses at regular intervals. Miles [47] sought the natural frequencies of a finite periodic mono-coupled beam system resting on an arbitrary number of simple supports. Heckl investigated a two-dimensional periodic structure consisting of a rectangular grillage of interconnected uniform beams which had both flexural and torsional stiffness [48]. In his high frequency analysis he considered the multiple reflection and transmission processes as flexural waves in one beam element impinge on the junctions with adjacent beams. An equation for the propagation constants was established in terms of the reflection and transmission

coefficients which relate to a single wave in just one infinite beam when it impinges on the junction with just one other infinite beam. Fundamentally the control of acoustic wave transmission in one-dimensional periodic (or nearly periodic) structures can be tackled in a solution based on the band structure resulted from transfer matrix method [49]. The comprehensive theoretical computations of band structures have also been well-documented for acoustic waves in periodic structures by Kushwaha and Mod [50]. The influence of heavy damping has been investigated as a means of reducing stress levels [51], it was found structure theory was well suited to lightly damped as well as to heavily damped finite periodic structures. Large areas of periodic building structures consist of uniform plates and shells with identical stiffeners at regular intervals, and research into their natural frequencies, modes and random response levels was required with a view to predicting stress levels and fatigue endurance. The fundamental or central ideas of structure characterization used in these areas were introduced by Mead [52]. In his context, a quadratic and well-posed spectral problem was studied to determine the wave propagation constants of a periodic system. This work was extended by proposing a second order matrix equation leading to the propagation constants of a periodic system [53]. Four different methods of calculating the structure-borne sound propagation in beams with many non-resonant discontinuities were demonstrated by Heckl [54], and most of these methods took the coupling between longitudinal and flexural waves into account. Later a mathematical model for the coupling of waves that propagate in a periodically supported Timoshenko beam was presented for the calculation of coupled wave transmission in such structures [55]. Furthermore, the propagation characteristics of coupled longitudinal and flexural waves in beam-type transmission paths with asymmetric loads in the form of resonant columns were theoretically analyzed and experimentally examined by Friss and Ohlrich

[56, 57]. The developments of this area enlighten the approach for the transmission of multi-coupled coupled waves in multi-layered strutures.

1.3 OBJECTIVES

The objectives of this thesis are:

- ✓ to propose the indices for assessing the stability of a vibration-isolated building services system and provide an insight into the selection of the inertia block for the vibratory system;
- ✓ to propose the transfer matrix method to investigate the characteristic wavetypes that propagate in a infinite or semi-infinite periodic coupling beam structure;
- ✓ to conduct experiment studies to analyze the structure-borne sound energy transmission in a finite dual-layered beam structure with connection branches;
- ✓ to study the structure-borne sound power transmission under the mono-coupling condition and multi-coupling condition at the pconnection branches of a finite periodic dual-layered beam structure; and investigate the approach to control the power transmission in the periodic structures;
- ✓ to study the effect of the interaction between two coherent vibratory machines on he power transmitted to a coupling dual-layered floor plate and the level of power transmissibility for isolation.

CHAPTER 2. PERFORMANCE OF A VIBRATION-ISOLATED SYSTEM WITH AN INERTIA BLOCK

2.1 INTRODUCTION

Structure-borne noise problem in modern buildings usually come from some vibratory building services equipments. Vibration control of the building services equipments is of engineering importance. There are basically two major tasks involved in the control of vibratory machines: one is to reduce significantly the overall structure-borne sound power transmitted from the vibratory equipment to the floor, and the other is to ensure the stability of the isolated vibratory system.

In engineering, resilient isolators are widely used in buildings to isolate vibratory equipment, such as water pumps, standby generators, and chillers, and the "force transmissibility" method is commonly adopted in industry to assess the performance of vibration isolation [5, 1, 58]. In this method, "isolation efficiency" is the criterion used to assess the performance of vibration isolation. However, its accuracy has been criticized, since it is based on the vibratory force transmitted through a single contact point of a simple vibratory system, usually the dynamic actions and interactions between the supporting points of a multi-point vibratory equipment and the flexible floor is neglected. Using the method based on multi-point source mobility descriptor and total power to describe structure-borne sound transmission appears more viable, because the interaction and phase difference of motions between the complex source and the receiver structure have to be considered [6]. In the light of the usefulness of knowing the overall structure-borne sound power emission, the source descriptor, together with the coupling function, was proposed by Mondot, Petersson and Plunt [6-8], and then further developed by Fulford and Gibbs [13-15] to establish the structure-borne sound power delivered by a multi-point connected system. The effect of

floor mobility on structure-borne sound power transmitted from multi-point sources to the floor structure [59] was later clarified, and for movable foundation structures such effect in the conditions without and isolators was evaluated by Mak and Su [41]. The further method of “power transmissibility” was developed by Mak et al. [42, 43]. In this method, power transmissibility was proposed as the criterion for use in evaluating the performance of vibration isolators for building services equipment mounted on a floor.

Despite the advantage in terms of the reduction in structure-borne sound power transmitted to the floor, the use of vibration isolators may lead to excessive rocking motions of the vibratory equipment in some region, which would influence the running of machines. Although large vibration motions are common in the efficient use of isolators to reduce the vibratory action transmitted on mounting structures, a significant increase in the vibration and rocking motions of isolated machines is an unwanted problem. The vibratory velocity level is often taken as an indicator of the vibration status of a machine and is used to compare the stability of different mounting systems for general purpose machines excited by frequency-independent forces [44]. Increasing the damping of isolators would reduce the vibration level of vibratory machines. As increasing the damping of isolators reduces the performance of vibrator isolators [43], in some conditions the viscoelastic structural elements are used to design frequency-dependent damping of springs for vibration isolation system [45], of which the high damping can limit the vibration amplitude in low frequencies near resonances and the decreased damping values at high frequencies can achieve effective isolation. In building engineering, lightly-damped isolators, such as coil metal springs, are usually used to isolate vibratory building services equipment, so an inertia block is commonly used to enhance the stability of the isolated vibratory machine.

Although inertia blocks are widely used in conjunction with vibration isolators, the selection of an inertia block is commonly based on some crude methods or the experiences of individual engineers. No comprehensive guidelines for the selection of inertia blocks or indices for assessing the effect of inertia blocks on the stability of a vibratory system are available. Apart from vibration isolation, the purpose of maintaining "stability" of the mounted vibratory system is to control the vibration velocity and rotational velocity of mounted machines so that the vibrating and rocking motions will not adversely affect the mounting and the normal operation of machines. To assess the effect of inertial blocks on the stability of the isolated system, a vibratory machine model, with four mounting points and in which the mass distribution is uneven and the exciting force is eccentric, is used. The structure-borne sound power transmitted from the multi-point machine to the structure and the levels of the vertical and rotational motions of the vibratory system mounted with different inertia blocks are investigated analytically. The mounted vibration velocity level and the rotational velocity level are proposed and used to assess the stability of the isolated vibratory system in different mounting conditions.

2.2 THEORETICAL MODELS OF VIBRATION-ISOLATED SYSTEMS

2.2.1 THE SYMMETRICALLY PLACED EVEN MASS SYSTEM

A vibratory machine model of even mass distribution M_0 with four symmetrical contact points as shown in Fig. 2.1(a) is placed symmetrically on a square concrete floor.

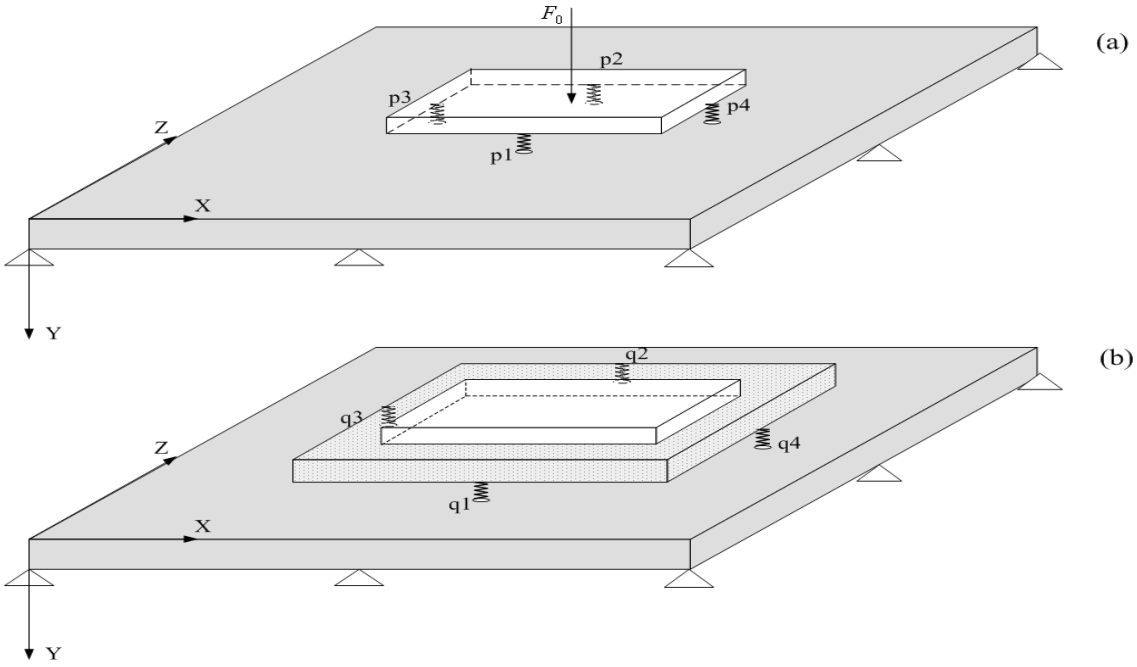

Fig. 2.1 (a) Vibratory machine of even mass distribution with four symmetrical contact points placed symmetrically on the simply-supported square concrete floor plate; (b) vibratory machine of even mass distribution attached to an inertia block with four symmetrical contact points placed symmetrically on the floor plate.

It is assumed that the machine is effectively driven by a source vibratory inherent force F_0 at the center of gravity. The free velocity vector of the source is given by

$$[V_{SO}] = V_0[1 \quad 1 \quad 1 \quad 1]^T \tag{2.1}$$

$$V_0 = \frac{F_0}{j\omega M_0} \tag{2.2}$$

where V_0 is the effective free velocity of the source. It should be noted that each component of the free velocity vector expresses the degree of vertical vibration velocity at the corresponding contact point, the 'vector' does not indicate a kind of multi-degree

vibratory motion. Since the components of force and velocity at all contact points are equal, the machine can be thought of as an effective simple source driven by the vertical vibratory force as shown in Fig. 2.2(a).

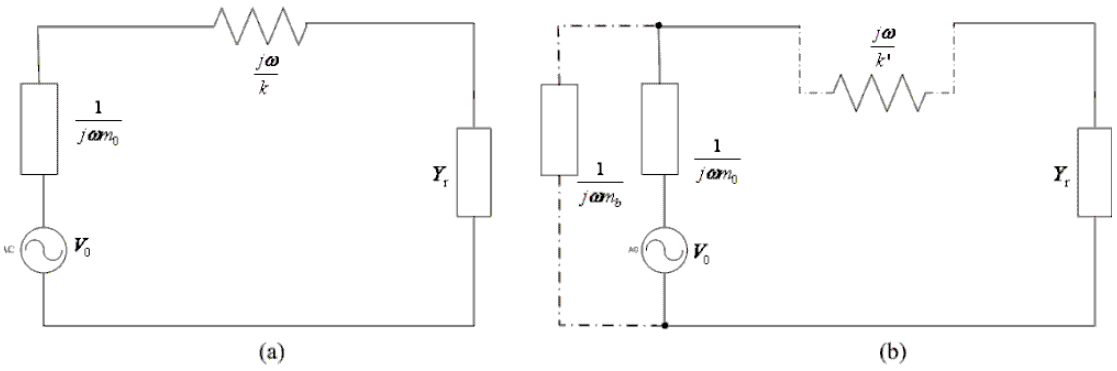

Fig. 2.2 (a) Equivalent circuit diagram of the simple model of a vibrating machine mounted on the flexible floor; (b) equivalent circuit diagram of the simple model of the isolated machine with inertia block.

The transmitted force through every spring isolator is therefore given by:

$$F_{\mathrm{T}} = \frac{V_0}{1/j\omega m_0 + j\omega/k + Y_{p\mathrm{r}}} = \frac{F_0/4}{1-(\omega/\omega_0)^2 + j\omega m_0 Y_{p\mathrm{r}}} \tag{2.3}$$

where $Y_{pr} = Y_{pi1} + Y_{pi2} + Y_{pi3} + Y_{pi4}$ for $i = 1,2,3,4$ is the effective floor mobility [43] at each contact point with the spring isolator, where $Y_{\mathrm{p}ii}$ is the point mobility of p_i, and $Y_{\mathrm{p}ik}$ is the transfer mobility between the contact point p_k and p_i, $m_0 = M_0/4$ is the effective mass distributed on each mounting point, $j = \sqrt{-1}$ and ω_0 is the natural frequency of system that is given by

$$\omega_0 = \sqrt{\frac{k}{m_0}} = \sqrt{\frac{g}{\delta_0}} \tag{2.4}$$

where k is the axial spring stiffness, g is the gravitational acceleration, and δ_0 is the static deflection. As the machine model is placed on an inertia block of mass M_b as shown in Fig. 2.1(b) and 2.2(b), new springs are selected to maintain the same static deflection (Section 6.5.4, Chapter 6 of Ref. [1]):

$$k^{'} = \frac{(M_0 + M_b)}{M_0} k = \frac{(m_0 + m_b)}{m_0} k \tag{2.5}$$

where $m_b = M_b / 4$ is the effective mass of the inertia block distributed on each mounting point. Note that the parameter with apostrophe (') means the parameter is for the system with the inertia block.

The free velocity vector of the source with the inertia block is:

$$[V_{SO}] = V_0^{'}[1 \quad 1 \quad 1 \quad 1]^{\mathrm{T}} \tag{2.6}$$

$$V_0^{'} = \frac{M_0}{M_0 + M_b} V \tag{2.7}$$

The transmitted force through an isolating spring to the floor is given by

$$F_{\mathbf{T}}^{'} = \frac{F_0 / 4}{1 - (\omega / \omega_0)^2 + j\omega(m_0 + m_b)_0 Y_{q\mathbf{r}}} \tag{2.8}$$

where $Y_{qr} = Y_{qi1} + Y_{qi2} + Y_{qi3} + Y_{qi4}$ for $i = 1,2,3,4$, which is the effective floor mobility at the new contact points on which the inertia block is placed as shown in Fig. 2.1 (b).

To assess the performance of vibration isolation, the active structure-borne sound power that is transmitted to the floor must be obtained [42]. For the machine that is symmetrically placed on the floor without isolators, the transmitted active power is

$$P_{(ns)} = \frac{1}{2} \frac{4}{\left|1 + j\omega m_0 Y_{p\mathbf{r}}\right|^2} \left|\frac{F_0}{4}\right|^2 \mathbf{Re}\left(Y_{p\mathbf{r}}\right) \tag{2.9}$$

For the machine spring with isolators, the total transmitted power $P_{(s)}$ is

$$P_{(s)} = \frac{4\left|F_T\right|^2}{2} \mathbf{Re}\left(Y_{pr}\right) = \frac{1}{8} \frac{\left|F_0\right|^2 \mathbf{Re}\left(Y_{pr}\right)}{\left|1 - (\omega / \omega_0)^2 + j\omega m_0 Y_{pr}\right|^2} \tag{2.10}$$

For the source being placed on an inertia block with isolators, the transmitted power is

$$P_{(bs)} = 2\left|F_{\mathbf{T}}^{'}\right|^2 \mathbf{Re}\left(Y_{q\mathbf{r}}\right) = \frac{1}{8} \frac{\left|F_0\right|^2 \mathbf{Re}\left(Y_{qr}\right)}{\left|1 - (\omega / \omega_0)^2 + j\omega(m_0 + m_b) Y_{qr}\right|^2} \tag{2.11}$$

For the machine with spring isolators, the vibration velocity is defined as the velocity of the machine at the contact point with the spring isolator, and is given by

$$V_{pi} = \frac{j\omega m_0 Y_{pr} - (\omega/\omega_0)^2}{1-(\omega/\omega_0)^2 + j\omega m_0 Y_{pr}} V_0 \tag{2.12}$$

For the machine that is placed on the inertia block with isolators, the vibration velocity is defined as the velocity of the machine and the inertia block at the contact point with the spring isolator, and is given by

$$V_{qi} = \frac{j\omega(m_0+m_b) Y_{qr} - (\omega/\omega_0)^2}{1-(\omega/\omega_0)^2 + j\omega(m_0+m_b) Y_{qr}} \frac{m_0}{m_0+m_b} V_0 \tag{2.13}$$

These values represent of vibration motion of a resiliently mounted vibratory system related to the free velocity of source. The smaller average vibration velocity, the less active is the vibratory motion of the isolated system.

2.2.2 4-POINT UNEVEN MASS MACHINE ISOLATED WITHOUT AND WITH INERTIA BLOCK

For the model of the vibratory system with N contact points which is described by the source characteristics, the free velocity can be defined as $N\times1$ vector $[V_S]$ and source mobility can be defined as $N\times N$ matrix $[Y_S]$. As described in Ref. [6, 10], retaining the basic model of a single-point vertical excitation and motion structure, while incorporating the interactions of N contact points, the relation between the components of vibration velocity and that of transmitted force can be expressed as $V_{\mathrm{p}i} = Y_{\mathrm{p}i1}F_{\mathrm{p}1} + \ldots Y_{\mathrm{p}ii}F_{\mathrm{p}i} + \ldots + Y_{\mathrm{p}iN}F_{\mathrm{p}N}$. Here $Y_{\mathrm{p}ik}$ are the transfer mobility components from the mounting point p_k to p_i, and $V_{\mathrm{p}i}$ is the actual velocity at point pi due to all excitation components of the system. The items of $Y_{\mathrm{p}ii}$ represent the direct path between the components of force and velocity at a same point, and the other items of $Y_{\mathrm{p}ik}$ ($i = k$) represent the coupling paths between different contact points for the components of dynamic force and velocity under study.

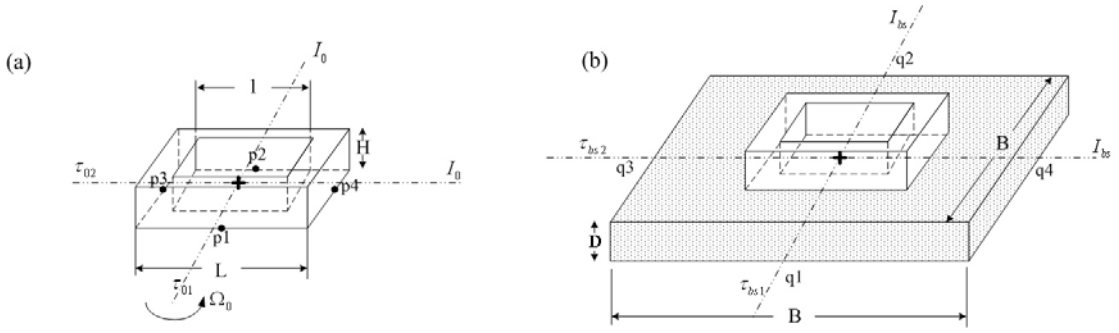

Fig. 2.3 (a) Model of the machine of even mass and its dimensions; (b) the model of the machine placed on the inertia block and its dimensions.

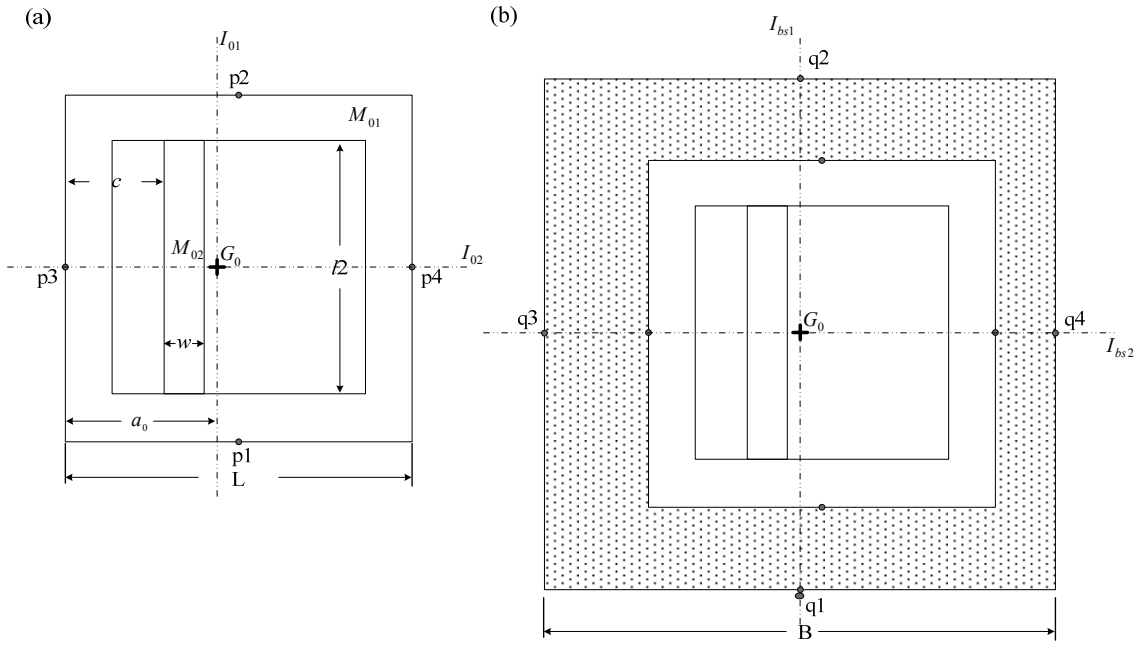

Fig. 2.4 (a) Plan view of the structure and dimension parameters of the uneven-mass machine. (b) plan view of the balanced setting with the inertia block.

As the model shown in Fig. 2.3(a) and the plan view shown in Fig. 2.4(a), the machine, which is assumed to be a rigid body in the interested low frequency region, consists of two parts – one is the symmetrical hollow rectangular part with four mounting points on the midpoints of every external side, and the other is an embedded rectangular engine part in uneven mass distribution. The whole mass of machine is

$$M_0 = M_{01} + M_{02} \tag{2.14}$$

where M_{01}= the mass of the hollow rectangular part of which L = the each external side length, l_2 = the internal side length, H = the height, and M_{02}= the mass of the

embedded rectangular engine part, of which l_2 = the long side length, H = the height, w = the width, c = the distance between the even mass embedded part and the external side of p3. There is a transverse distance between the center of gravity and the geometrical center, the location of the gravity center, and the moments of inertia around the axes throughout its center of gravity are given by

$$a_0 = \frac{M_{01}L + M_{02}(2c+w)}{2(M_{01}+M_{02})} \tag{2.15}$$

$$I_{01} = M_{01}\frac{L^2 + l_2^2 + H^2}{12} + M_{02}\frac{w^2 + H^2}{12} + \frac{M_{01}M_{02}}{4(M_{01}+M_{02})}(L - 2c - w)^2 \tag{2.16}$$

$$I_{02} = M_{01}\frac{L^2 + l_2^2 + H^2}{12} + M_{02}\frac{H^2 + l_2^2}{12} \tag{2.17}$$

In this case, to describe the source mobility including the multi interactions among the mounting points p1- p4 of the machine, a matrix form is used for the estimation of structure-borne sound by mobility method, which is given by

$$[Y_S] = \frac{1}{j\omega M_0}\begin{pmatrix} 1+\alpha_{11}+\alpha_{12} & 1+\alpha_{11}-\alpha_{12} & 1-\alpha_{13} & 1+\alpha_{14} \\ 1+\alpha_{11}-\alpha_{12} & 1+\alpha_{11}+\alpha_{12} & 1-\alpha_{13} & 1+\alpha_{14} \\ 1-\alpha_{13} & 1-\alpha_{13} & 1+\alpha_{33} & 1-\alpha_{34} \\ 1+\alpha_{14} & 1+\alpha_{14} & 1-\alpha_{34} & 1+\alpha_{44} \end{pmatrix} \tag{2.18}$$

where the coefficients of the matrix are given by

$$\alpha_{11} = \frac{M_0(l_0 - 2a_0)^2}{4I_{01}},\ \alpha_{12} = \frac{M_0 l_0^2}{4I_{02}},\ \alpha_{33} = \frac{M_0 l_0^2}{I_{01}},\ \alpha_{13} = \frac{M_0 l_0(l_0 - 2a_0)}{2I_{01}}$$

$$\alpha_{14} = \frac{M_0(l_0 - a_0)(l_0 - 2a_0)}{2I_{01}},\ \alpha_{34} = \frac{M_0 l_0(l_0 - a_0)}{I_{01}},\ \alpha_{44} = \frac{M_0(l_0 - a_0)^2}{I_{01}}$$

In the section, assuming that the source machine is effectively driven the inherent force F_0 at the center of the embedded engine part, the free velocity vector of the source machine is given by

$$[V_{S0}] = [V_{S1} \quad V_{S2} \quad V_{S3} \quad V_{S4}]^T \tag{2.19}$$

in which V_{Si} (i =1, 2, 3, 4) are the vibratory free velocities of four mounting points, which can be given by

$$V_{S1} = V_{S2} = V_0 - F_0 \frac{(a_0 - c)^2}{I_{01}},$$

$$V_{S4} = V_0 + F_0 \frac{(a_0 - c)}{I_{01}} a_0, \; V_{S3} = V_0 - F_0 \frac{(a_0 - c)}{I_{01}} (l_0 - a_0)$$

As the machine is directly mounted on the floor, the dynamic force vector and structure-borne power transmitted to the floor are given by

$$[F_{Tns}] = ([Y_S] + [Y_{rs}])^{-1} [V_{S0}] \tag{2.20}$$

$$[V_{r(ns)}] = [Y_{rs}][F_{(ns)}] \tag{2.21}$$

$$P_{(ns)} = \frac{1}{2} [F_{Tns}]^{*\mathrm{T}} \, \mathbf{Re}([Y_{rs}])[F_{Tns}] \tag{2.22}$$

the floor mobility matrix for the contact points on the floor that support the ma chine, and the components $V_{ri(ns)}$ of $[V_{r(ns)}]$ (i =1…N) are the corresponding vibr ation velocities at the points on the floor, as shown in Fig. 2.5(a).

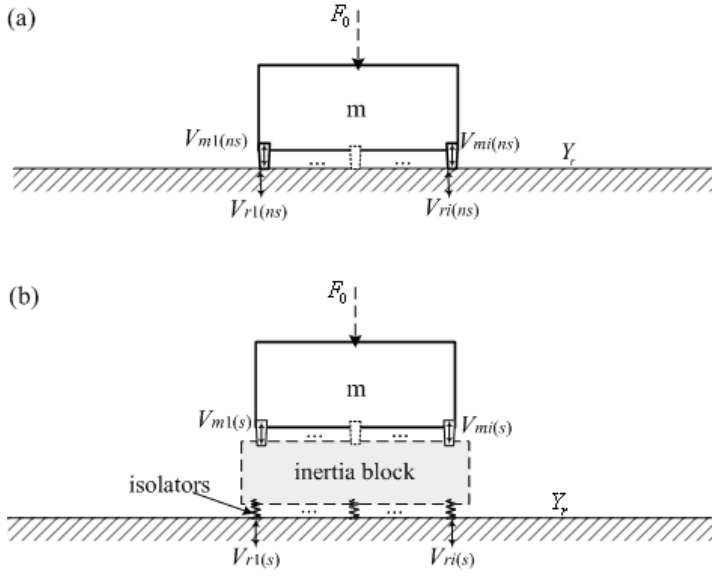

Fig. 2.5 (a) Definition of the vibration velocities of a multi-point vibratory machine that is mounted without vibration isolators or inertia block, and the velocities of the supporting flexible floor, (b) definition of the vibration velocities of the vibratory machine that is mounted with inertia block and vibration isolators, and the vibration velocities of the supporting floor.

When the isolated machine is combined with the inertia block as shown in Fig. 2.3(b) and Fig. 2.4(b), the center of gravity of the machine is located on the center of inertia block so that mass distribution of the combined system is balanced. The moments of inertia around the two horizontal axial throughout the gravity center of the combined vibratory source with the inertia block can be expressed as:

$$I_{Sb1} = I_{01} + M_b \frac{B^2 + H_b^2}{12} + \frac{M_0 M_b}{4(M_0 + M_b)}(H_0 + H_b)^2 \tag{2.23}$$

$$I_{Sb2} = I_{02} + M_b \frac{B^2 + H_b^2}{12} + \frac{M_0 M_b}{4(M_0 + M_b)}(H_0 + H_b)^2 \tag{2.24}$$

for the combined source of the machine with inertia block, the source mobility matrix is given by

$$[Y_{Sb}] = Y_{b0} \begin{pmatrix} 1+\beta_{u2} & 1-\beta_{u2} & 1 & 1 \\ 1-\beta_{u2} & 1+\beta_{u2} & 1 & 1 \\ 1 & 1 & 1+\beta_{u1} & 1-\beta_{u1} \\ 1 & 1 & 1-\beta_{u1} & 1+\beta_{u1} \end{pmatrix} \tag{2.25}$$

where the coefficients of the matrix of combined source mobility are derived by

$$\beta_{u1} = \frac{(M_0 + M_b)B^2}{4I_{sb1}}, \beta_{u2} = \frac{(M_0 + M_b)B^2}{4I_{sb2}}$$

Driven by the same inherent force of the machine, the new free velocity vector for the combined source with inertia block is given by

$$[V_{Sb}] = [V_{Sb1} \quad V_{Sb2} \quad V_{Sb3} \quad V_{Sb4}]^{\mathrm{T}} \tag{2.26}$$

$$V_{Sb1} = V_{Sb2} = V_0' - F_0 \frac{(a_0 - c)^2}{I_{Sb1}},$$

$$V_{Sb3} = V_0' - F_0 \frac{(a_0 - c)}{2I_{Sb1}} B, \quad V_{Sb4} = V_0' + F_0 \frac{(a_0 - c)}{2I_{Sb1}} B$$

where V_{Sbi} (i =1, 2, 3, 4) are the free vibratory velocities of four mounting points on the combined inertia block. Herein, $[V_S'] = [V_{Sb}]$ is the new free velocity and $[Y_S'] = [Y_{Sb}]$

is the new source mobility corresponding to the new mounting points of the source combined with inertia block. With the installation of the spring isolators, the vector of the dynamic forces and the active power transmitted to the floor can be calculated by

$$[F_{Ts}] = \left([Y_S^{'}] + \frac{j\omega}{k^{'}} [I] + [[Y_{rs}^{'}]] \right)^{-1} [V_S^{'}] \tag{2.27}$$

$$P_{(s)} = \frac{1}{2} [F_{Ts}]^{*T} \, \mathbf{Re}([[Y_{rs}^{'}]])[F_{Ts}] \tag{2.28}$$

Where $[Y_{rs}^{'}]$ is the floor mobility matrix for the new contact points q_i (i =1, 2, 3, 4) on the floor that support the combined source with inertia block. The vibration velocity vectors of the supporting floor and the isolated machine are given by

$$[V_{r(s)}] = [Y_{rs}^{'}] \, [F_{Ts}] \tag{2.29}$$

$$[V_{m(s)}] = [T_{ms}] \left(\frac{j\omega}{k} [I] + [Y_{rs}] \right) [F_{Ts}] \tag{2.30}$$

where $[T_{ms}]$ is the transfer matrix of source vibration velocity between the mounting points of the inertia block and the points of the machine (if there is no inertia block, $[T_{ms}]$ will be an identity matrix). In the form of $[V_{m(s)}] = [V_{m1(s)} \quad ... \quad V_{mN(s)}]^{T}$, the vector $[V_{m(s)}]$ expresses the corresponding velocities at the mounting points of the isolated machine, and $[V_{r(s)}] = [V_{r1(s)} \quad ... \quad V_{rN(s)}]^{T}$ expresses the vibration velocities at the N contact points supporting the vibration-isolated system on the floor, which are defined as shown in Fig. 2.5(b). (Eq. 2.31 for floor mobility)

2.2.3. THE ASSESSMENT INDICES FOR ISOLATED VIBRATORY SYSTEMS

For the multi-point vibratory machine mounted on a flexible floor, to accurately assess the vibration isolation system for structure-borne sound attenuation, the level of power transmissibility is used to evaluate the performance of vibration isolators, which is defined as

$$\gamma_s = 10\log\frac{P_{(s)}}{P_{(ns)}} \tag{2.32}$$

To estimate the stability of the multi-point vibratory system mounted on a real floor, the effect of floor mobility should not be neglected as it will affect the vibratory motion of the supporting floor structure, particularly, at frequencies near resonance modes of the floor. The level of vibration velocity transmissibility is adopted herein to evaluate the isolation effect on the vibration response of the supporting foundation, which is given by

$$\lambda_{rs} = 20\log\frac{\frac{1}{N}\sqrt{\sum_{i=1}^{N}\left|V_{ri(s)}\right|^2}}{\frac{1}{N}\sqrt{\sum_{i=1}^{N}\left|V_{ri(ns)}\right|^2}}$$

$$= 10\log\sum_{i=1}^{N}\left|V_{ri(s)}\right|^2 - 10\log\sum_{i=1}^{N}\left|V_{ri(ns)}\right|^2 \tag{2.33}$$

where $V_{ri(ns)}$ (i=1…N) is the vibration velocity at the ith contact point on the flexible floor supporting a vibratory machine that is directly mounted without the inertia block and vibration isolators, while $V_{ri(s)}$ is the velocity at the ith contact point on the floor supporting the machine that is mounted with isolators. Also, based on the free velocity of the source characteristics for multi-point machines excited by frequency-dependent forces, the mounted vibration velocity level of the vibratory machine is proposed to evaluate the stability of the isolated vibratory machine, which is defined by

$$\delta_{vm} = 10\log\sum_{i=1}^{N}\left|V_{mi(s)}\right|^2 - 10\log\sum_{i=1}^{N}\left|V_{Si}\right|^2 \tag{2.34}$$

where V_{Si} is the free velocity at the *i*th contact point on the source machine and $V_{mi(s)}$ is the velocity at the *i*th contact point of the vibratory machine that is mounted with the inertia block and vibration isolators. Moreover, the mounted rotational velocity level is proposed to evaluate the rocking motion of the vibratory multi-point machine mounted with the inertia block and vibration isolators, which is given by

$$\delta_{\omega m} = 20\log\frac{\frac{1}{N}\sqrt{\sum_{i=1}^{N}\left|\hat{\omega}_m \times \left(\hat{r}_{mi} - \hat{r}_{m0}\right)\right|^2}}{\frac{1}{N}\sqrt{\sum_{i=1}^{N}\left|V_{Si}\right|^2}};$$

$$= 10\,\mathbf{log}\sum_{i=1}^{N}\left|V_{mi(s)} - V_{m0(s)}\right|^2 - 10\,\mathbf{log}\sum_{i=1}^{N}\left|V_{Si}\right|^2 \qquad (2.35)$$

where V_{m0} is the vibration velocity at the center of gravity of the machine. Thus, the influence of isolating equipments on the vibrating and rocking motion of a vibratory machine can be analyzed as a normalized level.

2.3 ANALYSIS OF THE VIBRATION-ISOLATED SYSTEMS WITH VARIOUS INERTIA BLOCKS

2.3.1 THE PARAMETERS OF VIBRATORY SYSTEM AND THE SETTING CONDITIONS FOR ANALYZED CASES

In the first case study, the machine with four supporting springs is placed symmetrically on the square concrete floor, as shown in Fig. 2.6(a). The same machine mounted on the concrete inertia block with four supporting is shown in Fig. 2.6(b).

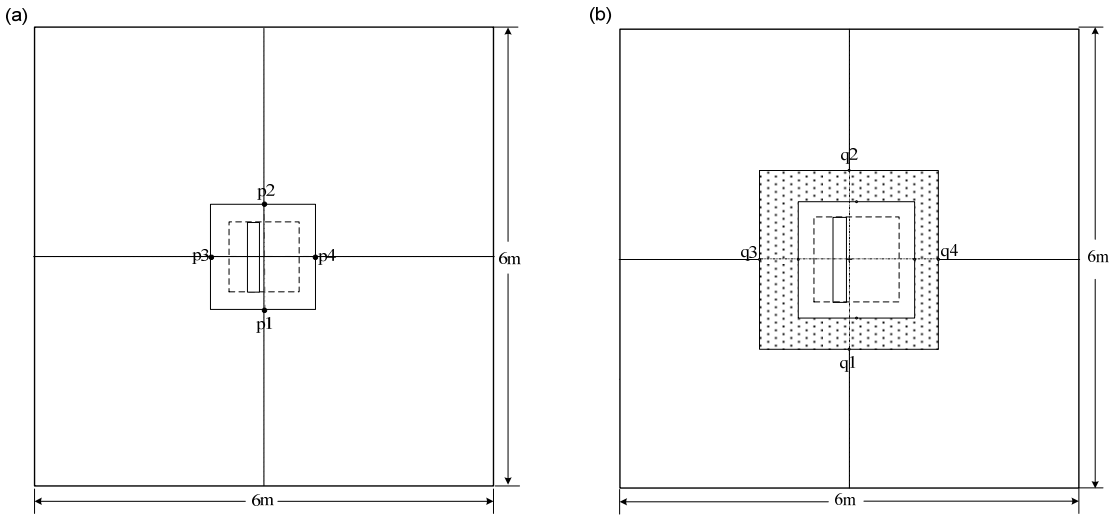

Fig. 2.6 (a) The plan view of the machine with uneven mass symmetrically mounted with four vibration isolators on the simply-supported floor plate. (b) The plane view of the machine mounted on the inertia block with four vibration isolators placed symmetrically on the floor.

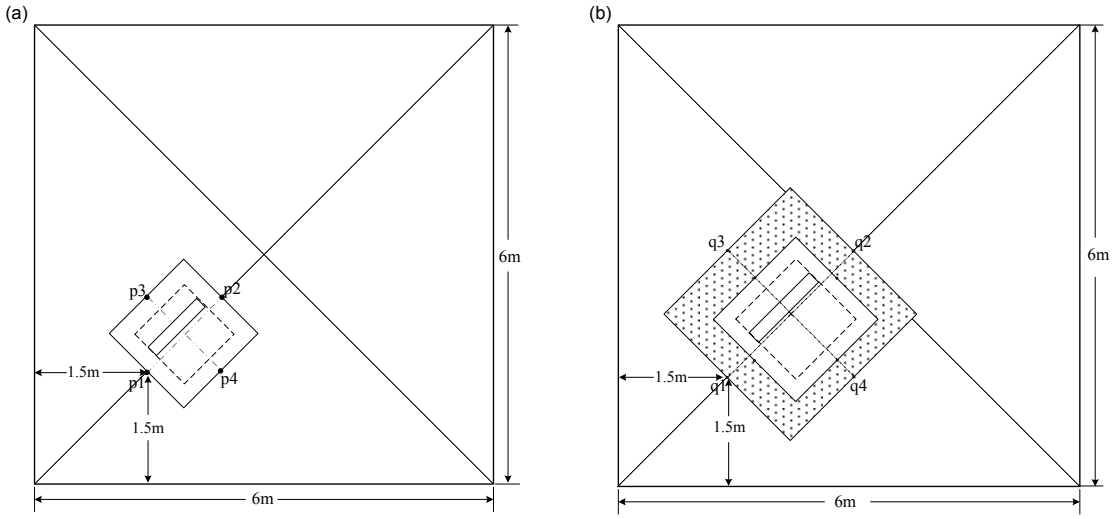

Fig. 2.7 (a) The plan view of the machine with uneven mass asymmetrically mounted with four vibration isolators on the simply-supported floor plate. (b) The plane view of the

machine mounted on the inertia block with four vibration isolators placed asymmetrically on the floor.

The dimensions and parameters of the steel machine model with uneven mass distribution are as follows: l_0 =1.294m; l_2 =1.185m; H = 0.32m; steel density $\rho_s = 7.85\times10^3\, kg/m^3$; the mass of the exterior body part of the machine $M_{01} = 700\,\text{kg}$ and of the internal engine part $M_{02} = 550\,\text{kg}$; $w = 0.27\,m$; and c = 0.575m. The four springs of the same stiffness are selected for the ideal natural frequency in vertical direction $f_0 = \frac{1}{2\pi}\sqrt{\frac{4k_0}{M_0}} = 12\,\text{Hz}$ with a low damping ratio ζ= 0.005, correspondingly for the two degrees of motions around two horizontal axes the natural frequencies are $f_1 = \frac{1}{2\pi}\sqrt{\frac{k_0 l_0}{I_{01}}} = 15.4\,\text{Hz}$ and $f_2 = \frac{1}{2\pi}\sqrt{\frac{k_0 l_0}{I_{02}}}$ =15 Hz. The inertia block, as a concrete cuboid body, is selected with a density $\rho_c = 2.8\times10^3\,\text{kg/m}^3$ and a side length of its square plane area L_B = 2.0m, the thickness (H_b) of which is varied for the different mass of the inertia block M_b (from 1-5.5 times the total machine mass M_0). To evaluate the influence of additional inertia blocks on the inertia of isolated sources, the ratio of the combined inertia of source is defined as $\beta = \sqrt{\frac{M_b(I_{sb1}+I_{sb2}-I_{01}-I_{02})}{M_0(I_{01}+I_{02})}}$. The physical parameters of the concrete floor are primarily based on the values given in [8], of which the density $\rho_c = 2.8\times10^3\,\text{kg/m}^3$, Young's modulus $E = 2.1\times10^{10}\,\text{N/m}^2$, loss factor $\eta = 2\times10^{-2}$, Poisson's Ratio $\mu = 0.2$, and thickness $d = 0.26\,\text{m}$. The boundaries of the square plate are simply supported, with the side length $L_a = 6\,\text{m}$, so that the floor mobility matrix, including the point mobility and transfer mobility for the multi supporting points, can be calculated using the developed analytical equations (whose mathematical functions are derived as in Ref. [61] and [40] p.322-327). The typical value of loss factor used in the thesis is based on the work of ref. [62].

The springs that support the machine with the inertia block are chosen to maintain the same static deflection [1, 58] with a same damping ratio ζ= 0.005 so that the ideal natural frequency in vertical direction is also 12 Hz. Then the different natural frequencies in two degrees of rocking motion around two horizontal axes correspondingly are $f_1 = \frac{1}{2\pi}\sqrt{\frac{k_b L_B}{I_{sb1}}}$ and $f_2 = \frac{1}{2\pi}\sqrt{\frac{k_b L_B}{I_{sb2}}}$. The details of the different natural frequencies corresponding to the vibratory systems in various ratios of the combined inertia of source are shown in Table. 2.1. In this case, the major working frequency region of the machine is assumed to be from 50 to 200 Hz that is larger than 3.3 times of f_0 for typical engineering design, and the frequency range interested by our study is 5 to 200 Hz in the figures for the analysis.

	Lightly uneven mass distribution			Heavy uneven mass distribution		
	f_0 Hz	f_1 Hz	f_2 Hz	f_0 Hz	f_1 Hz	f_2 Hz
without inertia block	12	15.4	15	12	17.2	15
with inertia block β_1	12	9.14	9.08	12	9.50	9.08
with inertia block β_2	12	6.46	6.44	12	6.59	6.44
with inertia block β_3	12	4.41	4.4	12	4.45	4.4

Table. 2.1 The natural frequencies in 3-degrees of freedom for the isolated vibratory systems without and with the inertia blocks in various ratios of the combined inertia of source *β*.

In the second case study, the vibratory machine with highly uneven mass distribution (c = 0.235m) is both asymmetrically mounted on the floor plate with springs only, as shown in Fig. 2.7(a), and isolated with the springs and inertia blocks, as shown in Fig. 2.7(b). Similar to the first case, the four springs of same stiffness supporting the

machine are selected for the ideal natural frequency in vertical direction f_0 = 12 Hz, and the natural frequencies in two degrees of motion around two horizontal axes correspondingly are f_1 = 17.2 Hz and f_2 = 15 Hz. The inertia block and springs that support the machine of heavy uneven mass distribution with the various inertia blocks are also chosen same as in the first case. The details of the different natural frequencies corresponding to the vibratory systems in various ratios of the combined inertia of source are also listed in the Table. 2.1.

2.3.2 COMPARISON AND ANALYSIS OF DIFFERENT VIBRATION-ISOLATED SYSTEMS

For a symmetrically placed machine with slightly uneven mass distribution that is driven by a force acting on the engine part M_{02}, the three thickness of the additional inertia block is selected corresponding to the ratios of the combined inertia of source are about β_1 = 2.4, β_2 = 4.4 and β_3 = 8.8. It can be seen from Fig. 2.8(a) that, at the frequency range 160Hz > f > 40Hz, the levels of power transmissibility (γ_s) for the system with the different inertia blocks are similar and do not, when compared to those for the system without the inertia block, change significantly at most frequencies. The slight differences at various frequencies are due to the change in floor mobility at the different supporting points on the floor. When the frequency increases to f > 160Hz, all the levels are quite small so the difference is not considerable. It is noted that the peak of power transmissibility at the frequency around 15Hz, which is corresponding to the resonance of rocking motion of the isolated uneven machine without inertia block, is cancelled after the insertion of inertia block, because the natural frequency of rocking motion f_1 of the isolated machine with inertia block is decreased by the combination with the inertia blocks (as shown in Table. 2.1). Besides, the peak at the frequencies

around 20Hz (which is in the ideal vibration isolation region $>\sqrt{2}f_0$) would move to a little higher range of frequency after the installation of bigger inertia block. Basically, the use of the inertia block or the additional mass of the inertia block does not change the performance of vibration isolation.

It can be seen from Fig. 2.8(b) that the curves of the level of vibration velocity transmissibility (λ_{rs}) at various ratios of the combined inertia of source are nearly the same in the whole studied region. This means that the change in the inertia of attached inertia block does not significantly change the excited vibration of the receiver floor. Compared to systems with the inertia block, the level of vibration velocity transmissibility for the system without the inertia block fluctuates at higher levels at most of the frequency range from 65 to 200 Hz except the narrow regions of two resonance peaks, but it is lower than the levels of. vibration velocity transmissibility for the systems with inertia blocks at the frequencies from 40 to 65 Hz. The mounted rotational velocity levels ($\delta_{\omega m}$) of the isolated vibratory machine, without and with the inertia blocks at various ratios of the combined inertia of source, are plotted in Fig. 2.8(c). It is found that the values of the mounted rotational velocity level of the isolated machine gradually decrease from -12 dB to -26 dB in the working region of machine (f > 50Hz) as β increases from β_1 = 2.4 to β_3 = 8.8. This means that the rotational velocity of the vibration system caused by the uneven mass distribution can be reduced by the additional inertia of the inertia block. Therefore, the use of or the additional mass of the inertia block improves the stability of the vibration isolation system while maintaining the performance of the vibration isolators in the working region. The mounted vibration velocity levels (δ_{vm}) of the isolated vibratory machine, without and with the inertia blocks at various ratios of the combined inertia of source, are plotted in Fig. 2.8(d). It is found that the values of the mounted vibration velocity level of the isolated machine

gradually decrease from 0 to -18 dB in the isolation region as β increases from 0 (i.e., without the inertia block) to β_3 = 8.8. This means that the vibration velocity of the isolated machine is near to the free velocity of the machine at most frequencies in the isolation region. The additional mass of the inertia block does reduce the vibration velocity of the isolated machine, so that the stability of the system is improved.

For good vibration isolation, it is necessary to reduce more than 99% of the structure-borne sound power transmitted from the source to the receiving structure and to reduce more than 90% of the transmitted vibration amplitude of the floor directly supporting the machine. The selected vibration isolators, together with the inertia block, should ensure that the level of power transmissibility of $\gamma_s \leq$ -20(dB) and the level of vibration velocity transmissibility of $\lambda_{rs} \leq$ -20(dB) can be satisfied in the vibration isolation region. The purpose of using additional inertia blocks is to control the rocking motion of the isolated machine. The average amplitude of the vibratory velocity of the isolated machine should be less than one-third of its free velocity, and the average amplitude of the rolling motion of the isolated machine should be less than 6% of the pure rolling motion, at the same amplitude, of its free velocity. Therefore, the suitable mass of the inertia block should be about two times the mass of the machine, as the ratio of the combined inertia of source of β_1 can satisfy the requirements of $\delta_{vm} <$ -10 dB and $\delta_{\omega m} <$ -20 dB in the mounting condition.

(a)

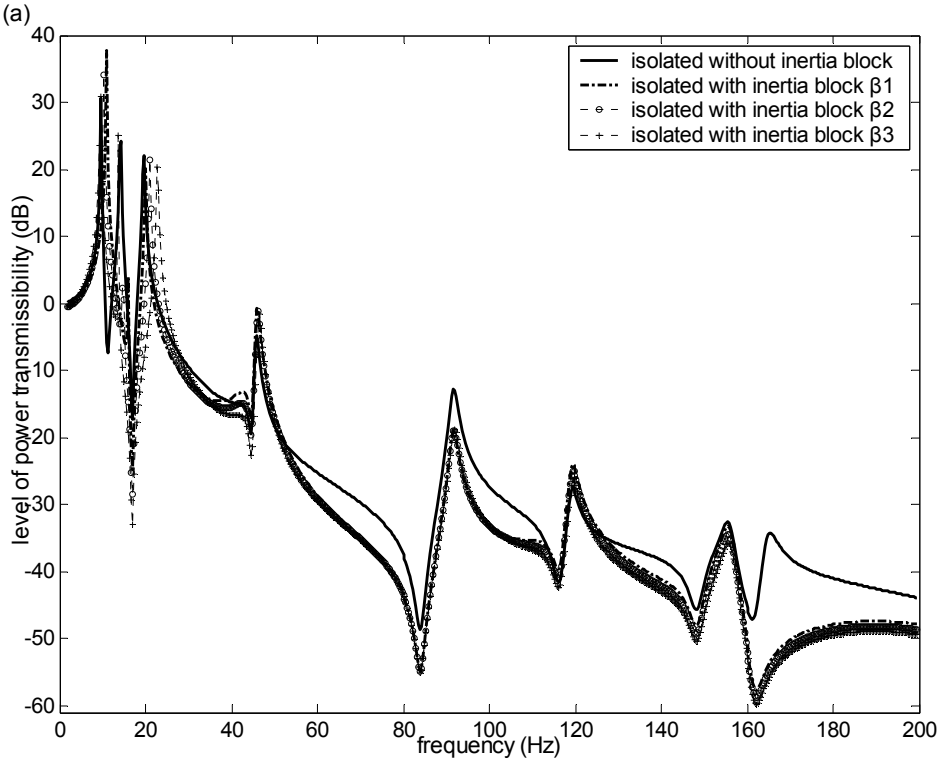
isolated without inertia block
isolated with inertia block β1
isolated with inertia block β2
isolated with inertia block β3
level of power transmissibility (dB)
frequency (Hz)
40
30
20
10
0
-10
-20
-30
-40
-50
-60
0
20
40
60
80
100
120
140
160
180
200

(b)

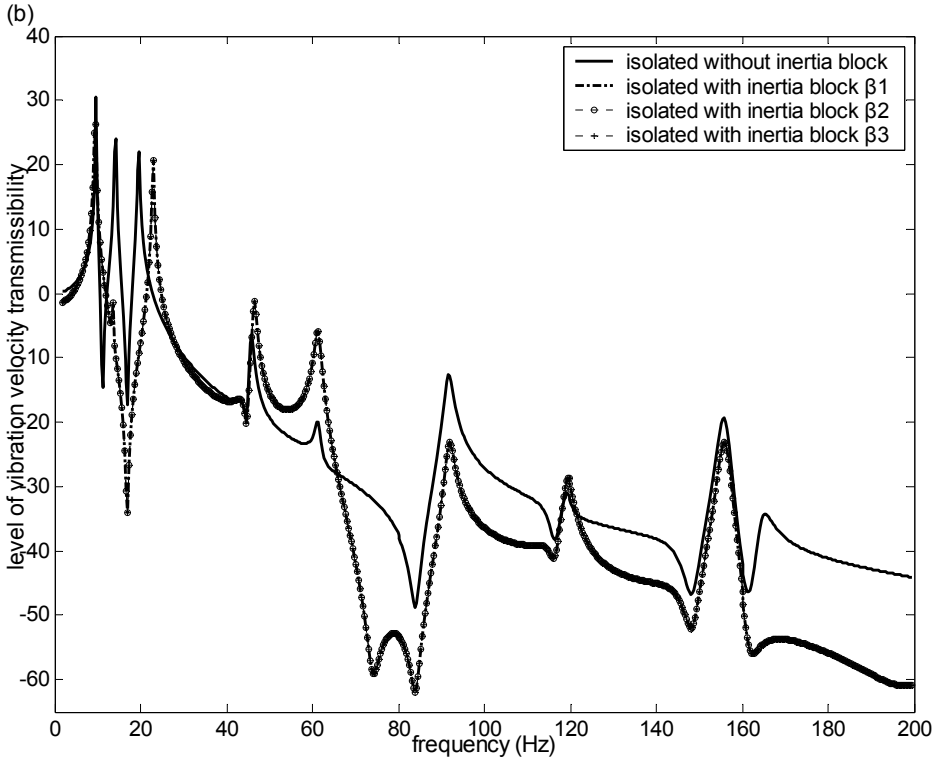
isolated without inertia block
isolated with inertia block β1
isolated with inertia block β2
isolated with inertia block β3
level of vibration velocity transmissibility
frequency (Hz)
40
30
20
10
0
-10
-20
-30
-40
-50
-60
0
20
40
60
80
100
120
140
160
180
200

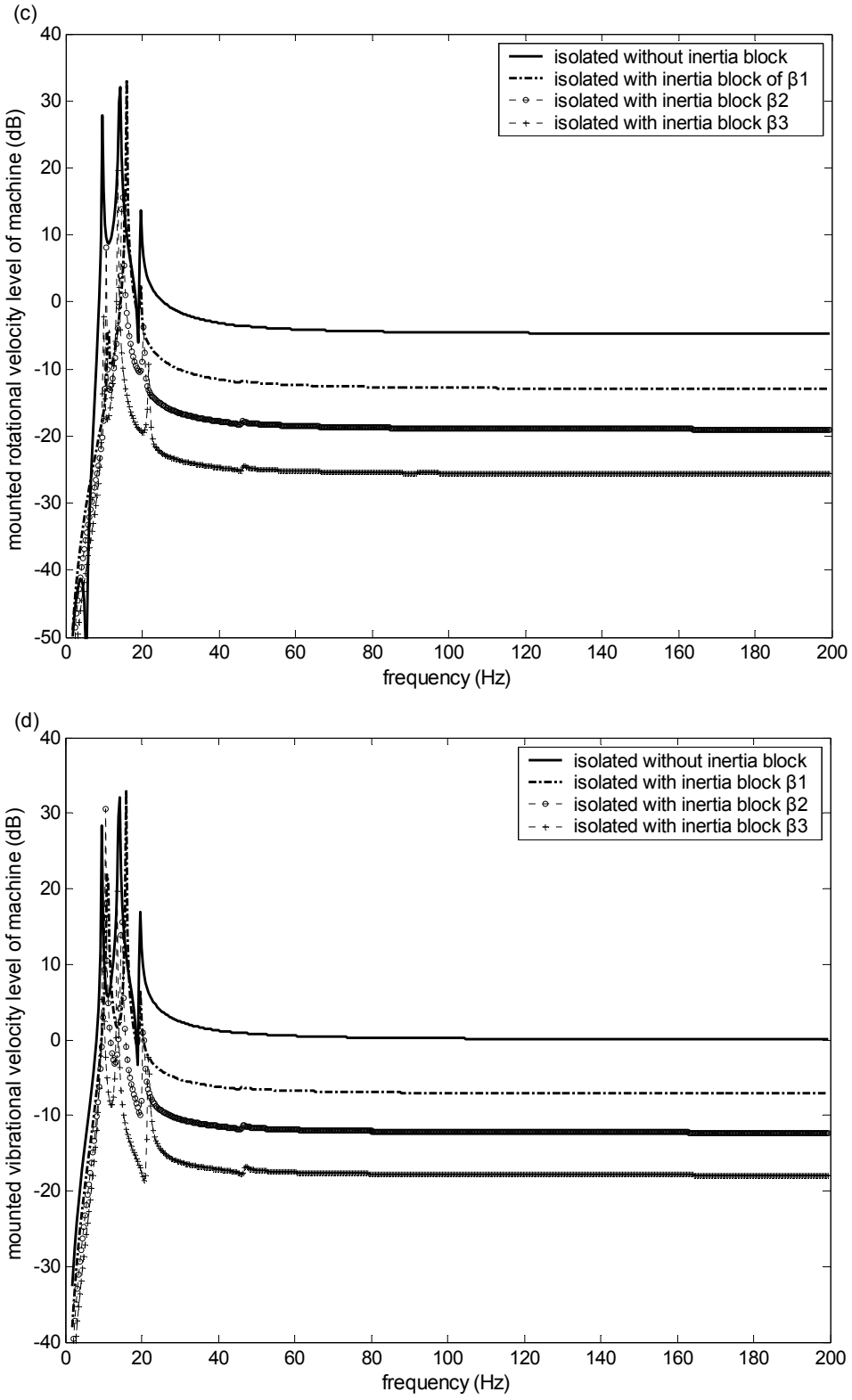

Fig. 2.8 Performance indices for the vibration isolation systems for the symmetrically placed machine of light uneven mass distribution, in the cases without and with the inertia blocks in various ratios of the combined inertia of source β. (a) The level of power transmissibility; (b) the level of vibration velocity transmissibility; (c) the mounted vibration velocity level of the vibratory machine; (d) the mounted rotational velocity level of the machine.

In the case of the machine with highly uneven mass distribution asymmetrically mounted on the floor plate without and with the inertia blocks, it can be seen from Fig. 2.9(a) that γ_s for the system with the inertia block with different β does not, when compared with γ_s for the system without the inertia block, change significantly in the isolation region at most frequencies (f>50 Hz). It can be seen from Fig. 2.9(b) that the curves of λ_{rs} at various ratios of the combined inertia of source are almost the same in the isolation region at most frequencies. This again indicates that the change in the mass of the inertia block does not significantly change the excited vibration of the receiver floor. It can be seen from Fig. 2.9(d) that the effect of inertia blocks on the δ_{vm} for the machine with highly uneven mass distribution is also very similar to the effect of inertia blocks on the δ_{vm} for the machine with slightly uneven mass distribution. Fig. 2.9(c) shows that, under the same mounting conditions, the values of $\delta_{\omega m}$ for the machine with highly uneven mass distribution are significantly higher than those of the machine with slightly uneven mass distribution. The values of the $\delta_{\omega m}$ for the isolated machine gradually decrease from -6 dB to -25 dB in the isolation region as β increases from 2.4 to 8.8. In order to meet the same requirements (i.e., δ_{vm} < -10 dB and $\delta_{\omega m}$ < -20 dB) as those in the first case study, the suitable mass of the inertia block should be >β_3. This again indicates that, basically, the use of the inertia block or the additional mass of the inertia block does not change the performance of vibration isolation but can improve the stability of the isolated vibratory system. The results reveal that, in order to enhance the stability of the vibration isolation system in machines with highly uneven mass distribution, an inertia block with a larger mass is required for a mounted vibratory machine.

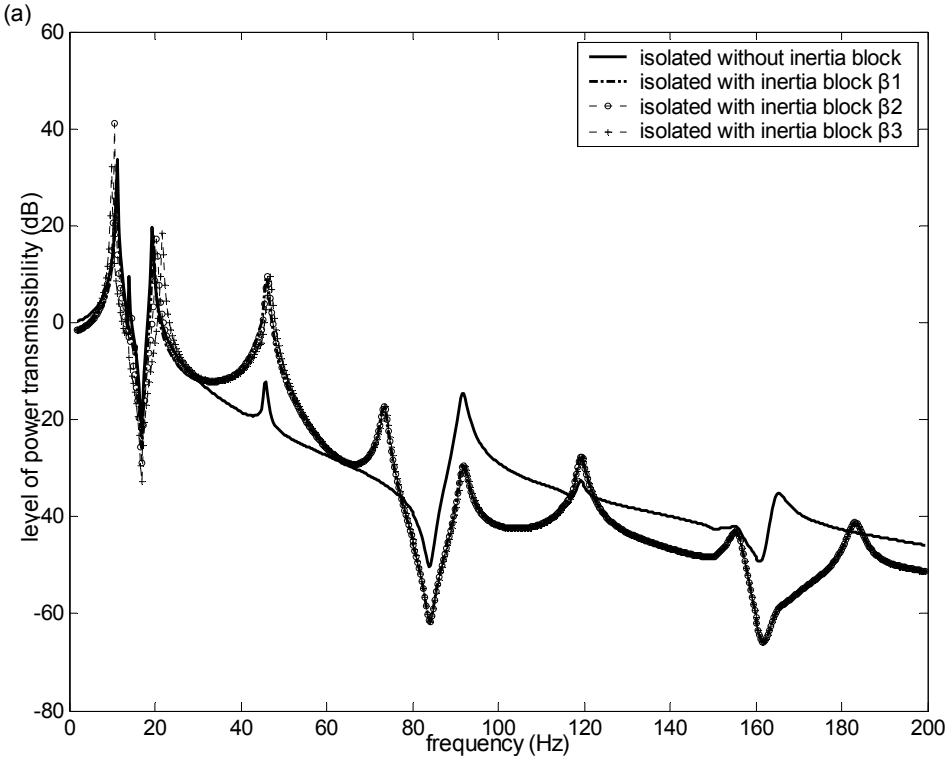
(a)
isolated without inertia block
isolated with inertia block β1
isolated with inertia block β2
isolated with inertia block β3
level of power transmissibility (dB)
frequency (Hz)
60
40
20
0
-20
-40
-60
-80
0
20
40
60
80
100
120
140
160
180
200

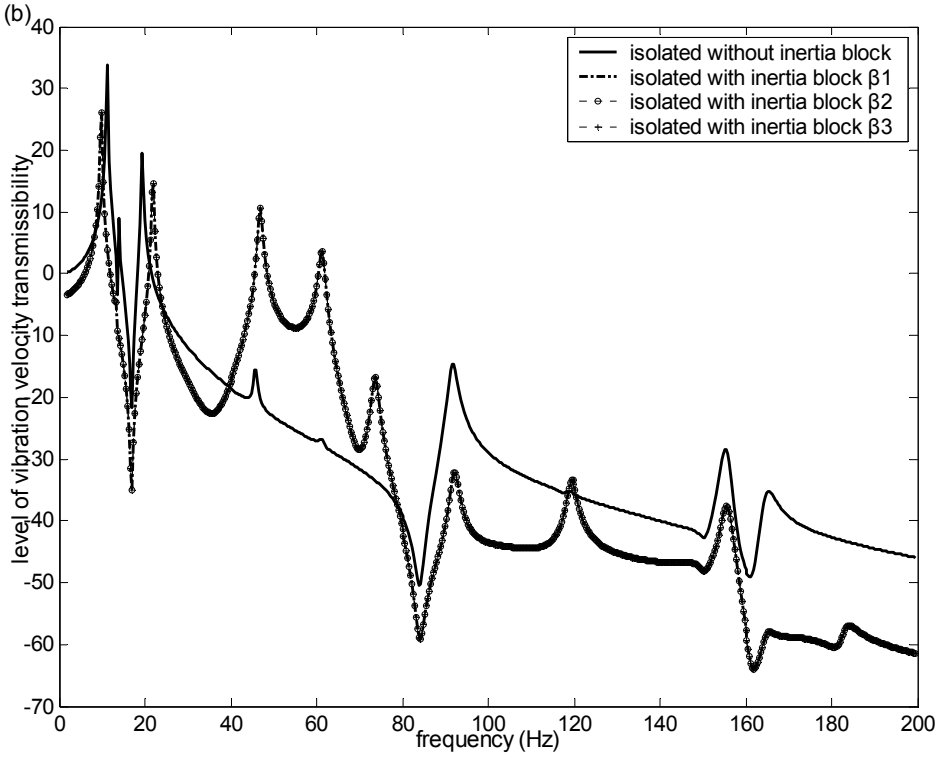
(b)
isolated without inertia block
isolated with inertia block β1
isolated with inertia block β2
isolated with inertia block β3
level of vibration velocity transmissibility
frequency (Hz)
40
30
20
10
0
-10
-20
-30
-40
-50
-60
-70
0
20
40
60
80
100
120
140
160
180
200

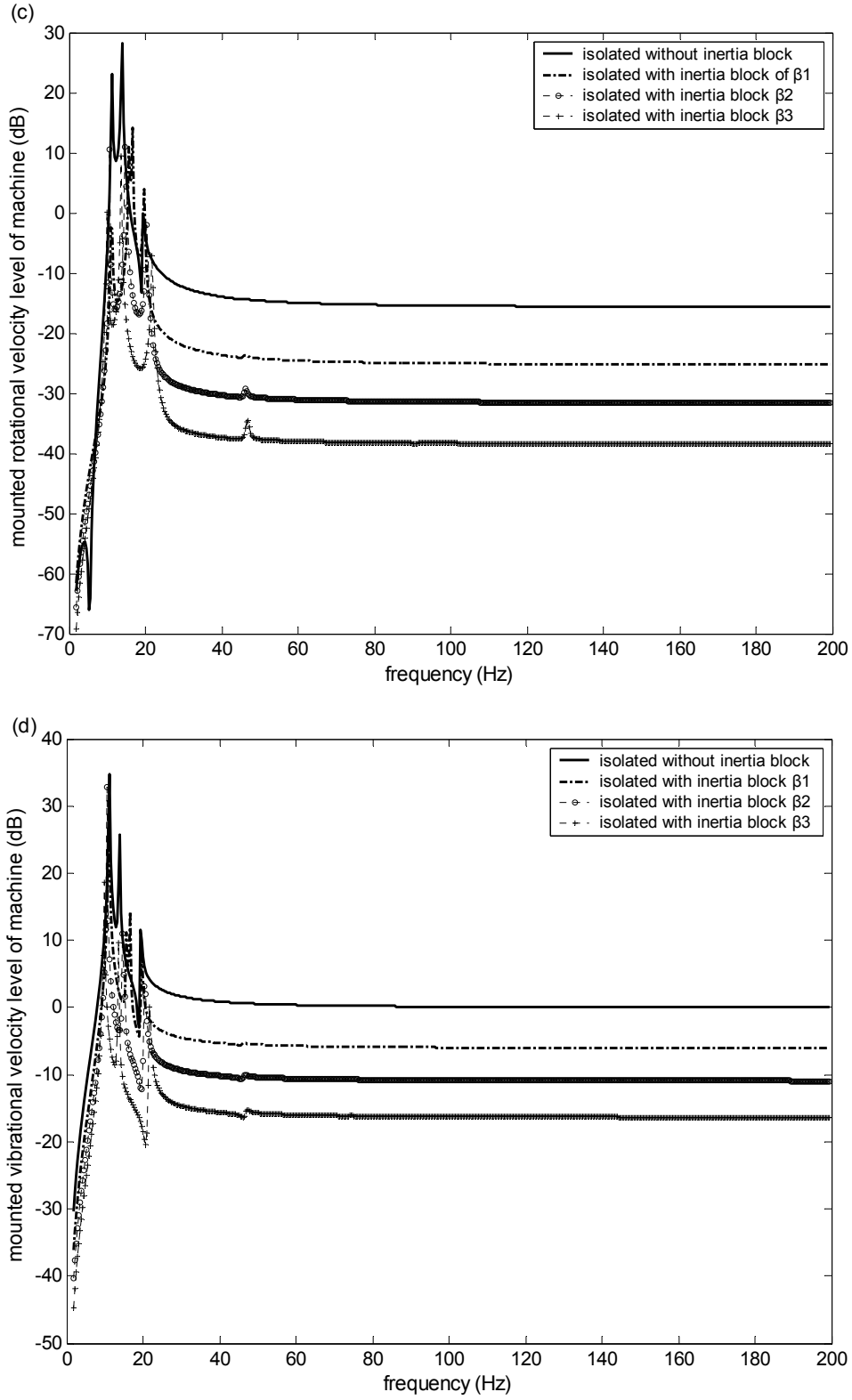

Fig. 2.9 The performance indices for the vibration isolation systems for the asymmetrically placed machine of heavy uneven mass distribution, in the cases without and with the inertia blocks in various ratios of the combined inertia of source β. (a) The level of power transmissibility; (b) the level of vibration velocity transmissibility; (c) the mounted vibration velocity level of the vibratory machine; (d) the mounted rotational velocity level of the machine.

2. 4. CONTRIBUTION AND SUMMARY

The fundamental source-receiver model of a vibration-isolated system is represented by an electrical analogy, and the complex model is applied to a multi-point source machine that vibrates in three degrees of freedom and asymmetrically mounted on a flexible floor with isolators in vertical direction. Furthermore, the developed model is used to estimate the isolation performance for an isolated uneven vibratory machine with an inertia block.

In the analysis of this chapter, the level of power transmissibility, the level of vibration velocity transmissibility, the mounted vibration velocity level, and the mounted rotational velocity level of the vibratory machine are proposed in order to assess the performance of vibration isolation and the stability of isolated multi-point vibratory building services equipment. The results primarily indicate that the use of an inertia block does not mainly affect the performance of vibration isolation. Instead, it decreases the vibration velocity and rotational velocity of the isolated vibratory machine, so that it can increase the stability of the vibratory system, regardless of whether the machine has slightly or highly uneven mass distribution. It is also found that, for the machine with slightly uneven mass distribution placed symmetrically on a floor plate, the suitable inertia block of which the ratio of the combined inertia of source is about 4. For the machine with highly uneven mass distribution placed asymmetrically on the floor, the ratio of the combined inertia of source of the additional inertia block should be larger than 8. The results reveal that, for the mounted vibratory machine, an inertia block with a larger mass can reduce the vibration and rotation of the isolated vibratory machine. As a result, it enhances the stability of the isolated vibratory system of machines with highly uneven mass distribution in 3 degrees of freedom. Therefore, in addition to proposing indices for assessing the stability of the vibratory

building services system, this chapter provides an insight into the selection of inertia blocks based on the mass distribution of an isolated vibratory machine.

CHAPTER 3. CHARACTERISTIC WAVETYPES OF THE FLEXURAL-LONGITUDINAL MOTION IN PERIODIC COUPLING DUAL-LAYERED BEAM STRUCTURES

3.1 INTRODUCTION

A number of building structures, bridges, container ship structures, and steel-reinforced concrete constructions are built from an assembly of a number of same or similar structure elements, of which the frames are typically coupled in a spatially identical manner to form a so-called "periodic structure." The excited vibration and transmission of the mechanical waves in these structures—from side to side in a bridge or layer to layer in a building—often give rise to structure-borne noise problems in the connected spaces and can sometimes even be harmful to the stability of the entire structure. When they propagate through frame structures that contain many connection branches, these structure-borne sound waves are coupled and reflected by each connector. The reflected and transmitted waves are then coupled and reflected again by other connectors. This process is physically repeated and sets off infinite multi-interactions between the coupling connections and propagating waves in a periodic structure, which forms the dispersion bands of structure-borne sound waves.

Early on, the dispersion bands of waves in periodic waveguides were studied for the electro-magnetic waves in solids [46], thus promoting our basic understanding of the properties of conductors, semi-conductors, and the like. Since the late 1980s, the optical wave bands in media with periodical modulation have been extensively studied, and these studies have led to a number of practical applications, including the advanced design of photonic crystals [63] and waveguide devices [64]. All of these studies have brought researchers deeper insight into the dispersion properties of periodic structures and have helped them to develop methods for the theoretical calculation of wave

propagation. In acoustics, the classical problem of plane sound wave transmission in one-dimensional periodic media can be tackled in an exact manner via the transfer matrix method [49]. The theoretical computations of band structures have also been well-documented for sound waves in periodic acoustic structures by Kushwaha and Mod [50]. Enhanced wave transmission was modeled in rib-reinforced floors about 50 years ago by using a beam that was periodically loaded with eccentric attachments because of wave coupling [65]. Four different methods of calculating the structure-borne sound propagation in beams with many non-resonant discontinuities were demonstrated by Manfred Heckl [54] and three of these methods took the coupling between longitudinal and flexural waves into account. The fundamental concept for the characterization of a periodic structure with multi-coupling was introduced by Mead [52]. In this context, a quadratic and well-posed spectral problem was studied to determine the propagation constants of coupled waves for a periodic system. The continued work was extended by Mead [53], which developed a second order matrix equation leading to the propagation and natural modes of the multi-coupled wave motion a damped periodic structure. Several years ago, a mathematical model for the coupling of waves that propagate in a periodically supported Timoshenko beam was presented by Maria Heckl [55]. Furthermore, the propagation characteristics of coupled longitudinal and flexural waves in beam-type transmission paths with asymmetric loads in the form of resonant columns were theoretically analyzed [56] and experimentally examined [57] by Friss and Ohlrich. However, little understanding of the fundamental physical propagation characteristics of the coupling acoustic waves in multi-layered structures has been gained from these studies. It is because they are commonly concerned with models of a single-channel waveguide that comprises the independent beam-type components or uncoupled wave transmission path in the structure. Therefore, the analytical study reported in this article

investigated the characteristics of the multi-coupling flexural and longitudinal waves that propagate in a periodic dual-beam type waveguide with structural connection branches. The transfer matrix method is developed by using the concept based on the propagation constants [52, 53] of the waves in a periodic structure so that it avoids the problems from inversion of ill-conditioned matrices and the cumulative errors. The developed method is therefore explicit and appropriate for the calculation of the coupled waves in the coupling beam structure.

3.2 THEORETICAL MODEL

3.2.1 SIMPLE MODEL OF A PERIODIC DUAL-BEAM STRUCTURE WITH A TRANSVERSE CONNECTION

The research of this chapter examines the band structure of flexural-longitudinal wave propagation in a dual-beam coupling structure that is periodically connected with transverse branches. A simplified model is shown in Fig. 3.1. The structure-borne sound consists of the flexural waves and longitudinal waves that propagate in two horizontal beams—A and B are coupled at each connection with a vertical branch C_i. The beams and branches discussed theoretically are even, straight, isotropic, and homogeneous, and the following physical parameters are assumed. $\rho_{(1,2,3)}$= the density of beams A and B and branch C_i, $B_{(a,b,c)0}$= the bending stiffness of beams A and B and branch C_i, $E_{(A,B,C)}$= the Young's modulus of beams A and B and branch C_i, $k_{(A,B,C)f}$= the flexural wave numbers of beams A and B and branch C_i, $k_{(A,B,C)l}$= the longitudinal wave numbers corresponding to the acoustic speeds of the longitudinal wave $c_{(1,2,3)}$ of beams A and B and branch C_i. The characteristics of the wave types and the energy transmission of the coupled flexural-longitudinal waves in a semi-infinite periodic dual-beam structure is calculated for analysis in a case study.

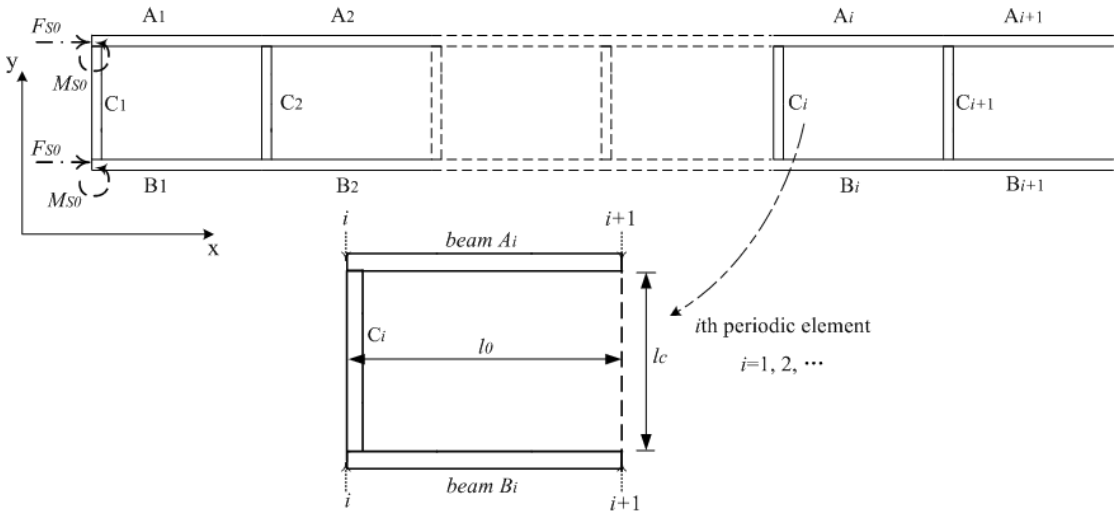

Fig. 3.1 Scheme of the semi-infinite periodic dual-beam structure and the excitations on the structure

3.2.2. WAVE TRANSFER MATRIX AND PROPAGATION CONSTANTS OF THE CHARACTERISTIC WAVE TYPES

In the analytical model of this research, the coupled wave components of the complex velocity (horizontal, vertical, and rotational) and force (horizontal, vertical, and moment) vectors are used for describing the coupled wave motions and response in the dual-beam structure. For the mathematical derivation based on the theoretical fundamentals of the propagation and coupling of structure-borne sound waves in thin beam structures [40], all of the analytical equations of this study are based on the harmonic wave of separate frequency ω_n with time dependence suppressed. Normally the longitudinal and flexural waves in a beam can be expressed in the form of the independent wave velocity components. In addition, the longitudinal-flexural waves can be described by the beam velocities and the corresponding forces caused by the wave motions. At the connections of every periodic element, the vector consisting of velocity and force components can be related to the vector of the flexural-longitudinal waves that propagate through the beams in a matrix form as follows.

$$\begin{bmatrix} \mathrm{V}_n \\ \mathrm{F}_n \end{bmatrix} = [S_{VF}]\,[v_w], \tag{3.1}$$

$$[v_w] = \begin{bmatrix} v_{wA} \\ v_{wB} \end{bmatrix} = [S_{VF}]^{-1} \begin{bmatrix} \mathrm{V}_n \\ \mathrm{F}_n \end{bmatrix}, \tag{3.2}$$

where the velocity vectors of the flexural and longitudinal wave components are expressed as

$$[v_{wA}] = \left[v_{Af}^{+} \;\; v_{Afj}^{+} \;\; v_{Af}^{-} \;\; v_{Afj}^{-} \;\; v_{Al}^{+} \;\; v_{Al}^{-} \right]^{\mathrm{T}}, \; [v_{wB}] = \left[v_{Bf}^{+} \;\; v_{Bfj}^{+} \;\; v_{Bf}^{-} \;\; v_{Bfj}^{-} \;\; v_{Bl}^{+} \;\; v_{Bl}^{-} \right]^{\mathrm{T}},$$

of which "+" donates the wave components propagating in the positive x-direction, "-" donates the components going in the negative x-direction, "f", "fj" and "l" donate the propagating flexural, nearfield flexural and longitudinal wave components respectively. The vectors of the velocities and forces of the two beam channels – indicated by the subscripts "a" and "b", are expressed as

$$[\mathrm{V}_n] = \left[V_{ya} \;\; V_{yb} \;\; \omega_a \;\; \omega_b \;\; V_{xa} \;\; V_{xb} \right]^{\mathrm{T}}, \; [\mathrm{F}_n] = \left[F_{ya} \;\; F_{yb} \;\; M_a \;\; M_b \;\; F_{xa} \;\; F_{xb} \right]^{\mathrm{T}}.$$

Where V_x, V_y and ω are the x-degree, y-degree and rotational velocities in the beam, and F_x, F_y and M are the x-degree force, y-degree force and moment acting on a beam. To describe the relationship between the independent flexural-longitudinal waves and the velocities-forces in two beams, the waves to motions-actions transfer matrix $[S_{VF}]$ takes on the matrix form:

$$[S_{VF}] = [\, S_{V1} \;\; S_{V2} \;\; S_{V3} \;\; S_{F1} \;\; S_{F2} \;\; S_{F3}]^{\mathrm{T}}, \tag{3.3}$$
$$S_{Vi} = \begin{bmatrix} D_{Vai} & \mathbf{O}_{6\times1} \\ \mathbf{O}_{6\times1} & D_{Vbi} \end{bmatrix}, S_{Fi} = \begin{bmatrix} D_{Fai} & \mathbf{O}_{6\times1} \\ \mathbf{O}_{6\times1} & D_{Fbi} \end{bmatrix},$$

in which the matrix are derived by

$$D_{V(a,b)1}=\begin{bmatrix}1\\1\\1\\1\\0\\0\end{bmatrix},\quad D_{V(a,b)3}=\begin{bmatrix}0\\0\\0\\0\\1\\1\end{bmatrix},\quad D_{Va2}=\begin{bmatrix}-jk_{Af}\\-k_{Af}\\jk_{Af}\\k_{Af}\\0\\0\end{bmatrix},$$

$$D_{Vb2}=\begin{bmatrix}-jk_{Bf}\\-k_{Bf}\\jk_{Bf}\\k_{Bf}\\0\\0\end{bmatrix},\quad D_{Fa1}=\begin{bmatrix}jR_{AF}\\-R_{AF}\\-jR_{AF}\\R_{AF}\\0\\0\end{bmatrix}\ \text{and}$$

$$D_{Fb1}=\begin{bmatrix}jR_{BF}\\-R_{BF}\\-jR_{BF}\\R_{BF}\\0\\0\end{bmatrix},\quad D_{Fa2}=\begin{bmatrix}R_{AM}\\-R_{AM}\\R_{AM}\\-R_{AM}\\0\\0\end{bmatrix},\quad D_{Fb2}=\begin{bmatrix}R_{BM}\\-R_{BM}\\R_{BM}\\-R_{BM}\\0\\0\end{bmatrix},$$

$$D_{Fa3}=\begin{bmatrix}0\\0\\0\\0\\R_{Al}\\-R_{Al}\end{bmatrix},\quad D_{Fb3}=\begin{bmatrix}0\\0\\0\\0\\R_{Bl}\\-R_{Bl}\end{bmatrix},\quad R_{Al}=\rho_1 c_1,\quad R_{Bl}=\rho_2 c_2,$$

$$R_{AM}=\frac{B_{a0}k_{Af}^2}{j\omega_n},R_{BM}=\frac{B_{b0}k_{Bf}^2}{j\omega_n},\quad R_{AF}=\frac{B_{a0}k_{Af}^3}{j\omega_n},\quad R_{BF}=\frac{B_{b0}k_{Bf}^3}{j\omega_n}.$$

It is clear that the y-degree velocities and forces, rotational velocities and moments in the beams A and B are resulted from the flexural wave motions, while the x-degree velocities and forces in two beams are resulted from the longitudinal wave motions. It should be noted that the wave-coupling effect in a periodic dual-beam structure is caused by the vertical connections. By introducing the dynamic continuity conditions at the interfaces that are vertically connected with the branch beams, the relationship

between the velocities and the forces of the coupled flexural and longitudinal waves at the connections of dual-beam structure can be characterized as a 12 x 12 coupling transfer matrix that can be expressed as

$$\begin{bmatrix} \mathrm{V}_n \\ \mathrm{F}_n \end{bmatrix}_i^+ = [W_{\mathrm{C}}] \times \begin{bmatrix} \mathrm{V}_n \\ \mathrm{F}_n \end{bmatrix}_i^- \tag{3.4}$$

where $\begin{bmatrix} \mathrm{V}_n \\ \mathrm{F}_n \end{bmatrix}_i^-$ and $\begin{bmatrix} \mathrm{V}_n \\ \mathrm{F}_n \end{bmatrix}_i^+$ denote the velocity and force vectors of the beam on the left and right side of the connection points on beam A-B with C*i*. Based on the dynamic equilibrium on two sides of a branch C*i*, the wave-coupling matrix $[W_{\mathrm{C}}]$ is given by

$$[W_{\mathrm{C}}] = \begin{bmatrix} \mathrm{I}_6 & \mathrm{O}_6 \\ -Z_{\mathrm{C}w} \times T_{\mathrm{C}v} & \mathrm{I}_6 \end{bmatrix}, \tag{3.5}$$

in which the transfer elements are given by

$$Z_{\mathrm{C}w} = \begin{bmatrix} Z_{Cl} & \mathrm{O}_{2\times4} \\ \mathrm{O}_{4\times2} & Z_{Cf} \end{bmatrix}, \quad Z_{\mathrm{C}l} = \begin{bmatrix} R_{\mathrm{c}l} & -R_{\mathrm{c}l} \\ -R_{\mathrm{c}l}\phi_{Cl}^{-j} & R_{\mathrm{c}l}\phi_{Cl}^{j} \end{bmatrix}$$

$$Z_{Cf} = \begin{bmatrix} \Omega_{Mc} & -\Omega_{Mc} & \Omega_{Mc} & -\Omega_{Mc} \\ -\phi_{Cf}^{-j}\Omega_{Mc} & \phi_{Cf}^{-1}\Omega_{Mc} & -\phi_{Cf}^{j}\Omega_{Mc} & \phi_{Cf}\Omega_{Mc} \\ j\Omega_{Fc} & -\Omega_{Fc} & -j\Omega_{Fc} & \Omega_{Fc} \\ -j\phi_{Cf}^{-j}\Omega_{Fc} & \phi_{Cf}^{-1}\Omega_{Fc} & j\phi_{Cf}^{j}\Omega_{Fc} & -\phi_{Cf}\Omega_{Fc} \end{bmatrix}.$$

$$T_{\mathrm{C}v} = \begin{bmatrix} T_{Cl} & \mathrm{O}_{2\times4} \\ \mathrm{O}_{4\times2} & T_{Cf} \end{bmatrix}, \quad T_{Cl} = \begin{bmatrix} 1 & 1 \\ \phi_{Cl}^{-j} & \phi_{Cl}^{j} \end{bmatrix}^{-1},$$

$$T_{Cf} = \begin{bmatrix} 1 & 1 & 1 & 1 \\ \phi_{Cf}^{-j} & \phi_{Cf}^{-1} & \phi_{Cf}^{j} & \phi_{Cf} \\ -jk_{Cf} & -k_{Cf} & jk_{Cf} & k_{Cf} \\ -jk_{Cf}\phi_{Cf}^{-j} & -k_{Cf}\phi_{Cf}^{-1} & jk_{Cf}\phi_{Cf}^{j} & k_{Cf}\phi_{Cf} \end{bmatrix}^{-1},$$

$$R_{\mathrm{c}l} = \rho_3 c_3, \quad \phi_{Cl} = e^{k_{Cl}h}, \quad \phi_{Cf} = e^{k_{cf}h}, \quad \Omega_{Mc} = \frac{B_{0C}k_{Cf}^2}{j\omega_n}, \quad \Omega_{Fc} = \frac{B_{0C}k_{Cf}^3}{j\omega_n}.$$

The new flexural and longitudinal waves that are excited in the branch will result in the velocities and forces acting on the two connection sides of the branch with the beams A

and B, so that the flexural and longitudinal waves will be coupled there. Moreover, the transfer matrix of the longitudinal and flexural waves propagating in the continuous beam period (whose length = d) is given by

$$[v_w]_{i+1}^{-} = [P_{wv}][v_w]_i^{+} \quad . \tag{3.6}$$

$$[P_{wv}] = \begin{pmatrix} P_{Af} & \mathrm{O} & \mathrm{O} & \mathrm{O} \\ \mathrm{O} & P_{Al} & \mathrm{O} & \mathrm{O} \\ \mathrm{O} & \mathrm{O} & P_{Bf} & \mathrm{O} \\ \mathrm{O} & \mathrm{O} & \mathrm{O} & P_{Bl} \end{pmatrix}, \quad P_{Af} = \begin{pmatrix} e^{-jk_{Af}d} & 0 & 0 & 0 \\ 0 & e^{-k_{Af}d} & 0 & 0 \\ 0 & 0 & e^{jk_{Af}d} & 0 \\ 0 & 0 & 0 & e^{k_{Af}d} \end{pmatrix},$$

$$P_{Bf} = \begin{pmatrix} e^{-jk_{Bf}d} & 0 & 0 & 0 \\ 0 & e^{-k_{Bf}d} & 0 & 0 \\ 0 & 0 & e^{jk_{Bf}d} & 0 \\ 0 & 0 & 0 & e^{k_{Bf}d} \end{pmatrix}, \quad P_{Al} = \begin{pmatrix} e^{-jk_{Al}d} & 0 \\ 0 & e^{jk_{Al}d} \end{pmatrix}, P_{Bl} = \begin{pmatrix} e^{-jk_{Bl}d} & 0 \\ 0 & e^{jk_{Bl}d} \end{pmatrix}.$$

It is generally understood that the flexural and longitudal waves can propagate independently through the dual-beam part between the connnection branches without coupling. Therefore, the transfer relationship of the waves in the continuous beam part can be described by using the diagonal matrices. On the whole, the coupled wave transmission in the periodic structure can be expressed as

$$\begin{bmatrix} \mathrm{V}_n \\ \mathrm{F}_n \end{bmatrix}_{i+1}^{-} = [U_e] \times \begin{bmatrix} \mathrm{V}_n \\ \mathrm{F}_n \end{bmatrix}_i^{-}, \tag{3.7}$$

where the entire periodic transfer matrix is given

$$[U_e] = [S_{VF}]\,[P_{wv}]\,[S_{VF}]^{-1}[W_{\mathrm{C}}].$$

According to the Bloch wave theory [66], for a linear acoustic system, when the acoustic waves are propagating through a semi-infinite one-dimensional periodic structure, the wave motions can be described as the characteristic wave-types of Bloch waves. Then the relationship between velocity vector $[\mathrm{V}_n]_i$ and force vector $[\mathrm{F}_n]_i$ at the two periodic connection points nearby satisfies the form

$$[\mathrm{V}_n]_{(i)}^{-} = \sum_{j=1}^{N} \mathrm{v}_{j,(i)} [\xi_{jn}],\ [\mathrm{F}_n]_{(i)}^{-} = \sum_{j=1}^{N} \mathrm{f}_{j,(i)} [\zeta_{jn}], \tag{3.8}$$

$$\begin{bmatrix} \mathrm{v} \\ \mathrm{f} \end{bmatrix}_{(i+1)} = e^{\mu} \begin{bmatrix} \mathrm{v} \\ \mathrm{f} \end{bmatrix}_{(i)}. \tag{3.9}$$

This represents a problem on the eigen value vector for the transfer matrix $[U_e]$, where $\mu_j = \pm(\mu_{j\mathrm{R}} + j \cdot \mu_{j\mathrm{I}})$ are the pair of jth eigen values—the frequency-dependent complex propagation constants for the corresponding pair of the N characteristic wave types (N = 6 for this periodic structure). Correspondingly the characteristic wave types are formulated by the eigen vectors $[\xi_{jn}\ \ \zeta_{jn}]^{\mathrm{T}}$, which take on the form $[\xi_{jn}] = [X^j_{Vxa}, X^j_{Vxb}, X^j_{\omega a}, X^j_{\omega b}, X^j_{Vya}, X^j_{Vyb}]^{\mathrm{T}}$ and $[\zeta_{jn}] = [X^j_{Fxa}, X^j_{Fxb}, X^j_{Ma}, X^j_{Mb}, X^j_{Fya}, X^j_{Fyb}]^{\mathrm{T}}$.

As the "attenuation constant" of the coupled wave type, the real part $\mu_{j\mathrm{R}}$ expresses the exponential decay rate for the jth characteristic wave type that propagates through a periodic beam element, whereas the imaginary part $\mu_{j\mathrm{I}}$ is defined as the "phase constant," of which the cosine value describes the phase transfer of the jth characteristic wave type that propagates through each element. If the propagation constants of the positive-going wave types are defined as $\mu_j = \mu_{j\mathrm{R}} + j \cdot \mu_{j\mathrm{I}}$ ($0 \le |\mu_{j\mathrm{I}}| < 2\pi$), then, correspondingly, the real and imaginary parts of the propagation constants ought to be negative. For the frequency-dependent wave propagation in a periodic structure, the frequency domain is classified into pass bands, i.e. frequencies at which the coupled waves travel through the periodic structure with little loss, and forbidden bands, i.e. frequencies at which the coupled waves propagating in the periodic structure are evanescent. In an ideal case as the damping factor is negligible, a pair (positive and negtive- going) of characteristic wave types yield up to a pair of pure imaginary propagation constants at any frequency within the pass bands, which indicates the

coupled waves propagating through the periodic structure will not decay. On the other side, the real parts of propagation constants are nonzero at the frequencies within the forbidden bands, which indicates the coupled waves will be attenuated as propagating through the periodic structure. The zone of larger attenuation constants, i.e. $|\mu_{jR}|$ means that the corresponding wave-type is in the stronger forbidden band of the periodic structure. In the semi-infinite structure, only the positive-going propagation constant $\mu_j = -|\mu_{jR}| - j|\mu_{jI}|$ is the resonable solution, because neither $+|\mu_{jI}|$ nor $+|\mu_{jR}|$ for a negtive-going wave type is physically possible for the phase retardation and energy decay in propagation.

3.3 ANALYSIS FOR THE TRANSMISSION OF COUPLED WAVES

3.3.1. SETTINGS AND PARAMETERS USED IN COMPUTATION

The numerical analysis and choice of the physical parameters for a semi-infinite periodic structure was designed to investigate and reveal the coupling effects of wave propagation. All of the computations and matrix manipulations were conducted using MATLAB. Aluminum was chosen as the beam material, of which the Young's modulus is $E_0 = 6.9 \times 10^{10}$ N/m^2 with loss factor $\eta = 0.002$ and density $\rho_0 = 2700$ kg/m^3. The two equal beams are semi-infinite along the x-direction and periodically connected by the transverse beams with a same rectangular cross-section. The thickness and width of the beam cross-section are $h_0 = 11$ mm and $d_0 = 50$mm respectively, the periodic element length is $l_0 = 550$ mm and the length of transverse connection beam is $l_c = 500$ mm. The results in the frequency domain computed for the analysis and the discussion herein of the characteristic coupled waves are normalized by using the non-dimensional frequency parameter Ω_n as Ref. [56], which is given by

$$\Omega_n = \left(k_f l_0\right)^2 = \omega_n \left(12\rho_0 / E_0\right)^{1/2} \left(l_0 / h_0\right), \tag{3.10}$$

where k_f is the real wave number for the free flexural waves that are propagating in beams A and B.

3.3.2 PROPAGATION CONSTANTS AND THE CHARACTERISTIC WAVE TYPES

Basically, there are six characteristic wave types for the coupled wave motions that propagate in the semi-infinite periodic coupling beam structure, which all contain both positive-going and negative-going longitudinal and flexural wave motions in the beams because of the multi-coupling at the beam connections. These characteristic wave types can be divided into two groups—symmetric and antisymmetric types—based on the different phase relationships of the wave motions between beams A and B. Herein the symmetric wave types are named because the phase differences of the y-degree velocities between beam A and beam B are π and the phase differences of the x-degree velocities between two beams are 0. They are like the mirror images from the symmetry axis of the dual-beam structure in x-direction. For the motions of antisymmetric wave types, the phase differences of the y-degree velocities between beam A and beam B are 0 and the phase differences of the x-degree velocities between two beams are π. They are like the inverted images from the symmetry axis of the dual-beam structure in x-direction. A further step to describe the propagation characteristics of the wave types is to use the dispersion of the propagation constants.

(a)

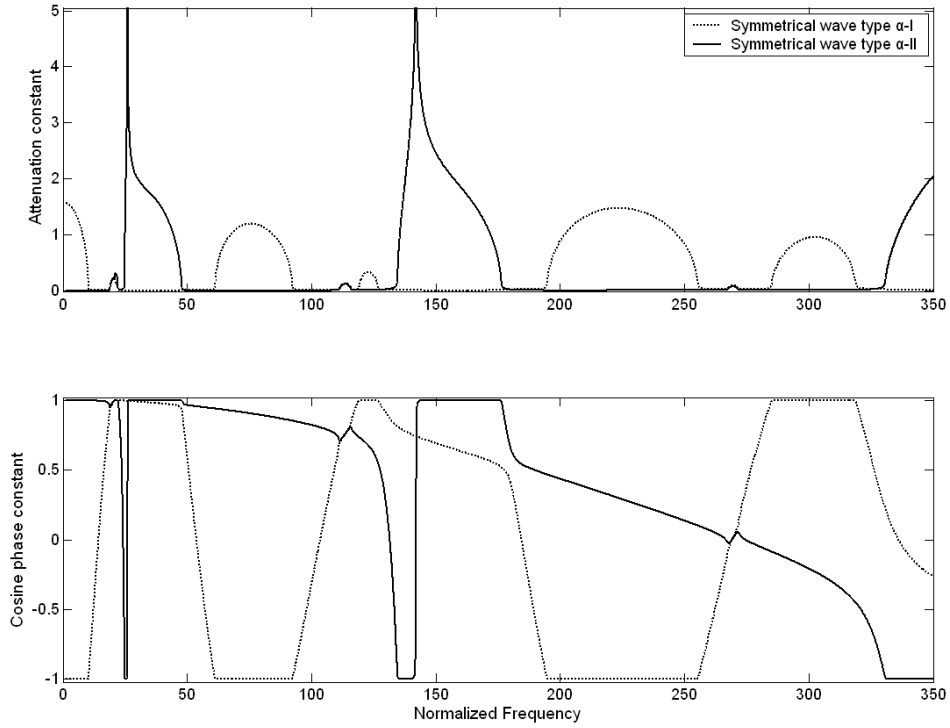
Symmetrical wave type α-I
Symmetrical wave type α-II
Attenuation constant
Cosine phase constant
Normalized Frequency

(b)

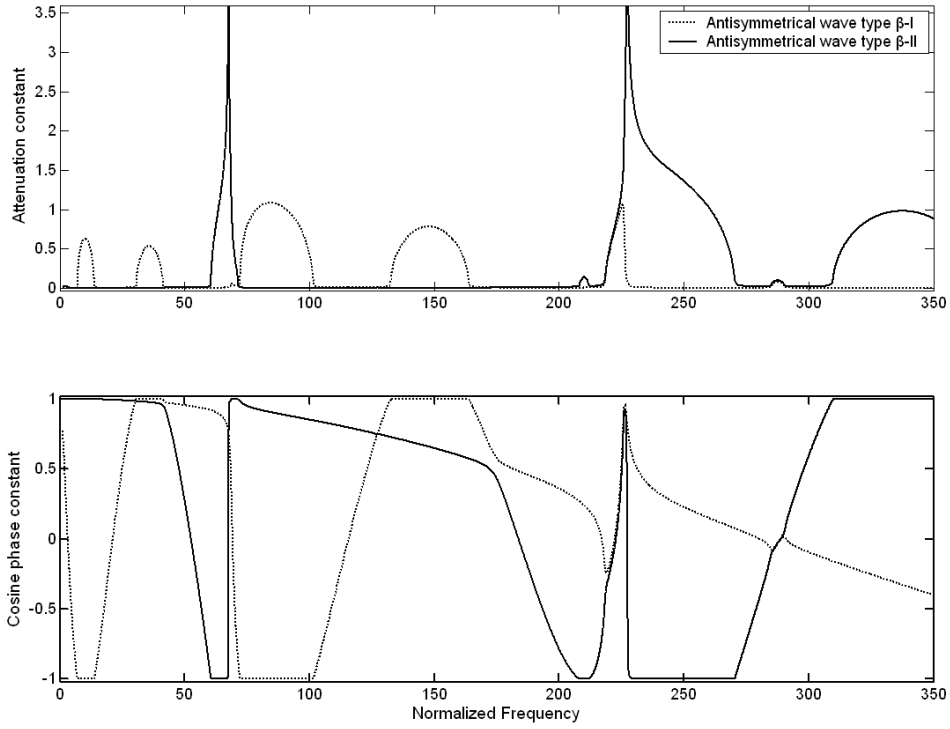
Antisymmetrical wave type β-I
Antisymmetrical wave type β-II
Attenuation constant
Cosine phase constant
Normalized Frequency

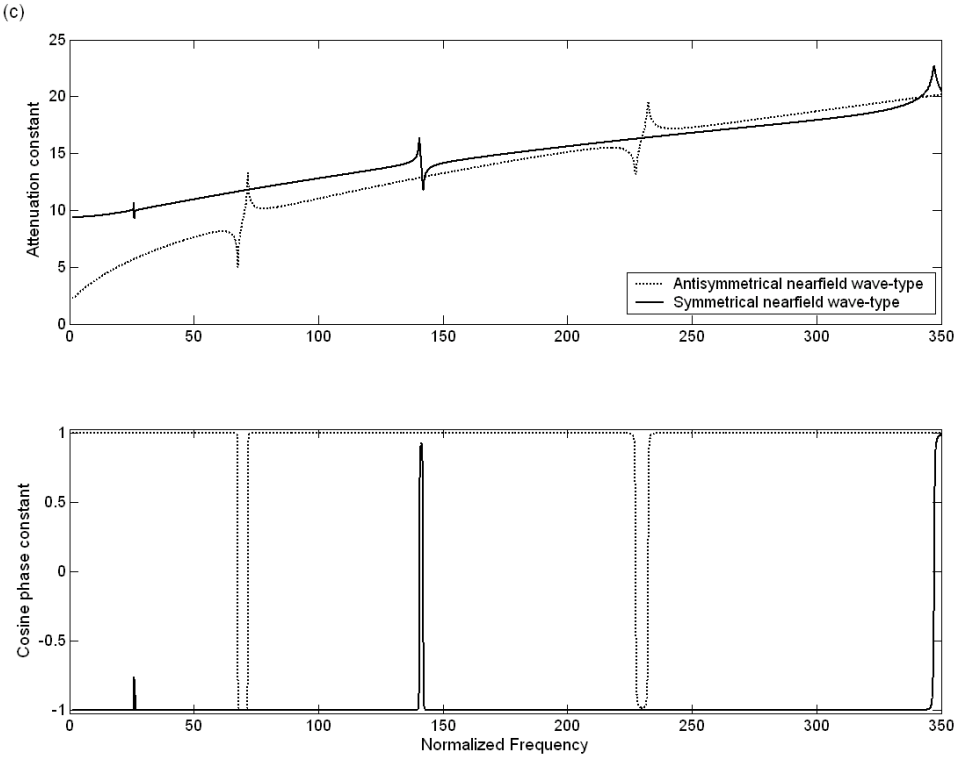

Fig. 3.2 Propagation constants of characteristic wave-types. (a) μ_R and cos(μ_I)of the symmetric flexural-longitudinal wave types: α-I and α-II; (b) μ_R and cos(μ_I)of the antisymmetric flexural-longitudinal wave types: β -I and β –II; (c) μ_R and cos(μ_I) of the symmetric and antisymmetric predominantly near-field wave types.

The computed results for the attenuation constants μ_R and cos(μ_I) for the characteristic wave types in the periodic beam structure are plotted in Figs. 3.2 (a), (b), and (c). It can be seen from Fig. 3.2(a) that the symmetric flexural-longitudinal wave motion is governed by two types: α-I and α-II. It is found that more attenuation zones belong to wave type α-I, and they fall off slowly and have broad forbidden bands. Those that belong to wave type α-II, which, for the most part, belong to the frequency region below Ω_n = 330, have pass bands, but two strong forbidden bands from nearly Ω_n = 25 to 47 and 133 to 177, where the attenuation constants of α-II fall off rapidly and have sharp peaks at around two significant symmetric resonant modes of the connecting beam branch. It should be noted that the values of cos(μ_I) are equal to 1 or -1 in most regions of the forbidden bands. As shown in Fig. 3.2(a), the two curves of cos(μ_I) for the two wave types overlap at certain normalized frequencies where the attenuation constant is non-zero. This implies that the propagation constants almost

become complex conjugates with the non-zero attenuation constant. Similarly, it can be seen from Fig. 3.2(b) that the antisymmetric flexural-longitudinal wave propagation is governed by two wave types: β-I and β-II. It is found that more attenuation zones that correspond to the forbidden bands of type β-I fall off slowly and have broad bands. Those of type β-II in most regions below $\Omega_n = 310$ have pass bands, but two significant forbidden bands from nearly 62 to 72 and 219 to 271, where the attenuation constants of β-II fall off rapidly and have two sharp peaks at around two strong antisymmetric resonant modes of the connecting beam branch.

Strong wave coupling occurs in the forbidden band gaps of the coupled longitudinal-flexural waves, as they are strongly attenuated through the periodic structure. In Fig. 3.2(c), the attenuation constants and $\cos(\mu_l)$ of the predominantly near-field wave types are plotted as symmetric and antisymmetric types. For the predominantly near-field waves, the attenuation constants are obviously larger than those for the other wave types, and all of the $\cos(\mu_l)$ values are almost equal to 1 or -1, which indicates that the energy of predominantly near-field waves decays dramatically as the waves propagate. As these two wave types are in the strong forbidden band regions, they can be ignored in the consideration of structure-borne sound transmission through a periodic structure.

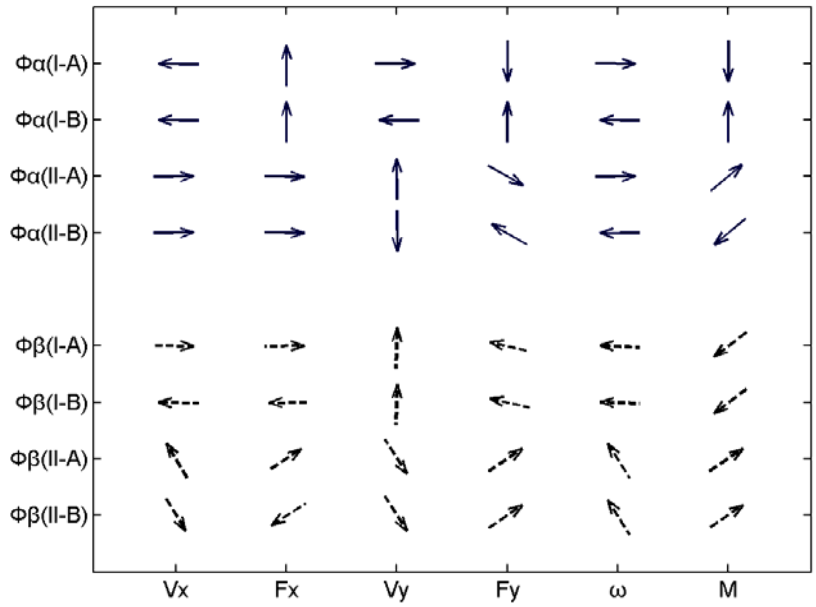

Fig. 3.3 Phase relationship of characteristic flexural-longitudinal wave vectors in normalized frequency $\Omega_n = 150$.

Fig. 3.3 shows the indicative results of the phase behavior of force-velocity vectors and further illustrates the phase relationship of the motions and actions between two beams. The phase vectors of the coupled flexural-longitudinal waves at the connection between beams A and B are chosen in the normalized frequency $\Omega_n = 150$. Remarkably, it can be observed that for symmetric wave types α-I and II, the phases of y-degree velocity V_y and rotational velocity ω of beam A are the reverse of those of beam B, and the phase of longitudinal velocity V_x of beam A is the same as that of beam B. In contrast, for antisymmetric wave types β-I and II, it is found that the phases of y-degree velocity V_y and rotational velocity ω of beam A are the same as those of beam B, whereas the phase of longitudinal velocity V_x of beam A is the reverse of that of beam B. As the frequency is chosen from the pass bands of wave types α-I and β-II, the phase vectors of their forces and moments point in different directions from their velocities and rotational velocities, which, in total, results in the positive energy flow constantly propagating along the periodic beams. However, the frequency is in the forbidden bands of wave types α-I and β-II, and almost all of the phase vectors of their forces and moments are perpendicular to the phase vectors of their velocity fields, which indicates

that the energy flow cannot continuously propagate through the periodic structure because of energy losses.

3.3.3 EXCITED MOTION AND ENERGY OF THE COUPLED WAVES IN A SEMI-INFINITE DUAL-LAYERED BEAM

In this section, the effect of wave coupling on the response of an ideal semi-infinite periodic structure to two synchronous point excitations is investigated via simulation using the analytical transfer matrix method. Two types of harmonic source excitations that synchronously act on the left side of the semi-infinite beams A and B (along the x-axis) are considered. They are defined as the standardized synchronous longitudinal (x-degree) forces of amplitude $F_{S0} = E_0 S_0$ and the synchronous moments of amplitude $M_{S0} = (E_0 I_0)/ l_0$, where I_0 is the second moment of area of the beam elements and S_0 is its cross-sectional area. The normalized force/moment levels of the propagating wave types through the first to fifth beam elements are plotted in Figs. 3.4(a) and 3.5(a) in the conditions of being excited by the longitudinal forces and moments, which are defined as $\hat{\mathrm{f}}_{in}^{j} = 20\log\left(\left|\mathbf{f}_{i,j}\right| / \left|F_{excit}\right|\right)$, where $\mathbf{f}_{i,j}$ corresponds to the normalized eigen vector ζ_{jn} satisfying the condition that $X_{FxA}^{j} = 1$ is being excited by the synchronous longitudinal forces, and $X_{MA}^{j} = 1$ is the excitation of the synchronous moments. In addition, the variations in the total flexural and longitudinal energy levels of every beam element are plotted in Figs. 3.4(b) and 3.5(b) in the forms given by

$$LE_{long} = 10\log\left[\rho_0 S_0 \left(\left|v_l^{+}\right|^2 + \left|v_l^{-}\right|^2\right) \int_{l_0} \cos^2 k_l x \cdot dx\right], \tag{3.11}$$

$$LE_{flex} = 10\log \rho_0 S_0 \left[\frac{1}{2}\left(\left|v_f^{+}\right|^2 + \left|v_f^{-}\right|^2\right) l_0 + \left|v_f^{+} v_f^{-}\right| \int_{l_0} \cos(2k_f x) \cdot dx\right] . \tag{3.12}$$

Herein the energy unit – J is suppressed because of the use of standardized excitations.

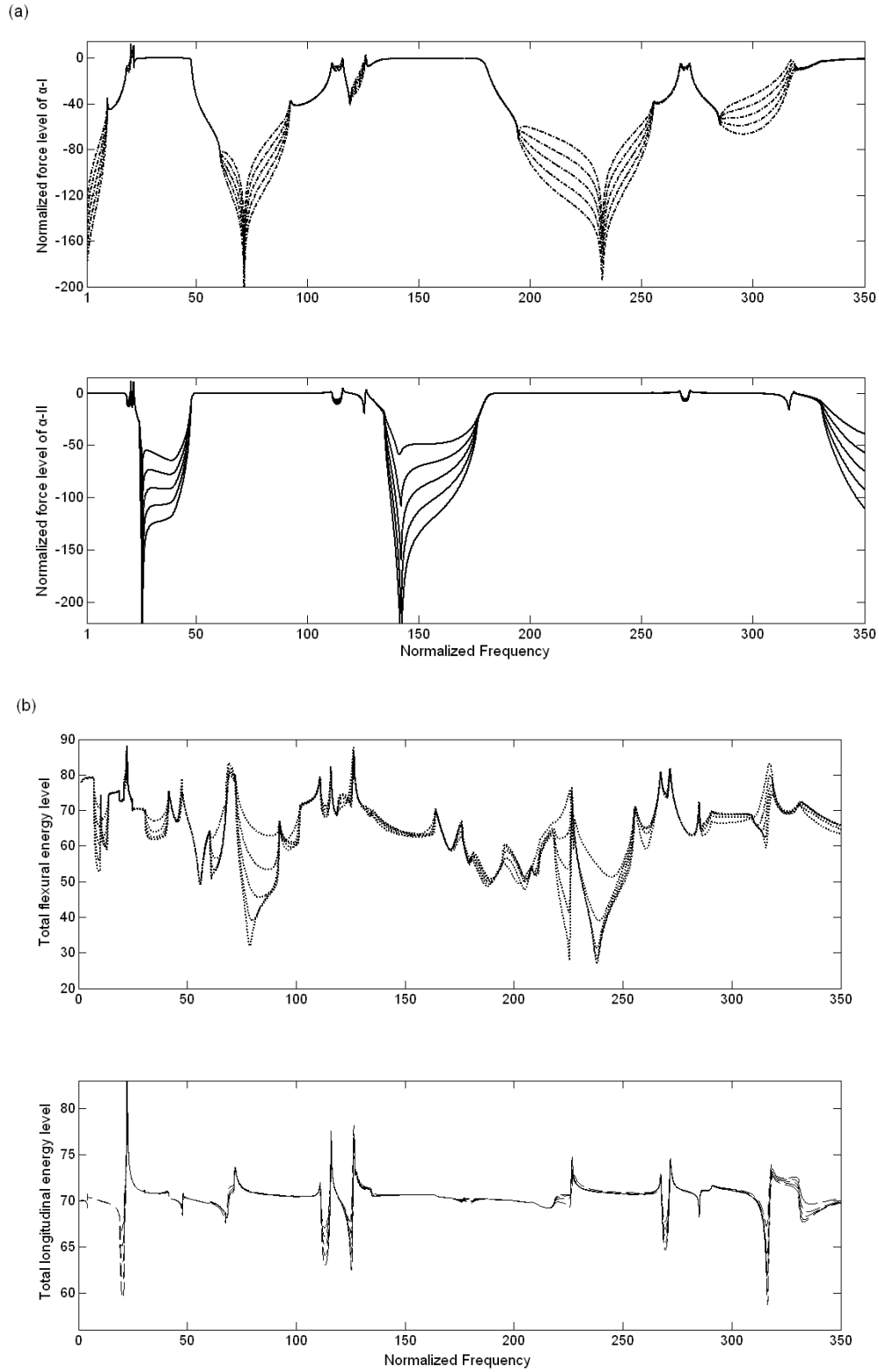

Fig. 3.4 Amplitude and energy transmission of coupled waves in response to the excitation of synchronous longitudinal forces. (a) The normalized force levels of the symmetrical wave types α-I and α-II that propagate through the first to fifth beam elements; (b) the total longitudinal and flexural energy levels of the five beam elements for synchronous longitudinal force excitation.

For a periodic structure that is being excited by the synchronous longitudinal forces F_{S0}, the normalized force levels of the symmetrical wave types α-I and α-II that

propagate through the first to fifth beam elements are plotted and shown in Fig. 3.4(a). The near-field wave types are neglected, as they decay significantly after propagating through a few elements, and the antisymmetric waves are omitted because they cannot be excited in this case. Notably, it can be seen from Fig. 3.4(a) that wave type α-I is excited at a low level and is attenuated significantly within the frequency regions of about Ω_n = 0 to 11, 65 to 90, 195 to 256, and Ω_n = 285 to 320 (which belong to the main forbidden bands of α-I) as it propagates through the structure, whereas wave type α-II is excited at a high level (i.e., the excited forces are near to the source excitation forces) and propagates through the structure without significant attenuation at those frequency regions. Similarly, wave type α-II is excited at a low level and is attenuated significantly within the frequency regions of about Ω_n = 25 to 48, 136 to 180, and Ω_n = 330 and above (which belong to the strong forbidden bands of α-II) as it propagates through the structure, whereas wave type α-I is excited at a high level and propagates through the structure without significant attenuation at those frequency regions. Fig. 3.4(b) shows the total longitudinal and flexural energy levels of the five beam elements. It should be noted from this figure that the total longitudinal energy is excited at a considerable level (near to 73), and the waves propagate through the structure without significant energy loss at most frequency regions, except for certain narrow zones that belong to the small forbidden bands of wave type α-I or α-II. Two prominent gaps in the curves of the total flexural energy level at the frequency regions that correspond to the strong forbidden bands of wave type α-I can be observed, as the total flexural energy level is mainly due to the coupling effect of the structure. On the other hand the total longitudinal energy level holds relatively steady at most frequencies, as the total longitudinal energy level is mainly due to the direct effect of the longitudinal source exciting forces. In fact, these two prominent gaps indicate that wave type α-I contributes most of the energy to the total flexural energy level, compared with wave

type α-II, at those frequency regions. This means that the energy contribution of coupled waves with respect to source excitation depends not only on the forbidden band of the wave types, but also on the energy ratios and combination of wave types.

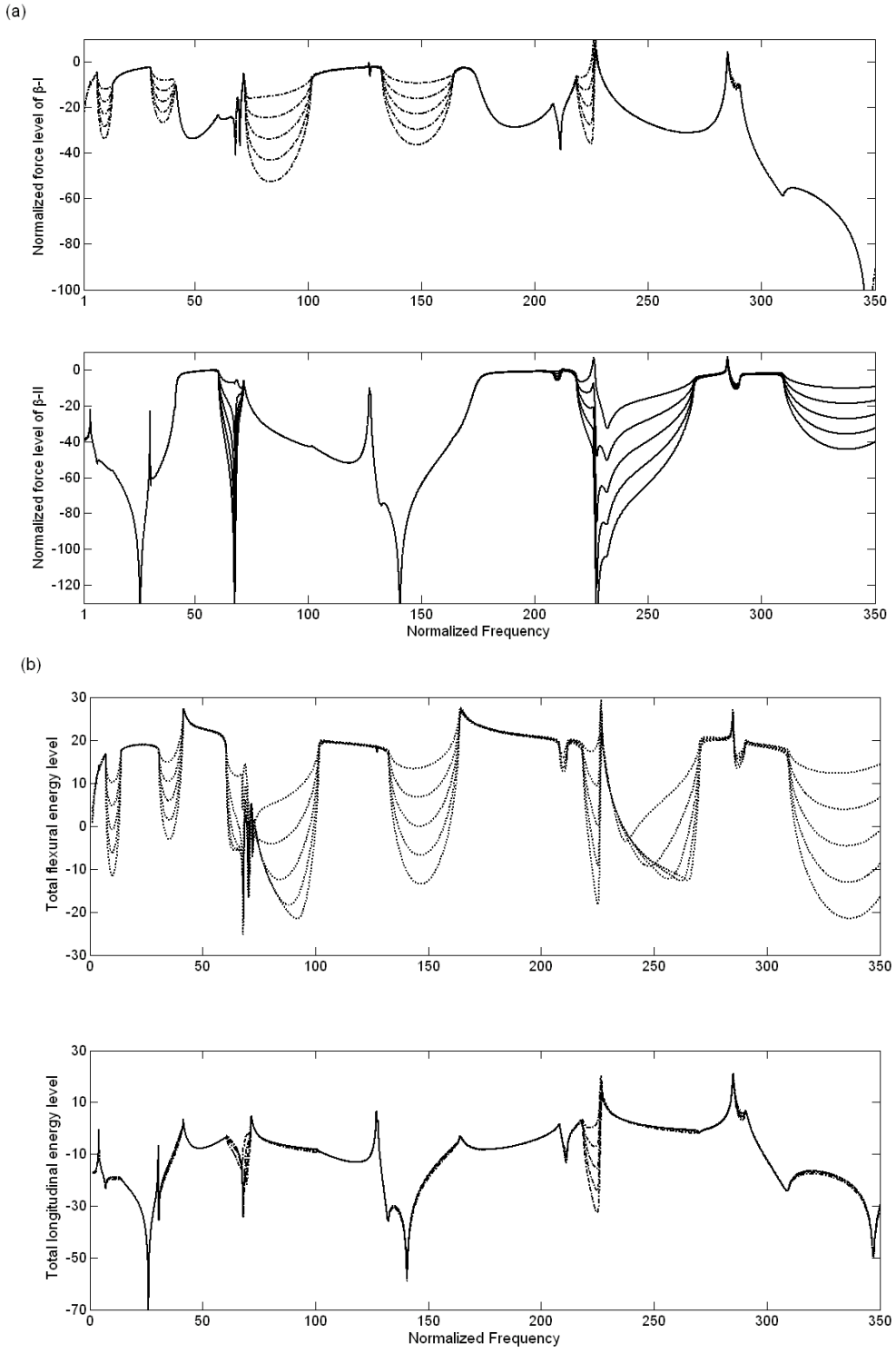

Fig. 3.5 Amplitude and energy transmission of coupled waves in response to the excitation of synchronous moments. (a) The normalized force levels of symmetrical wave types β-I and β-II that propagate through the first to fifth beam elements; (b) the total longitudinal and flexural energy levels of the five beam elements for synchronous moment excitation.

For a structure that is being excited by synchronous longitudinal forces M_{S0}, the normalized force levels of symmetrical wave types β-I and β-II that propagate through the first to fifth beam elements are plotted separately in Fig. 3.5(a). The near-field wave types and the antisymmetric waves are again neglected. Notably, it can be seen from Fig. 3.5(a) that the excited wave type β-I is excited at a low level and is attenuated significantly within the frequency regions of about Ω_f= 5 to 10, 30 to 40, 72 to 99, 132 to 164, and from 220 to 229, which belong to the main forbidden bands of β-I as it propagates through the structure. Besides, the wave type β-II is excited at a high level where the excited moments are near the source excitation moments and the wave type β-II propagates through the structure without significant attenuation at those frequency regions. Similarly, wave type β-II is excited significantly at a low level and is attenuated strongly within the frequency regions of about Ω_f= 11 to 21, 218 to 270, and Ω_f=311 and above (which belong to the strong forbidden bands of β-II) as it propagates through the structure, whereas wave type β-I is excited at a high level and propagates through the periodic structure without significant energy loss at those frequency regions. Fig. 3.5(b) shows the total longitudinal and flexural energy levels of the five beam elements for synchronous moment excitation. A comparison of the shapes of the curves of the total flexural energy level in Fig. 3.5(b) with those in Fig. 3.5(a) shows that the propagating flexural energy at frequencies approximately lower than 225 is mainly due to the transmission of wave type β-I, whereas the propagating flexural energy at frequencies approximately higher than 225 is mainly due to the transmission of wave type β-II. Fig. 3.5 again illustrates that the energy contribution of coupled waves with respect to source excitation depends on the forbidden band of the wave types and on the energy ratios and combination of wave types.

3.4 SUMMARY

A theoretical model based on a multi-coupling wave transfer matrix has been developed to study the phenomena of the coupled flexural-longitudinal wave motions that propagate in a tri-coupling dual-layered periodic beam structure. A lightly damped semi-infinite structure that consists of two equally thin semi-infinite beams connected with resonant branches has been numerically analyzed. The connection branches are the beams perpendicularly connected at regular intervals. This type of waveguide can simulate a one- to two-dimensional model of a column-beam frame for modern steel-concrete buildings or bridges simply. The computed results of the complex propagation constants that govern the transmission of wave types in periodic structures have clearly revealed the characteristics of pass and forbidden bands and the wave-coupling phenomena. It is found that there are six characteristic coupled wave types that propagate through such a structure, and these can be divided into symmetric and antisymmetric groups of flexural-longitudinal and predominantly near-field characteristic wave types. Their properties under different excitations are quantified from the computed transmission of the normalized amplitudes of the coupled wave types together with the maximum flexural and longitudinal energies along the wave-carrying components. It has been revealed that the structure-borne sound energy from the synchronous longitudinal excitations at two beams mainly propagate through the periodic structure in the form of one or two types of symmetric characteristic coupled flexural-longitudinal waves. In contrast, the structure-borne sound energy from the synchronous rotational sources that excite dual-channel beams mainly propagate along the periodic structure in the form of one or two types of antisymmetric characteristic coupled flexural-longitudinal waves. These results demonstrate that the energy contribution of coupled waves with respect to source excitation depends on the

forbidden band of the wave types and on the energy ratios and combination of wave types.

CHAPTER 4. EXPERIMENTAL STUDY OF VIBRATION TRANSMISSION THROUGH A FINITE COUPLING DUAL-LAYERED BEAM STRUCTURE

4.1 INTRODUCTION OF THE FUNDAMENTAL RESEARCH WORKS

To be able to predict the propagation of structure-borne sound through such structures, it is essential to know how to model the built-up structure to describe correctly the characteristics associated with the wave propagation. This is the case when statistical descriptions of the vibration field are applied [67], as well as when applying analytical descriptions [68, 69]. For analytical solutions, the most common approaches are the wave approach [52, 53] and transfer matrix method [70, 71]. It was showed that the bounding frequencies of wave propagation zones of a periodic system can be determined from element receptance matrices of the system [52, 53]. The propagation wave approach associated with the development of the Bloch wave theorem in solid state physics [72], can be applied most efficiently to infinite or semi-infinite periodic systems. On the other hand, the transfer matrix method provides a more convenient approach to the analysis of finite periodic structures where boundary conditions can be incorporated into the transfer matrix with ease. Other methods, such as Z-transform method [73], and Fourier transform method [74] had also been developed. Furthermore, an analytical solution was provided to predict wave propagation in infinite periodic supported beams and infinite periodic plates by using phased array receptance functions [75].

Most of the past research work on the coupling of wave motions is concerned with models of a single-layered structure made of independent structural coupling connections, and few studies have been conducted on the energy transmission of

coupled acoustic waves in multi-layer structures. The theoretical study [76] reported in the last chapter therefore investigated the fundamental characteristics of the multi-coupling flexural and longitudinal wave motions that propagate in an infinite structural coupling dual-layered beam with connection branches. The characteristics of a semi two-dimensional beam structure is considered because the coupling interaction between the waves at the connections and transmission paths through a three-dimensional structure is so complicated that the analytical predictions based on the series of approximations required can be very different from the experimental set up.

4.2 THEORETICAL MODEL OF A FINITE DUAL-LAYERED BEAM

4.2.1 FUNDAMENTALS FOR THE PERIODIC COUPLING DUAL-LAYERED BEAM STRUCTURE

A simplified model of a dual-layer beam structure that is periodically connected with transverse branches is shown in Fig. 4.1. The propagating longitudinal waves and flexural waves in two horizontal beams— A and B are coupled at two sides of each junction j= 1…N with connection branches C_j. The beams and branches analyzed in the theoretical model are even, straight, isotropic, and homogeneous, and the following physical parameters are assumed: $\rho_1 = \rho_2$ is the density of beams A and B and ρ_3 is the density of branch C, $B_{s1} = B_{s2}$ is the bending stiffness of beams A and B and B_{s3} is the bending stiffness of C, $E_1 = E_2$ is the Young's modulus of beams A and B and E_3 is the modulus of branch C, $k_{f1} = k_{f2}$ is the flexural wave number in beams A and B and k_{f3} is the flexural wave number in branch C, $k_{l1} = k_{l2}$ is the longitudinal wave number in beams A and B corresponding to the longitudinal wave speed c_1, and k_{l3} is the longitudinal wave number in branch C corresponding to the longitudinal wave speed c_3.

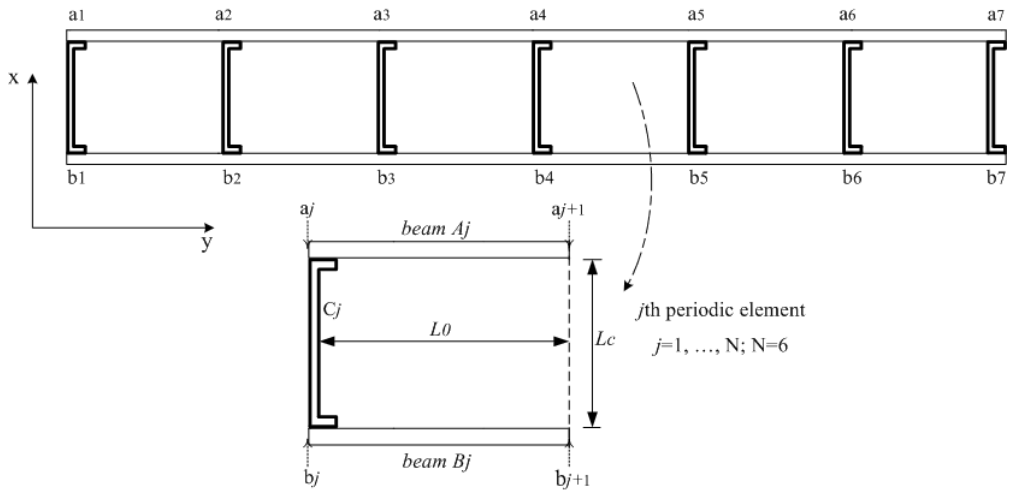

Fig. 4.1 Diagram and dimensional parameters of the finite periodic coupling dual-layered beam used in the research.

4.2.2 COUPLED WAVE MOTION AND MOBILITY OF A FINITE DUAL-LAYERED BEAM

In every dual-layer beam part between the connection branches of the periodic structure shown in Fig. 4.1, the propagation of longitudinal-flexural waves can be expressed as a transfer matrix of velocity (horizontal, vertical, and rotational) and force (horizontal, vertical, and moment) vectors, (all of the analytical equations herein are based on a harmonic wave with frequency ω_n with time dependence suppressed), as follows.

$$\begin{bmatrix} \mathrm{V}_{ab} \\ \mathrm{F}_{ab} \end{bmatrix}_{(j+1)^-} = [\Gamma_0] \begin{bmatrix} \mathrm{V}_{ab} \\ \mathrm{F}_{ab} \end{bmatrix}_{j^+} \tag{4.1}$$

$$[\mathrm{V}_{ab}] = [V_{ya} \;\; V_{yb} \;\; \omega_a \;\; \omega_b \;\; V_{xa} \;\; V_{xb}]^{\mathrm{T}}, \quad [\mathrm{F}_{ab}] = [F_{ya} \;\; F_{yb} \;\; M_a \;\; M_b \;\; F_{xa} \;\; F_{xb}]^{\mathrm{T}}$$

where the subscripts j^- and j^+ of the velocity $[\mathrm{V}_{ab}]$ vector and the force vector $[\mathrm{F}_{ab}]$ denote the position on the left and right side of a_j and b_j (the connection points on beams A-B with C_j), and $(j+1)^-$ is defined as the right end of jth beam element. Based on the theory of structure-borne sound waves [74], the transfer matrix for the propagation of uncoupled longitudinal and flexural waves in the parallel dual beam part

can be derived by

$$[\Gamma_0] = [S_{VF}][P_{wv}][S_{VF}]^{-1} \tag{4.2}$$

where the transfer matrices for coupled wave transmission are the same as the terms of the equations in Chapter 4. Thus, the entire periodic transfer matrix of the coupling wave transmission can be given by

$$\begin{bmatrix} \mathrm{V}_{ab} \\ \mathrm{F}_{ab} \end{bmatrix}_{(j+1)^-} = [U_e] \begin{bmatrix} \mathrm{V}_{ab} \\ \mathrm{F}_{ab} \end{bmatrix}_{j^-} \tag{4.3}$$

$$[U_e] = [W_{\mathrm{C}}] \times [\Gamma_0]$$

According to the Bloch wave in an acoustic system, when the coupled waves are propagating one-directionally through an infinite periodic structure, the relationship between the velocities and forces in two adjacent periodic elements can be expressed as:

$$[\mathrm{V}_{ab}]_{j^-} = [\xi_n][\mathrm{v}_n]_j \ , \ [\mathrm{F}_{ab}]_{j^-} = [\zeta_n][\mathrm{f}_n]_j \ \ , \ \ n = 1 \ldots 12 \tag{4.4}$$

$$\begin{bmatrix} \mathrm{v}_n \\ \mathrm{f}_n \end{bmatrix}_{j+1} = e^{\mu_n} \begin{bmatrix} \mathrm{v}_n \\ \mathrm{f}_n \end{bmatrix}_j \tag{4.5}$$

This represents a problem on the eigen-value vector for the transfer matrix $[U_e]$, where $\mu_n = \pm(\mu_{\mathrm{R}} + j \cdot \mu_{\mathrm{I}})_k$, k = 1...6, is the kth pair of eigen values — the complex propagation constants, and correspondingly the 6 pairs of eigen vectors are the characteristic wave types, which take on the normalized form

$$[\xi_n] = \left[1, X_{Vxb}^{(n)}, X_{\omega a}^{(n)}, X_{\omega b}^{(n)}, X_{Vya}^{(n)}, X_{Vyb}^{(n)}\right]^{\mathrm{T}}$$

$$[\zeta_n] = \left[1, X_{Fxb}^{(n)}, X_{Ma}^{(n)}, X_{Mb}^{(n)}, X_{Fya}^{(n)}, X_{Fyb}^{(n)}\right]^{\mathrm{T}}.$$

As the "attenuation constant" of the coupled wave type, the real part μ_{R} expresses the exponential decay rate of the characteristic wave type that propagates through a periodic beam element, whereas the imaginary part μ_{I} is defined as the "phase

constant," which describes the phase transfer of the characteristic wave type that propagates through each element. The propagation constants of the 6 positive-going wave types are defined as $-(\mu_R+\mu_I)_k$, in which the real and imaginary parts of the propagation constants ought to be positive. Ideally, where the damping factor of the beam structure is negligible, a characteristic wave type at any given frequency within a pass band yields up a pair of pure imaginary propagation constants. Of these, $\mu_n = -j\cdot\mu_{Ik}$ is the positive-going propagation constant and $+\mu_{Ik}$ is that of the negative-going wave type. In the forbidden band, the larger value of the real part μ_{Rk} means the stronger attenuation of the corresponding wave-type transmission in the periodic structure.

Engineering structures are usually made of several periodic elements. This means that reflections resulting from the boundaries cannot be neglected, and the periodic structure should be treated as a finite element number. The input mobility matrix of the left subsystem from jth element can be expressed as

$$[Y_{nn}]_j = [Y_{nn}]_{jR}\left(I + [Y_{nn}]_{jR}^{-1}[Y_{nn}]_{jL}\right)^{-1} \tag{4.6}$$

Then the solution of those mobility matrices can be implemented numerically for the finite periodic structure.

4.3. EXPERIMENT AND ANALYSIS OF VIBRATIONAL MOTION AND ENERGY TRANSMISSION IN A FINITE DUAL-LAYERED BEAM

4.3.1 CONDITIONS AND SETTINGS OF EXPERIMENT

The dimensions and physical parameters of the finite periodic structure were designed to allow comparisons of the results of the theoretical model with that of the experiment. The numerical calculations based on the theoretical model were conducted using MATLAB. The material of the two equal beam layers A and B is aluminum alloy, for which the Young's modulus is $E_{1,2} = 5.05 \times 10^{10}$ N/m^2 with an assumed loss factor $\eta_{1,2} = 0.01$ and density $\rho_{1,2} = 3220$ kg/m^3. The dimensions of the two equal beams with a rectangular cross-section are periodic element length $L_0 = 50$ mm, so its total length is 3.0 m, thickness $h_0 = 6.0$ mm, and width $d_0 = 38.1$ mm. The material of the connection branch is steel, for which the Young's modulus is $E_3 = 1.15 \times 10^{11}$ N/m^2 with assumed loss factor $\eta_3 = 0.011$ and density $\rho_3 = 7690$ kg/m.^{3} The dimensions of the branch are thickness $h_c = 1.54$ mm, width $d_c = 38.2$ mm, and length of its vertical beam component $L_c = 320$ mm. The attaching part on two sides of the connection branch, which has the same cross-section but a short length $l_s = 9.0$ mm, is perpendicular to the vertical part of the branch. The attaching part of the connection branch is fixed on a horizontal beam layer by two steel screws with nuts of a diameter of 4 mm. The total number of periodic elements of this finite periodic structure is six (j = 1,...,N and N = 6). The end terminations of this periodic structure are also modeled as the mobility matrix $[Y_C]$ of the same connection branch at the right boundary.

In the experiment, the dual-layer periodic beam structure was suspended on elastic strings so that it could ideally vibrate freely in all degrees (the model shown in Fig. 4.2). The structure was longitudinally excited at the left boundary of beam B by an electro-dynamic vibration exciter (LING Dynamic System Type V403), which was

driven by an amplifier (LING Dynamic PA300) that was fed with white noise. A force transducer (PCB ICP F-sensor) was set to measure the exciting force, and the vibrational responses of the beam structure were measured by two accelerometers (B&K Type 4394). The data acquisition and analysis were conducted with NI equipment (RIO-9233 and PXI-8187) using the LabVIEW program.

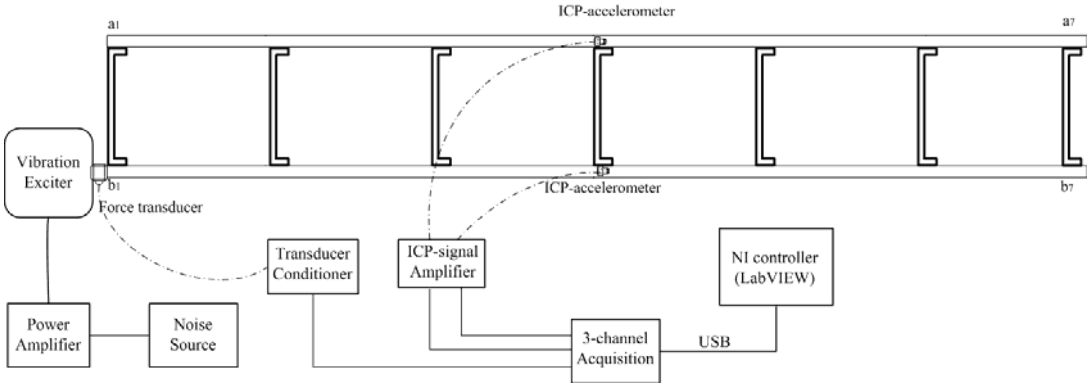

Fig. 4.2 Diagram of the settings of the dual-layered beam and measuring equipments.

4.3.2 TRANSFER MOBILITY UNDER A LONGITUDINAL FORCE EXCITATION

Being excited by the longitudinal force F_0 at the left boundary (near the first junction b_1) of the lower beam B, the experimental results of the longitudinal point and uni-layer transfer mobilities at the junctions, defined as $Y_{lx,bi} = V_{x,bj}/F_0$, are investigated in this section. The calculated and experimental results of the absolute value of $Y_{lx,bi}$ at the junctions $b1$, $b3$, $b5$, and $b7$ on beam B are shown in Figs. 4.3 (a)-(d) respectively.

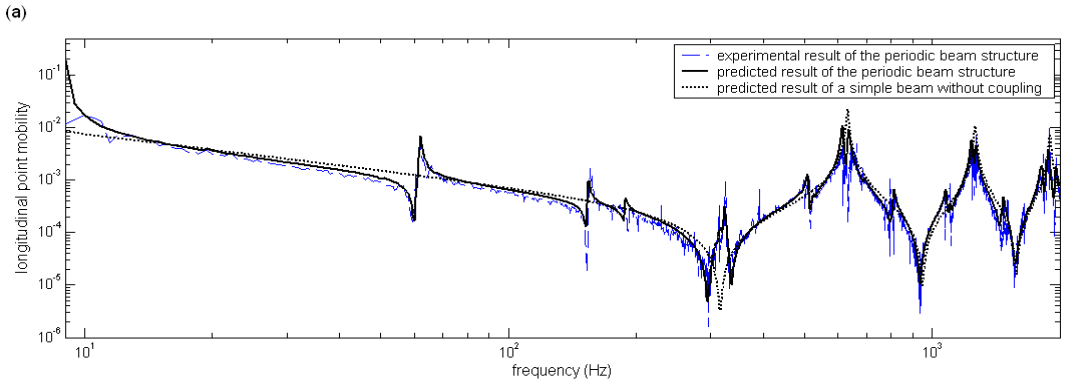

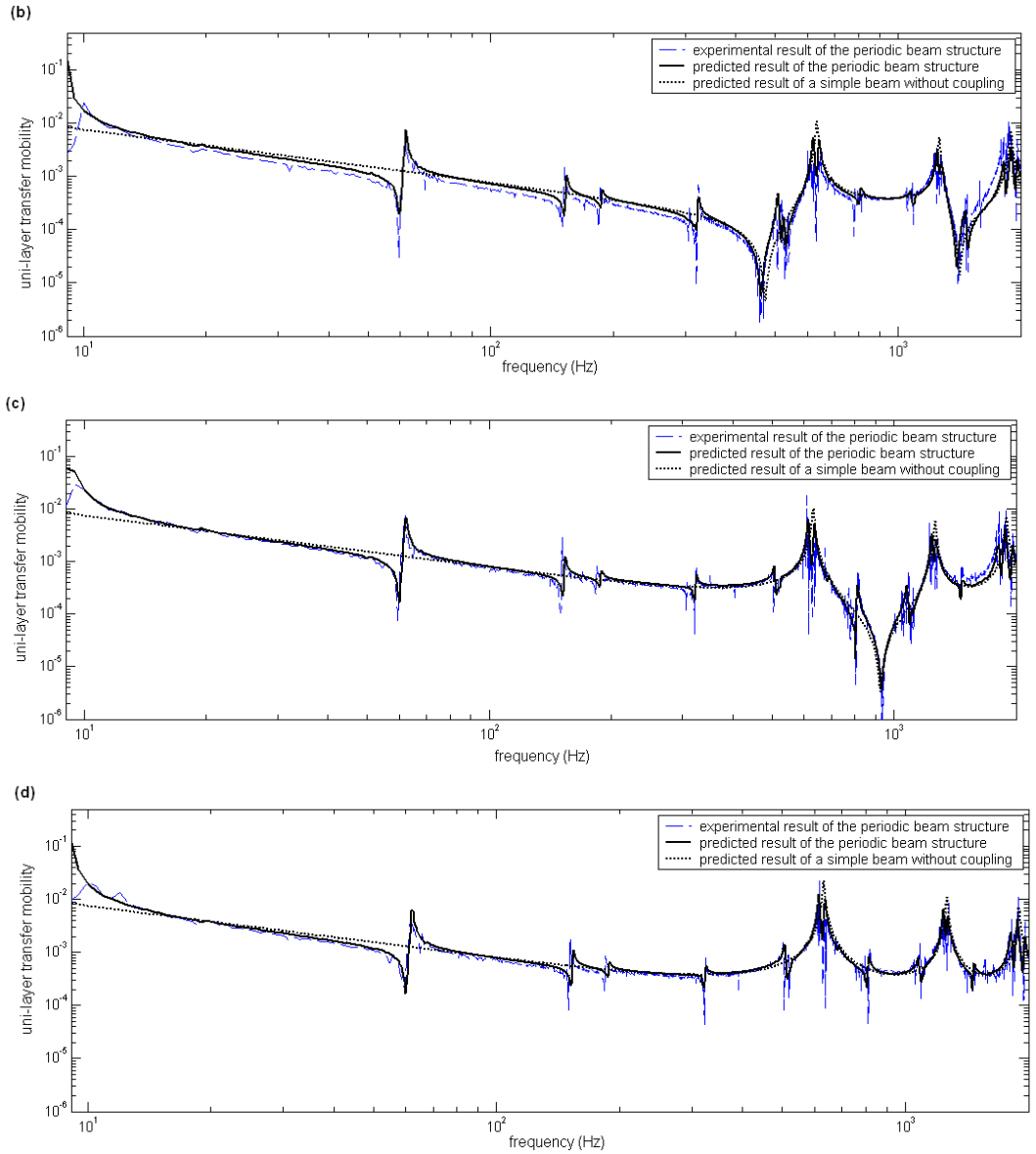

Fig. 4.3 Absolute values of the predicted and measured longitudinal uni-layer point and transfer mobilities at the b1, b3, b5, and b7 junctions on beam B. (a) Point mobility at *b*1; (b) transfer mobility at *b*3; (c) transfer mobility at *b*5; (d) transfer mobility at *b*7.

It can be observed that the predicted mobilities for the periodic beam structure agree well with the measured results. The derived theoretical model is therefore reliable and can be used to study the coupled wave transmission in the uni-layer of the periodic beam structure. Comparing with the predicted mobilities for the same positions of the same beam without the coupling connections, it can be seen in Fig. 4.3 that the uni-layer mobility curves of the coupling beam structure are similar to those of the single beam without coupling connection at most frequencies, though there are some

fluctuations at some frequencies. Notably, it can be seen from Figs. 4.3 (a)-(d) that at frequencies around 615, 1240, and 1870 Hz, three major peaks of the mobility curves for all junctions on beam B of the periodic beam structure are almost the same as the peaks for the corresponding positions on the single beam, which are at the longitudinal resonant modes of the finite single beam. Furthermore, unlike the mobility curves of the single beam, the point and uni-layer transfer mobility curves of the periodic coupling beam have some minor peaks at frequencies around 61, 104, 109, 121, 140, 800, 1020, and 1050 Hz, which mainly result from the flexural resonance of the connection branches. The amplitudes of these minor peaks are different for the different junctions but they occur at the same frequencies. Moreover, it is noted that for the point and transfer mobilities at the junctions of the periodic beam structure, the major peaks at around 615 and 1240 Hz are decomposed into two sub-peaks, which is due to the co-resonance effect of the coupling connection branches. The coupling effect resulting from the flexural motion of branches becomes stronger as the frequency increases so that the region of the main peak around 1870 Hz is decomposed into three sub-peaks.

4.3.3 THE CROSS-LAYER TRANSFER MOBILITY UNDER LONGITUDINAL FORCE EXCITATION

With the same excitation condition of the longitudinal force F_0, the experimental results of the longitudinal cross-layer transfer mobility, defined as $Y_{lx,ai} = V_{xaj}/F_0$, are investigated in this section. The calculated and experimental results of the absolute value of $Y_{lx,bi}$ at the junctions a1, a3, a5, and a7 on beam B are plotted in Figs. 4.4 (a)-(d) respectively.

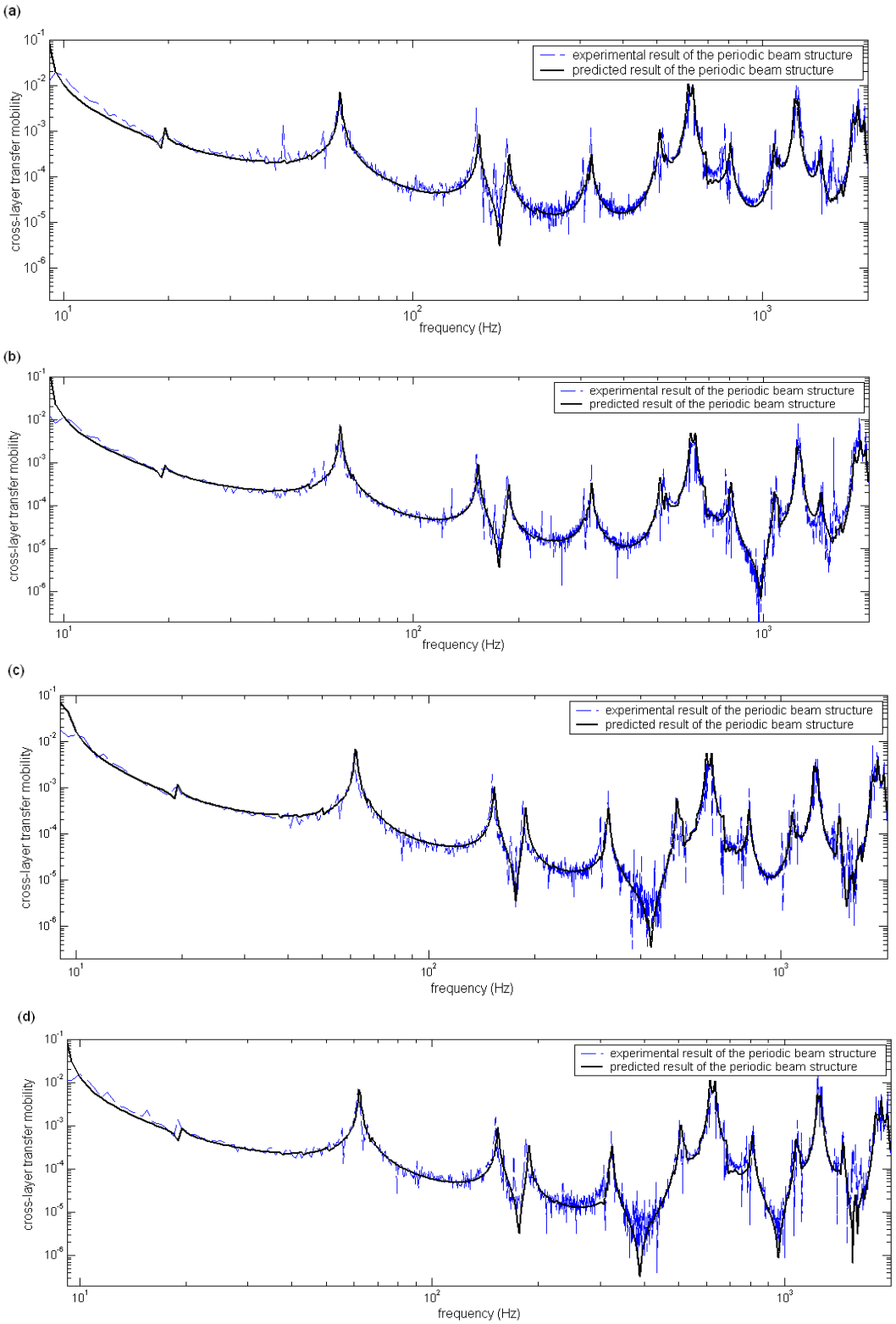

Fig. 4.4 Absolute values of the longitudinal cross-layer transfer mobility at the junctions on beam A. (a) Transfer mobility at a1; (b) transfer mobility at a3; (c) transfer mobility at a5; (d) transfer mobility at a7.

It can be seen from the figures that there is a general agreement between the curves of the predicted mobility and the measured mobility, especially for the peak frequency

regions that are of engineering interest. However, there are some deviations in some trough regions at relatively high frequencies because there are errors between the ideal coupling factors derived from lumped parameters in the theoretical model and the real frequency-dependent factors in the experiment. The derived theoretical model is therefore reliable and can be used to study the coupled wave transmission in the cross-layer of the periodic beam structure.

By comparing the results plotted in Figs. 4.4 with those in Figs. 4.3, it can be observed that the major peaks of the cross-layer transfer mobility curves are the same as those of the uni-layer mobility curves at the frequencies around 615, 1240, and 1870 Hz, and the minor peaks of the cross-layer mobility curves are the same as those of the uni-layer mobility curves at the frequencies around 61, 104, 109, 121, 140, 800, 1020, and 1050 Hz. The fluctuating amplitudes of the peaks of the cross-layer transfer mobilities are similar for all junctions of the periodic beam structure. In addition, most of the minor peaks of the cross-layer transfer mobility curves are larger than those of the uni-layer transfer mobility curves at the same frequencies. It can be understood that the longitudinal-flexural motion of beam A is due to the cross-layer transmission from the coupling connection branches. Moreover, the major peaks of the cross-layer transfer mobilities at frequencies around 615 and 1240 Hz are divided into two sub-peaks, and the major peaks of the cross-layer transfer mobilities at a frequency around 1870 Hz are divided into three sub-peaks with a broader frequency band.

4.3.4. THE CROSS-LAYER ENERGY TRANSMISSION

In this section, the effect of wave coupling on the cross-layer transmission of vibrational energy in the finite periodic structure is investigated using the transfer matrix method developed for the model. A standard longitudinal excitation acting on

the left side of b_1, which is defined as the normalized force $F_{S0} = E_0 S_0$, has been applied to study the levels of energy transmission of the coupled waves from the source through the junctions of periodic structure to the upper layer beam A. The levels of the cross-layer transmitted longitudinal $10\log\left(\mathrm{E}_{l(pot)} + \mathrm{E}_{l(kin)}\right)$ and the level of flexural energy density $10\log\left(\mathrm{E}_{f(pot)} + \mathrm{E}_{f(kin)}\right)$ at the beam junctions are plotted in Figs. 4.5, where $\mathrm{E}_{l(pot)}$ and $\mathrm{E}_{l(kin)}$ are the longitudinal potential and kinetic energy densities respectively, and $\mathrm{E}_{f(pot)}$ and $\mathrm{E}_{f(kin)}$ are the flexural potential and kinetic energy densities respectively.

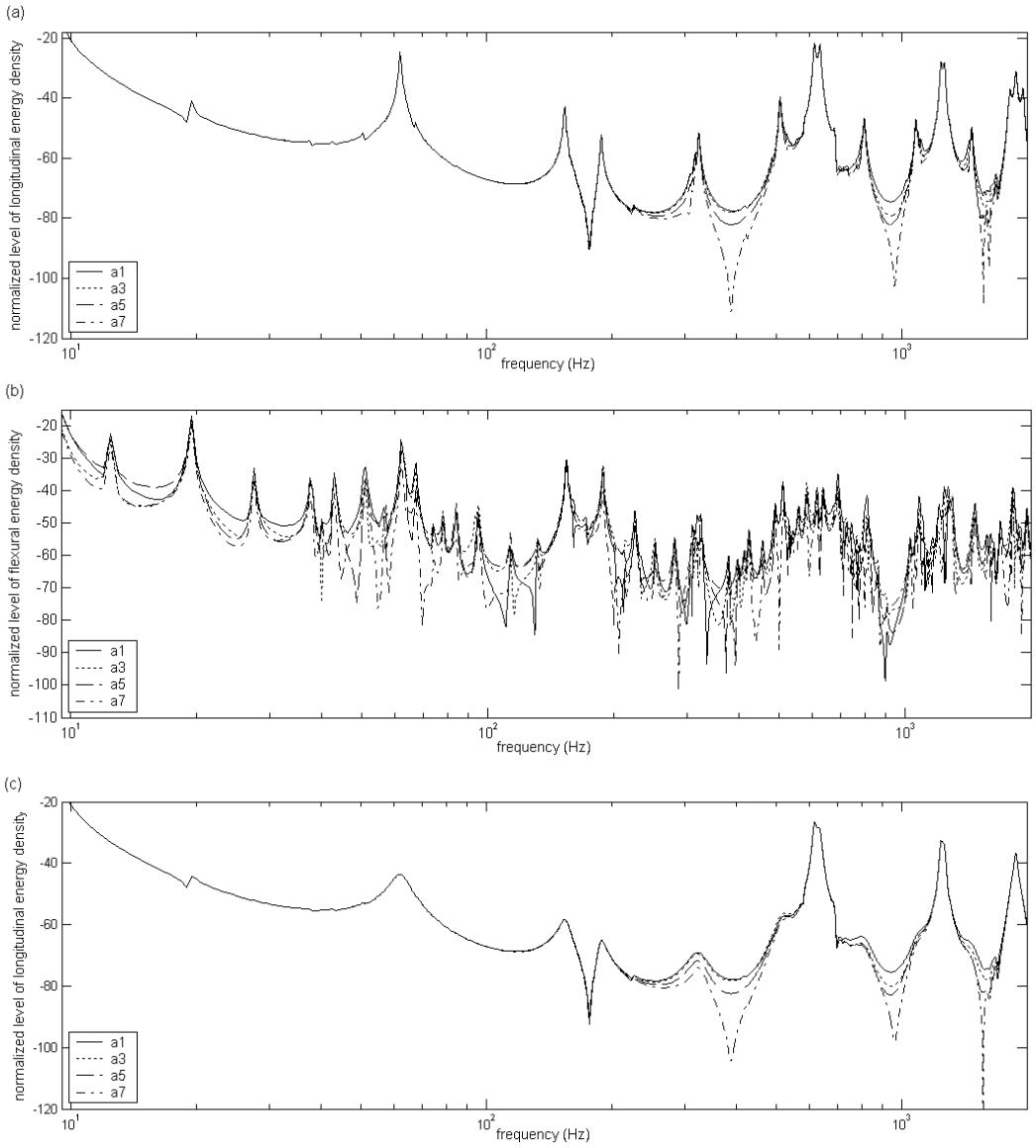

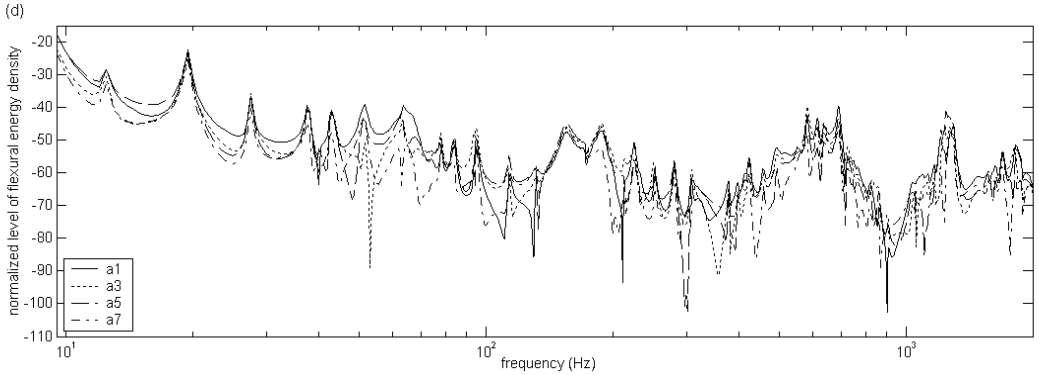

Fig. 4.5 Normalized levels of the longitudinal and flexural energy density at the cross-layer junctions from a1 to a7, excited by a longitudinal force, for different η_3. (a) longitudinal energy density at the cross-layer junctions, $\eta_3 = 0.011$; (b) flexural energy density at the cross-layer junctions, $\eta_3 = 0.011$; (c) longitudinal energy density at the cross-layer junctions, $\eta_3 = 0.1$; (d) flexural energy density at the cross-layer junctions, $\eta_3 = 0.1$.

It can be seen in Fig. 4.5(a) that the levels of the longitudinal energy transmitted to the cross-layer of the beam structure are generally proportional to the longitudinal cross-layer transfer mobilities on beam A. It can also be seen that due to the wave coupling at the junctions, the longitudinal energy transmitted from the branches to the cross-layer of the finite periodic structure is most significant at the longitudinal resonant modes of the finite beam (the major peaks), and is also prominent at the flexural resonant modes of the connection branches (the minor peaks). Fig. 4.5(a) shows that the curves of the normalized level of longitudinal energy density at different junctions (a1, a2, a5, and a7) overlap at most frequencies, though there are exceptions at some gap frequency regions. This implies that the cross-layer transmitted longitudinal energy propagates through the periodic structure without significant attenuation at most frequencies, though not at those gap frequency regions. It can be seen in Fig. 4.5(b) that the cross-layer transmitted flexural energy resulting from wave coupling is comparable to the cross-layer transmitted longitudinal energy. Apart from the peaks occurring at around the same frequency regions as those major peaks of the cross-layer transmitted longitudinal energy, a number of relatively small peaks can be

observed that resulted from the flexural resonance of the finite beam. No major peaks occur in the curves of the normalized level of flexural energy density. Fig. 4.5(b) shows that owing to the strong wave coupling at some resonance modes of the connection branch, such as around 20, 155, and 195 Hz, the cross-layer transmitted flexural energy is even larger than the cross-layer transmitted longitudinal energy. To investigate the effect of the damping of the connection branches on the cross-layer energy transmission, the levels of the cross-layer transmitted longitudinal and flexural energy are plotted in Figs. 4.5(c) and 4.5(d) correspondingly for the increase of the loss factor to $\eta_3 = 0.1$. It is observed that increasing the damping of the connection branch can only attenuate some peaks of the cross-layer transmitted energy at the flexural modes of the branch but cannot attenuate the peaks of the longitudinal resonance modes of the finite beams. This means that the cross-layer transmitted energy from wave coupling is mainly dominated by the modes of the finite beam rather than the modes of the connection branch. Changing the damping of branches, therefore, cannot control the structure-borne sound transmitted to the cross-layer in the major frequency regions.

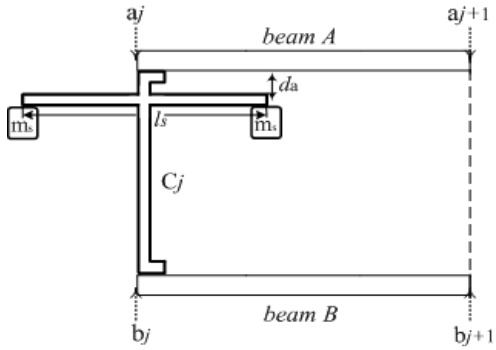

Fig. 4.6 The structure of periodic beam element with the attached cantilever on the connection branch.

A method designed to control the cross-layer transmission of vibration is shown in Fig. 4.6. A cantilever with symmetric mass at two boundaries is attached on the branch of every periodic element, in which the parameters used are width $d_c = 38.2$ mm, length $l_s = 0.38$ m, thickness $h_s = 1.4\ h_c$, and $m_s = 0.3$ kg. The corresponding levels of the

cross-layer transmitted longitudinal and flexural energy density are plotted in Figs. 4.7 (a) and(b).

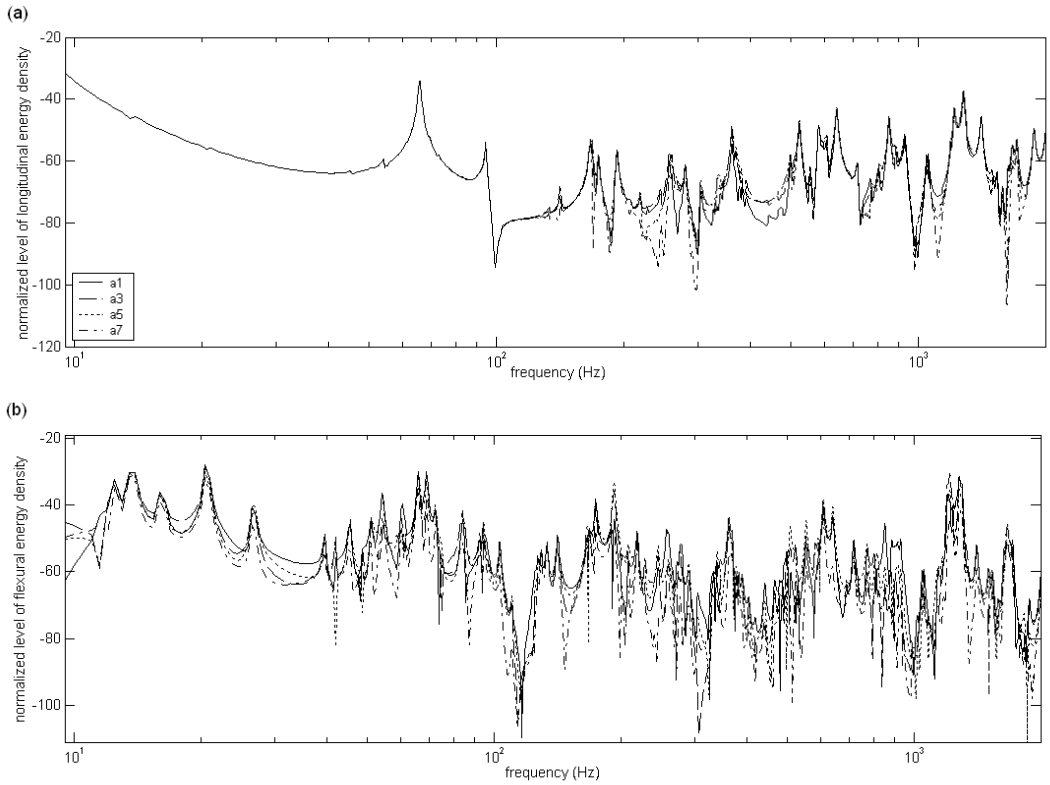

Fig. 4.7 Normalized levels of the longitudinal and flexural energy density of beam A at the junctions from a1 to a7, excited by a longitudinal force, in the condition of $\eta_3 = 0.011$, and the parameters of the attached cantilevers are $l_s = 0.38$m, $h_s = 1.4\ h_c$, and $m_s = 0.3$kg. (a) The normalized levels of longitudinal energy density at the cross-layer junctions with the attached cantilevers; (b) the normalized levels of flexural energy density at the cross-layer junctions.

In comparison with Figs. 4.5 (a) and (b), it can be observed in Figs. 4.7 (a) and (b) that the cross-layer transmitted longitudinal energy in the regions of major peaks around 615 and 1870 Hz can be significantly attenuated by the proposed method. The cross-layer vibration motions from coupled waves in the branches are significantly controlled by the attached cantilevers with mass at the resonance modes. This method can therefore be used to control the structure-borne sound transmission in multi-layer beam structures.

4.4 SUMMARY

In this chapter, the model based on a coupling transfer matrix method of longitudinal-flexural wave has been developed to study the dynamic characteristics of the longitudinal-flexural motions and energy transmission in a finite dual-layered beam structure. Based on the analytical equations of the model, numerical calculation is performed to predict the coupled wave motion excited by a longitudinal force in a finite periodic structure and the predicted results are compared with the experimental results. In the experiment, a lightly damped finite structure consisted of two equally thin beams with multiple resonant branches in the form of thin beams that were connected perpendicularly at regular intervals. The numerical results from the theoretical model generally agree well with the experimental results at the frequencies from 10 to 2000 Hz, which suggests that the developed model and solution method for a finite periodic coupling beam structure can be useful in most of the middle-low frequency region. Further, the cross-layer energy transmission of the coupled waves in the finite periodic dual-layered beam is then calculated and analyzed by using the verified model. The results reveal that the longitudinal energy transmitted in the cross-layer of finite periodic structure is enhanced not only at the longitudinal resonant modes but also the flexural resonant modes of the finite beam of connection branches due to the wave coupling of the structure. It is shown that the damping factor of the coupling connection could obviously influence most peaks of cross-layer transmitted energy of the coupled wave at the flexural resonant modes of connection branches, which suggests that some structure-borne sound control methods based on this model may be applied on the dual-layered beam structures.

CHAPTER 5. STRUCTURE-BORNE SOUND POWER TRANSMISSION THROUGH A SUPPORTED DUAL-LAYERED BEAM STRUCTURE

5.1 INTRODUCTION

Structures periodically consisting of similar elements are easy to be found in natural or manmade environments, of which a group of identical components are connected or coupled together at regular intervals to form a whole structure. The atomic lattices of pure crystals constitute perfect periodic coupling structures in nature, so the propagation of waves in periodic waveguides was studied for solids [46], thus promoting basic understanding of the electromagnetic properties of conductors or semi-conductors. The transmission of structure-borne sound excited by mechanical vibration in these similar structures—from side to side in a bridge or layer to layer in a building—often give rise to structure-borne noise problems in the connected spaces and can sometimes even be harmful to the stability of the entire structure.

The classical problem of acoustic wave transmission in one-dimensional periodic media can be tackled in an exact manner via the transfer matrix method [49]. Commonly in very a few cases like such simple structure the power is transmitted by just one type of wave motion .i.e. pure longitudinal wave, but in most of other cases of coupling structures it is transmitted simultaneously in combinations of multiple types such as longitudinal, torsional and flexural waves. As the different types of wave motions are coupled in each periodic connection or discontinuity, the process of coupling effect takes an important part of the structure-borne sound transmission in building structures. Early to 50 years ago the enhanced wave transmission in a

rib-reinforced floor due to wave coupling was modeled by using a beam that was periodically loaded with eccentric attachments [65]. Four different methods of calculating the structure-borne sound propagation in beams with many non-resonant discontinuities were demonstrated by Manfred Heckl [54], and three of these methods took the coupling between longitudinal and flexural waves into account. A series of work on multi-coupling of waves in periodic structures had been done by Mead, in which the characteristic wave-types that can propagate along a periodic structure were predicted by using the method of propagation constant [52], and the flexural-longitudinal wave coupling in a simple multi-supported beam was studied with the effect of damping [78]. More studies providing valuable insight into multiple coupling of waves propagation on general periodic engineering structures was concluded in the extensive literature review [53]. Transfer matrices were used by Roy and Plunkett to examine attenuation of flexural waves in an undamped beam with flexible but non-resonant ribs [70]. More recently, the propagation characteristics of coupled longitudinal and flexural waves in beam-type transmission paths with asymmetric loads in the form of resonant columns were theoretically analyzed [56] and developed experimentally [57] by Ohlrich.

Commonly the coupling of wave motions is concerned with the waveguide models of a single-layer beam that comprises independent beam-discontinuities, few studies about the structure-borne power transmission had been focused on the cross-layer power flow through a multi-layered beam structure in a flexible boundary supporting condition. Therefore the work in this chapter developed the analytical solution method for a finite dual-layer beam structure with periodic connection branches in the different conditions of simple coupling without longitudinal wave and multi-coupling of flexural and longitudinal waves. Based on the transfer matrix method, the propagation constants of the characteristic wave-types were derived and applied to analyze the structure-borne

sound transmission in a multi-coupling dual-layer beam structure [76] achieve the characteristics of a finite periodic dual-beam structure, and to investigate the structure-borne sound power transmitted through the periodic structure.

5.2 DEVELOPED TRANSFER MATRIX METHOD

5.2.1 PERIODIC DUAL-LAYERED BEAM STRUCTURE WITH TRANSVERSE CONNECTION

The research of this chapter is built on the model of a dual-layer beam structure that is periodically connected with transverse branches. A simplified model is shown in Fig.5.1. The structure-borne sound including flexural waves and longitudinal waves that propagate in two horizontal beams—A and B are coupled at two sides of each junction j=1…N with the connection branch C. Every side of two finite beams is vertically supported in y-direction on a long Timoshenko beam. The beams and branches analyzed in the theoretical model are even, straight, isotropic, and homogeneous, and the following physical parameters are assumed: $\rho 1 = \rho 2$ is the density of beams A and B and $\rho 3$ is the density of branch C, B_{sa} and B_{sb} are the bending stiffness of beams A and B, and B_{sc} is the bending stiffness of C, $E_a = E_b$ is the Young's modulus of beams A and B and E_c is the Young's modulus of branch C, k_{fa}, k_{fb} and k_{fc} are the flexural wave numbers in beams A, beam B and branch C, k_{la}, k_{lb} and k_{lc} are the longitudinal wave numbers in beams A, B and branch C corresponding to the longitudinal wave speeds c_{a0}, c_{b0} and c_{c0}.

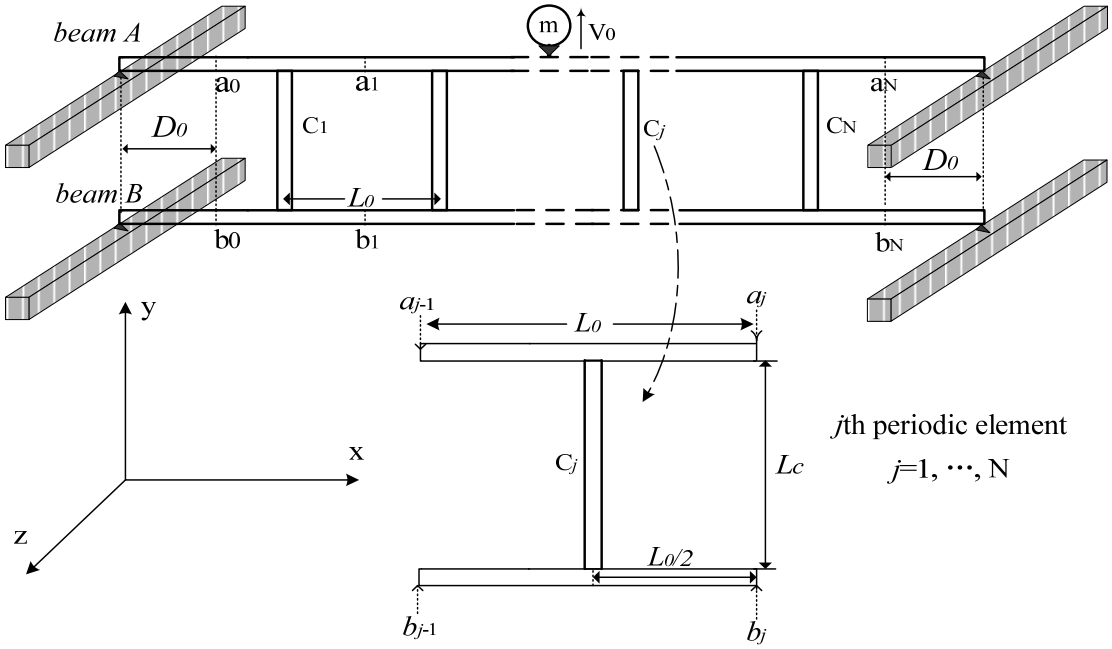

Fig. 5.1 Finite periodic coupling dual-beam structure and the supporting structure

5.2.2 WAVE TRANSFER MATRIX FOR DIFFERENT COUPLING CONDITIONS

In every dual-beam part between the connection branches of the periodic structure shown in Fig.5.1, the propagation of longitudinal-flexural waves can be expressed as the transfer matrix of velocity (horizontal, vertical, and rotational) and force (horizontal, vertical, and moment) vector

$$\begin{bmatrix} \mathrm{V}_n \\ \mathrm{F}_n \end{bmatrix}_{(a,b)_j^-} = [\Gamma_0] \begin{bmatrix} \mathrm{V}_n \\ \mathrm{F}_n \end{bmatrix}_{(a,b)_{j-1}^+} \tag{5.1}$$

$$[\mathrm{V}_n] = [V_{ya} \;\; V_{yb} \;\; \Omega_a \;\; \Omega_b \;\; V_{xa} \;\; V_{xb}]^{\mathrm{T}}, \;\; [\mathrm{F}_n] = [F_{ya} \;\; F_{yb} \;\; M_a \;\; M_b \;\; F_{xa} \;\; F_{xb}]^{\mathrm{T}}$$

where a_{j-1}, b_{j-1} is the left side position and a_j, b_j are the right side of jth periodic beam element, and branch Cj connects with the midpoints of jth beam element (all of the analytical equations in this chapter are based on the harmonic wave of separate frequency ω_n with time dependence suppressed), as follows. Based on the theory about structure-borne sound waves as [76], the transfer matrix for the propagation of

uncoupled longitudinal and flexural waves in the independent dual beam part can be derived by

$$[\Gamma_0]=[S_{VF}][P_{w0}][S_{VF}]^{-1} \tag{5.2}$$

where the transfer matrix for transforming wave components $[S_{VF}]$ takes on the form:

$$[S_{VF}]=\begin{bmatrix} D_{V1} & \mathrm{O} & D_{V2a} & \mathrm{O} & D_{V3} & \mathrm{O} & D_{F1a} & \mathrm{O} & D_{F2a} & \mathrm{O} & D_{F3a} & \mathrm{O} \\ \mathrm{O} & D_{V1} & \mathrm{O} & D_{V2b} & \mathrm{O} & D_{V3} & \mathrm{O} & D_{F1b} & \mathrm{O} & D_{F2b} & \mathrm{O} & D_{F3b} \end{bmatrix}^{\mathrm{T}} \tag{5.3}$$

in which the components of the matrix are given by

$$D_{V1}=\begin{bmatrix}1\\1\\1\\1\\0\\0\end{bmatrix},\quad D_{V2(a,b)}=\begin{bmatrix}-jk_{f(a,b)}\\-k_{f(a,b)}\\jk_{f(a,b)}\\k_{f(a,b)}\\0\\0\end{bmatrix},\quad D_{V3}=\begin{bmatrix}0\\0\\0\\0\\1\\1\end{bmatrix}\ \text{and,}$$

$$D_{F1(a,b)}=\begin{bmatrix}jR_{f(a,b)}\\-R_{f(a,b)}\\-jR_{f(a,b)}\\R_{f(a,b)}\\0\\0\end{bmatrix},\quad D_{F2(a,b)}=\frac{1}{k_{f(a,b)}}\begin{bmatrix}R_{f(a,b)}\\-R_{f(a,b)}\\R_{f(a,b)}\\-R_{f(a,b)}\\0\\0\end{bmatrix},\quad D_{F3(a,b)}=\begin{bmatrix}0\\0\\0\\0\\R_{l(a,b)}\\-R_{l(a,b)}\end{bmatrix},$$

where $R_{l(a,b)}=\rho_{(a,b)}c_{0(a,b)}$ and $R_{f(a,b)}=\dfrac{B_{s(a,b)}k_{f(a,b)}^3}{j\omega_n}$.

As the transfer matrix of all the wave components prapagating through each continous beam period (in the length of L_0), $[P_{wv}]$ is given by

$$[P_{wv}]=\begin{pmatrix} P_{fva} & 0 & 0 & 0 \\ 0 & P_{lva} & 0 & 0 \\ 0 & 0 & P_{fvb} & 0 \\ 0 & 0 & 0 & P_{lvb} \end{pmatrix} \tag{5.4}$$

where $P_{lv(a,b)} = \begin{pmatrix} e^{-jk_{f(a,b)}L_0} & 0 \\ 0 & e^{jk_{f(a,b)}L_0} \end{pmatrix}$ is the transfer matrix for the longitudinal wave propagation and $P_{fv(a,b)} = \begin{pmatrix} e^{-jk_{f(a,b)}L_0} & 0 & 0 & 0 \\ 0 & e^{-k_{f(a,b)}L_0} & 0 & 0 \\ 0 & 0 & e^{jk_{f(a,b)}L_0} & 0 \\ 0 & 0 & 0 & e^{k_{f(a,b)}L_0} \end{pmatrix}$ is that for flexural wave propagation. It is noted that the wave-coupling in a dual-layered beam structure is caused by the discontinuity of the connection with branches. By introducing the dynamic continuity conditions, the velocities are continuous and the forces are changed by the wave coupling at the vertical connection with the branch beams. The relationship between the velocities-forces of the coupled flexural and longitudinal waves can be characterized as a 12×12 coupling transfer matrix expressed as

$$\begin{bmatrix} \mathrm{V}_n \\ \mathrm{F}_n \end{bmatrix}_{(a,b)_j^+} = [\mathrm{W}_C] \begin{bmatrix} \mathrm{V}_n \\ \mathrm{F}_n \end{bmatrix}_{(a,b)_j^-} \tag{5.5}$$

where $\begin{bmatrix} \mathrm{V}_n \\ \mathrm{F}_n \end{bmatrix}_{(a,b)_j^-}$ and $\begin{bmatrix} \mathrm{V}_n \\ \mathrm{F}_n \end{bmatrix}_{(a,b)_j^+}$ denote the velocity and force vectors of the beam on the left and right side of the connection points on beam A-B with C_i, whereas the wave-coupling matrix $[\mathbf{W}_C]$ is given by

$$[\mathbf{W}_C] = \begin{bmatrix} \mathbf{I}_6 & \mathbf{O} \\ \mathrm{Z}_C & \mathbf{I}_6 \end{bmatrix} \tag{5.6}$$

In the assumed condition of mono-coupling that there is only y-directional action considered for every connection with branch, $[\mathrm{Z}_C]$ can be simplified as

$$[\mathrm{Z}_C] = \begin{bmatrix} \mathrm{Z}_{Cl} & \mathbf{O} \\ \mathbf{O} & \mathbf{O} \end{bmatrix}$$

where Z_{Cl} is the 2×2 y-longitudinal impendence matrix of branch C. While in the condition that the multi-coupling of longitudinal and flexural waves are considered, the transfer elements of $[Z_C]$ are given by

$$[Z_C] = -\begin{bmatrix} Z_{Cl} & \mathbf{O}_{2\times4} \\ \mathbf{O}_{4\times2} & Z_{Cf} \end{bmatrix} \times \begin{bmatrix} M_{Cl} & \mathbf{O}_{2\times4} \\ \mathbf{O}_{4\times2} & M_{Cf} \end{bmatrix}$$

$$Z_{Cl} = \begin{bmatrix} R_{cl} & -R_{cl} \\ -R_{cl}\phi_{Cl}^{-j} & R_{cl}\phi_{Cl}^{j} \end{bmatrix},\ Z_{Cf} = \begin{bmatrix} R_{CM} & -R_{CM} & R_{CM} & -R_{CM} \\ -\phi_{Cf}^{-j}R_{CM} & \phi_{Cf}^{-1}R_{CM} & -\phi_{Cf}^{j}R_{CM} & \phi_{Cf}R_{CM} \\ jR_{CF} & -R_{CF} & -jR_{CF} & R_{CF} \\ -j\phi_{Cf}^{-j}R_{CF} & \phi_{Cf}^{-1}R_{CF} & j\phi_{Cf}^{j}R_{CF} & -\phi_{Cf}R_{CF} \end{bmatrix}$$

$$M_{Cl} = \begin{bmatrix} 1 & 1 \\ \phi_{Cl}^{-j} & \phi_{Cl}^{j} \end{bmatrix}^{-1},\quad M_{Cf} = \begin{bmatrix} -jk_{fc} & -k_{fc} & jk_{fc} & k_{fc} \\ -jk_{fc}\phi_{Cf}^{-j} & -k_{fc}\phi_{Cf}^{-1} & jk_{fc}\phi_{Cf}^{j} & k_{fc}\phi_{Cf} \\ 1 & 1 & 1 & 1 \\ \phi_{Cf}^{-j} & \phi_{Cf}^{-1} & \phi_{Cf}^{j} & \phi_{Cf}^{1} \end{bmatrix}^{-1}$$

$$R_{cl} = \rho_c c_0,\ \phi_{Cl} = e^{k_{l3}L_c},\ \phi_{Cf} = e^{k_{f3}L_c},\ R_{CM} = \frac{B_{0C}k_{f3}^2}{j\omega_n}, R_{CF} = \frac{B_{0C}k_{f3}^3}{j\omega_n}$$

The entire periodic transfer matrix of the coupling wave transmission can be given by

$$\begin{bmatrix} V_n \\ F_n \end{bmatrix}_{i+1}^{-} = [U_e]\begin{bmatrix} V_n \\ F_n \end{bmatrix}_{i}^{-}. \tag{5.7}$$

where $[U_e] = [\Gamma_0] \times [W_C] \times [\Gamma_0]$.

Generally, according to the theory of Bloch wave, when the one-dimensional acoustic waves are propagating through a semi-infinite periodic structure, the amplitudes and phases of wave components are modulated periodically by the structure. Based on the derived wave transfer matrix and the linear transformation, to satisfy the continuity of the forces (moment actions) and the equilibrium of the volume velocities at the two ends of each periodic beam-branch element, the relationship between velocity vector $[V_n]_j$ and force vector $[F_n]_j$ at the two periodic connection points nearby can be expressed by

$$\begin{bmatrix} \mathrm{V}_n \\ \mathrm{F}_n \end{bmatrix}_j^- = \sum_{i=1}^{2N} s_{j,i} \begin{bmatrix} \xi_{in} \\ \varsigma_{in} \end{bmatrix} \tag{5.8}$$

$$s_{j,i+1} = e^{\mu_i} s_{j,i} . \tag{5.9}$$

This represents a problem on the eigen value vector for the transfer matrix $[U_e]$. The pair of *i*th eigen values $\mu_j = \pm(\mu_{j\mathrm{R}}+\mu_{j\mathrm{I}})$ of transfer matrix are the frequency-dependent complex propagation constants for the corresponding N pairs of the characteristic wave types (N = 6 for the studied periodic structure). Correspondingly, the eigen vectors $\begin{bmatrix} \xi_{in} & \varsigma_{in} \end{bmatrix}^{\mathrm{T}}$ are used to express the characteristic wave types, which take on the form $[\xi_{in}] = [X^i_{Vxa},\ X^i_{Vxb},\ X^i_{\Omega a},\ X^i_{\Omega b},\ X^i_{Vya},\ X^i_{Vyb}]^{\mathrm{T}}$ and $[\varsigma_{in}] = [X^i_{Fxa},\ X^i_{Fxb},\ X^i_{Ma},\ X^i_{Mb},\ X^i_{Fya},\ X^i_{Fyb}]^{\mathrm{T}}$. As the "attenuation constant" of the coupled wave type, the real part $\mu_{j\mathrm{R}}$ expresses the exponential decay rate for the *j*th characteristic wave type that propagates through a periodic beam element, whereas the imaginary part $\mu_{j\mathrm{I}}$ is defined as the "phase constant," of which the cosine value describes the phase transfer of the *j*th characteristic wave type that propagates through each element. If the propagation constants of the positive-going waves are defined as $+\mu_j$, then, correspondingly, the real and imaginary parts of the propagation constants ought to be negative. Ideally, in the case that the damping factor of the beam structure is negligible, a coupling wave type at any given frequency within a pass band yields up to a pair of pure imaginary propagation constants, of which $\mu_j = -\mu_{j\mathrm{I}}$ is the positive-directional propagation constant, and $+\mu_{j\mathrm{I}}$ for negtive-going transmission is physically impossible in a semi-infinite structure. the larger attenuation zone of the real part μ_{jR} means that the corresponding wave-type is in the forbidden band of the periodic structure so that it will decay quickly as it is propagating in the periodic structure.

5.2.3 CHARACTERISTICS OF THE FINITE PERIODIC BEAM STRUCTURE AND STRUCTURE-BORNE SOUND POWER TRANSMISSION

Engineering structures usually are made of a few periodic elements, which means that reflections resulted from the extreme boundaries cannot be neglected so that the periodic structure ought to be treated as finite element number. The direct mobility matrixes of the left *j*-elements and the right *N-j* elements subsystem are expressed by

$$[Y_{nn}]_{jL} = ([\zeta_+][e_d^{-j\mu}]r_L + [\zeta_-][e_d^{j\mu}])(-[\xi_+][e^{-j\mu}]r_L - [\xi_-][e_d^{j\mu}])^{-1} \tag{5.10}$$

$$[Y_{nn}]_{jR} = ([\zeta_+][e_d^{(N-j)\mu}]r_R + [\zeta_-][e_d^{(j-N)\mu}])([\xi_+][e^{(N-j)\mu}]r_R - [\xi_-][e_d^{(j-N)\mu}])^{-1} \tag{5.11}$$

Where r_L and r_R are the left and right reflection matrix derived from the mobility of boundary condition, $[\zeta_{(+,-)}]$ and $[\xi_{(+,-)}]$ correspondingly are the 6×6 normalized velocity and force matrix for the positive-going or negative-going characteristic wave types. Then the input mobility matrix of the total periodic beam at a_j, b_j is given by

$$[Y_{nn}]_j = [Y_{nn}]_{jR}\left(I + [Y_{nn}]_{jL}^{-1}[Y_{nn}]_{jR}\right)^{-1} \tag{5.12}$$

While the mobility matrix at the boundary of the beam structure $[Y_{nn}]_{Nj}$ is introduced, the structure-borne sound power transmitted into the structure can be given by

$$[P_{wt}]_N = \mathbf{Re}\left([V_t]_N^{*T}[Y_{Nj}]^{-1}[V_t]_N\right)$$

Where $[V_t]_N$ is the velocity vector at the boundary sides of the two-layer beam mounted on the supporting structure, which can be calculated by the transfer matrix method of characteristic wave types in section 5.2.2.

5.3. ANALYSIS FOR STRUCTURE-BORNE SOUND TRANSMISSION IN THE FINITE PERIODIC DUAL-BEAM STRUCTURE

5.3.1 CONDITIONS OF THE COMPUTATION FOR THE FINITE PERIODIC STRUCTURE

An analysis based on the theoretical model was conducted to investigate the effects of flexural and longitudinal wave coupling in a dual-layer beam structure on the structure-borne sound transmission. All of the numerical calculations of the analyzed model were conducted using MATLAB. The dimensions and physical parameters of the finite periodic structure were designed according to a normal engineering structure as explained in the followings, and are shown in Fig. 5.1. Steel was chosen as the material for the two equal periodic beams A and B, the Young's modulus of which was $E_0 = 2.16 \times 10^{11}$ N/m^2 with an assumed loss factor $\eta = 0.01$ and density $\rho = 7790$ kg/m^3. The beams A and B with a rectangular cross-section were assumed to be of a thickness $h_0 = 3.0$ cm, width $d_0 = 5.0$ cm, There were three cases: Case I: $L_A = L_B = 14.4$ m ($L_A = 12 \times 1.2$m), Case II: element length $L_0 = 1.2$m , and the whole length of a beam $L_A = L_B = 21.6$ m ($L_A = 18 \times 1.2$m),and Case III: $L_0 = 1.8$m, $L_A = L_B = 12 \times 1.8m= 21.6$ m. The same steel was also elected as the material for the connection branch with a rectangular cross-section, the dimensions of which were a thickness $h_c = 2.6$ cm, width $d_c = 5$ cm, and the length of branch $L_c = 2.5$ m. The periodic elements were symmetrically distributed from the center of the finite beam structure. The total number was N and the distance D_0 between a_0-b_0 and the left boundary of the beam structure was equal to the distance between a_N-b_N and the right boundary of the beam structure. The four sides of this periodic dual-beam structure were ideally vertically supported at the centers of four long Timosheko beams as the outside structure (only y-directional force and velocity were taken into account. The material of those four same supporting

Timosheko beams also was the steel, and the dimensions of the square cross section were assumed to be $h_T = d_T = 11$ cm. The force acting on every contact point supporting one side of the periodic dual beams was assumed to have a single degree of freedom in y-direction. An ideal simple source driven by a y-directional inherent force was mounted on beam A. As the wave coupling at the periodic connection was treated by transfer matrix method with lumped parameters, herein the analysis was applied in a mid-low frequency region from 1 to 1000 Hz. The level of power flow transmissibility being defined as $L_{(pt)} = 10\,\mathbf{log}\left(P_{t(a,b)} \Big/ P_{in} \right)$ was used for the analysis. Timoshenko beam in this study is defined as the thick beam with the shear stiffness taken into account, the point mobility at the center can be given by

$$Y_{Tb} = \frac{1}{2\omega m'} \frac{k_T^2 + k_I k_{II}}{k_I + k_{II}} \tag{5.13}$$

where k_T is the wave number of transverse wave in the beam, k_I and k_{II} are the complex waves numbers derived by

$$k_I = \frac{k_T^2 + k_l^2}{2} + \sqrt{\left(\frac{k_T^2 + k_l^2}{2} \right)^2 + \alpha k_B^4}$$

$$k_{II} = \frac{k_T^2 + k_l^2}{2} - \sqrt{\left(\frac{k_T^2 + k_l^2}{2} \right)^2 + \alpha k_B^4} \tag{5.14}$$

It is used to express the supporting structure into which structure-borne sound is going to transmitted in this chapter.

5.3.2 STRUCTURE-BORNE SOUND POWER TRANSMITTED THROUGH A FINITE PERIODIC STRUCTURE

The effect of wave coupling on the transmission of structure-borne sound through a finite periodic dual-beam structure was investigated by using the developed structure

model in the different conditions of connection. The levels of power flow transmissibility throughout beam A without connection branches to branch B are plotted in Fig. 5.2(a) , of which the structure-borne sound is transmitted from a source symmetrically placed on the middle a_9 (x=10.8m) of beam A and asymmetrically placed on the point a_6 (x=3.6m) of beam A. It can be seen that the level of power flow transmissibility of the beam A modulated on the similar small modes within the frequency range, and gradually decayed following a smooth trend. The modulation envelopes of the levels of power flow transmissibility were different for the different exciting positions. The amplitude of the modulation envelopes in the case of being excited at a_6 is significantly larger than that in the case of being excited at a_9, but they both decay with increasing frequencies.. It is because the structure-borne sound power of flexural wave in the beam was mainly attenuated by the decaying factor $k_f x$ of the evanescent part of flexural wave that becomes larger with increasing frequencies.

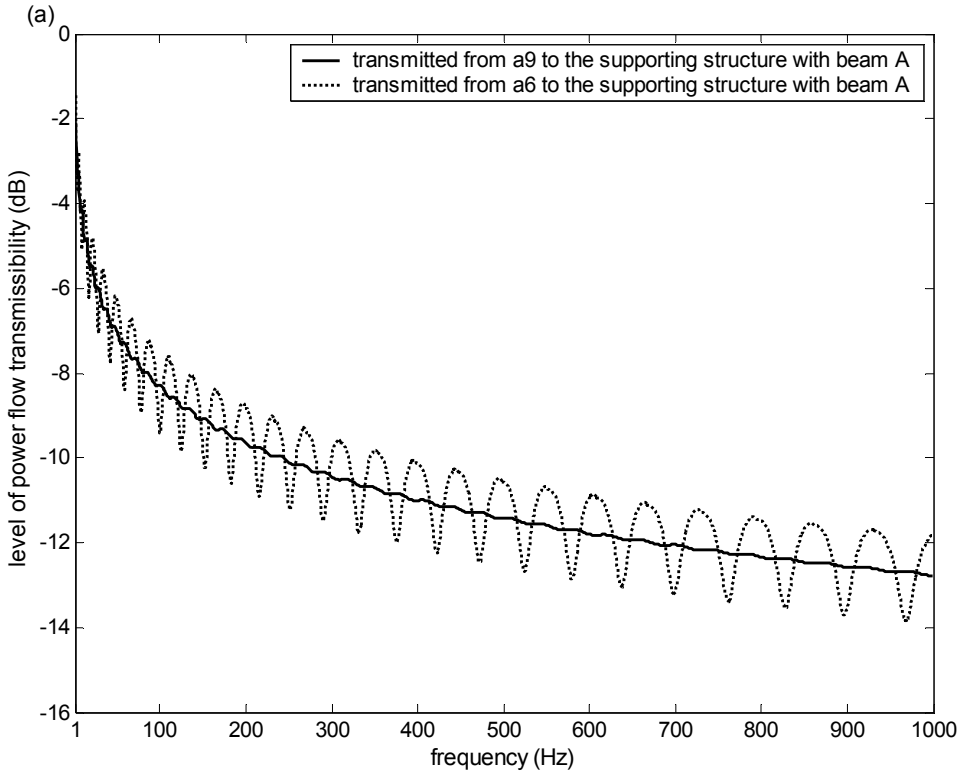

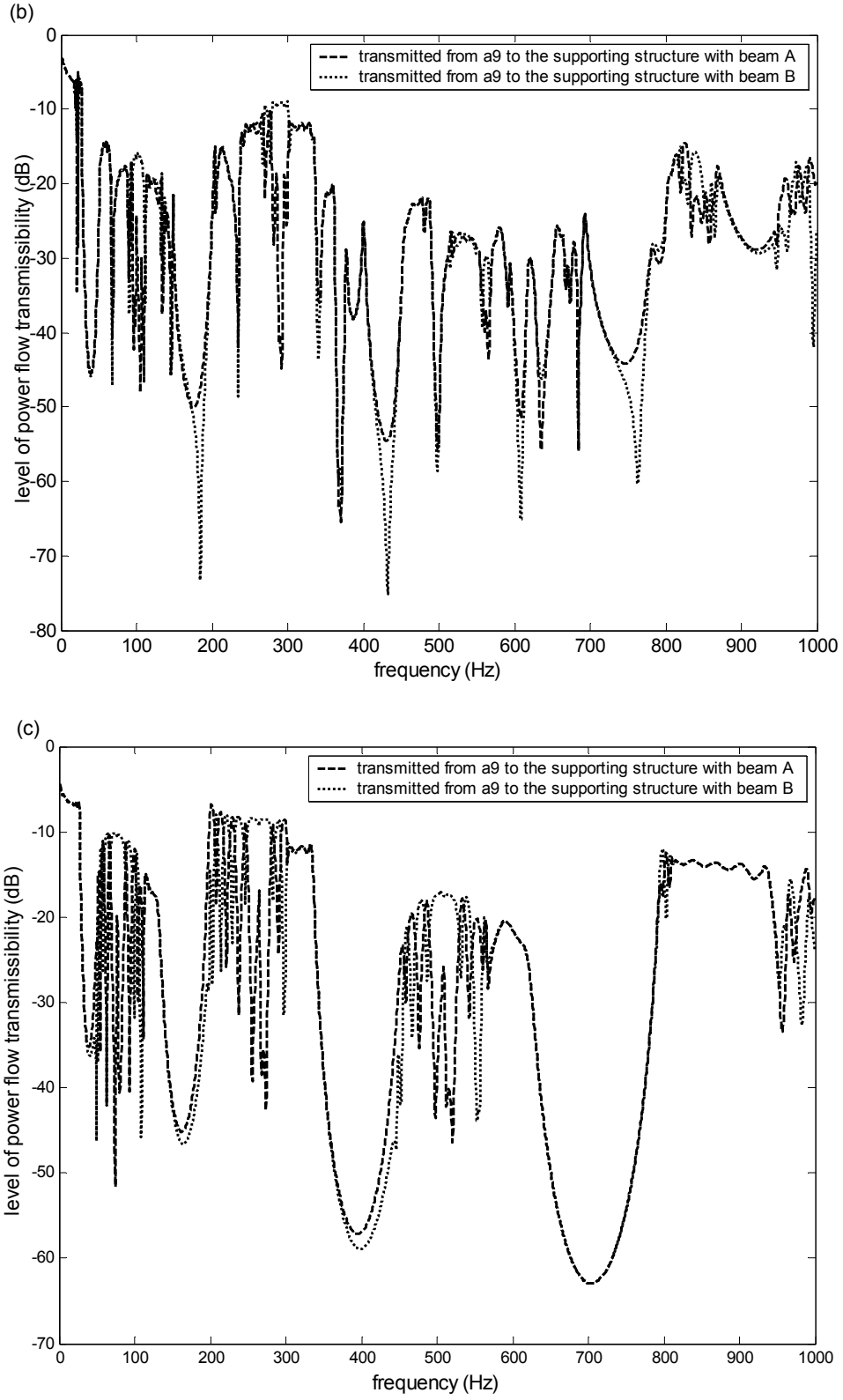

Fig. 5.2 levels of the structure-borne sound power flow transmissibility throughout the beams into the supporting structure ($L_A = L_B$ =21.6 m). (a) Excited on the middle point of a singly supported beam A without coupling branches; (b) excited on the middle point a_9 of the dual-beam structure in condition of multi-coupling of longitudinal and flexural wave; (c) excited on the point a_9 of the dual-beam structure in condition of mono-coupling without longitudinal motion.

Figs. 5.2(b) and 5.2(c) show the results when the dual-beam structure was periodically connected with B by 18 branches (N=18), of which the periodic element length L_0 = 1.2 m, the positions of a_0-b_0 were just on the left boundary and a_N-b_N were just on the right boundary of the beam structure (D_0 = 0). In the figures, for the structure-borne sound power that was transmitted from the source placed on a_9(x =10.8m) through two layers of the periodic beam structure into the supporting structure, the levels of the structure-borne sound power flow transmissibility were plotted in the conditions of multi-coupling and mono-coupling connection. It can be observed that the power of the structure-borne sound transmitted throughout the dual-layer beam to the supporting structure was mainly modulated by the coupling structure and did not decay with increasing frequencies. The transmitted power throughout the beam structure was slightly attenuated at the peak regions, in which the level of power flow transmissibility for the beam structure with coupling branches was higher than that without coupling branches. On the other hand, the transmitted power for the beam with coupling branches was attenuated to the levels lower than that without coupling branches in most frequencies except peak frequencies. Especially in the gaps, the decreased levels of power flow transmissibilty could be more than 50 dB. It also can be observed that at most frequencies below 350 Hz, the predicted level of power flow transmissibility for the mono-coupling beam structure is similar to that for the multi-coupling beam structure, but they became to be quite unlike while the frequency increased above 350Hz. This indicates the fact that the action of longitudinal wave plays a dominant role on the wave coupling in the beam structure at low frequencies. However, the action of flexural wave plays a more important role on the wave coupling in the beam structure as frequency increases. A calculation method based on the multi-coupling model of flexural and longitudinal waves is therefore

required for the accurate prediction of structure-borne sound transmission in a dual-layer beam structure.

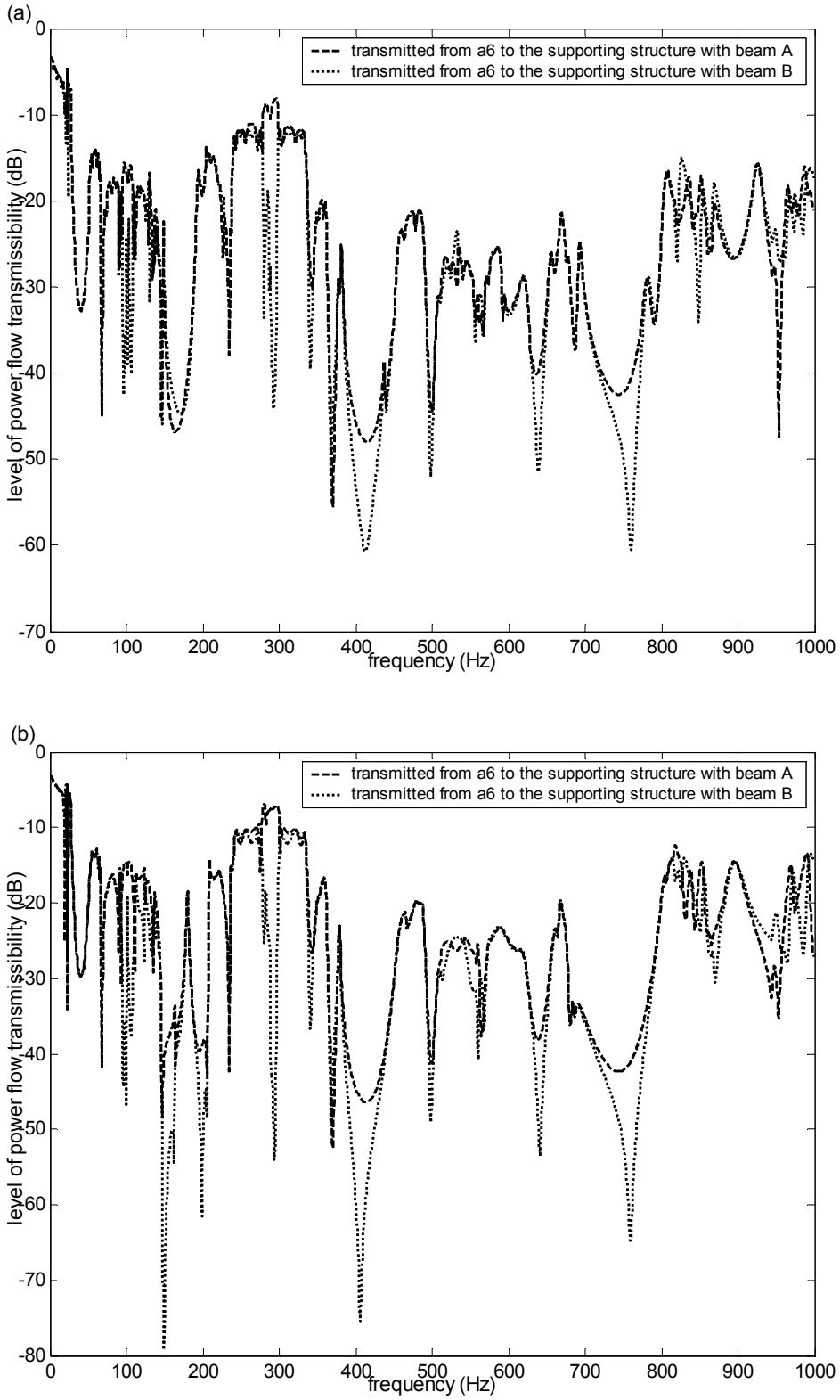

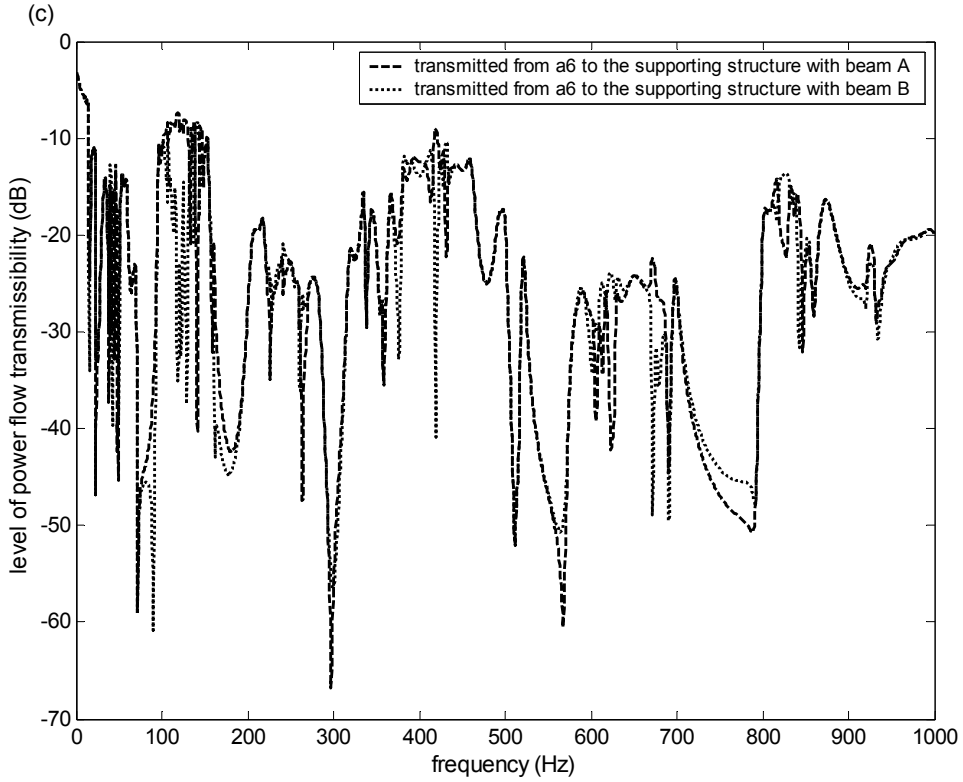

Fig. 5.3 levels of the structure-borne sound power flow transmissibility throughout the finite periodic dual-beam structure in condition of multi-coupling of longitudinal and flexural wave. (a) Excited on the a_6 of the dual-beam structure of which L_0 = 1.2m, L_A= 18L_0; (b) excited on the a_6 of the dual-beam structure of which L_0 = 1.2m, L_A= 12L_0; (c) excited on the a_6 of the dual-beam structure of which L_0 = 1.8m, L_A= 12L_0.

Fig. 5.3(a) and Fig. 5.3(b) show the results for the similar multi-coupling dual-beam structures (L_0 = 1.2m) periodically connected by 18 branches and 12 branches, respectively. It can be seen that in the case of being excited on the same position a_6, the band structures of the level of power flow transmissibility for the two beam structures of the same periodic elements were similar at most frequencies. It is believed that the transmitted power throughout the multi-coupling beam structure is less attenuated as there are fewer periodic elements in the beam structure. However, it can be seen from Fig. 5.3(a) and Fig. 5.3(b) that there were no significant difference in attenuation of power transmission between beam structure connected by 18 branches and 12 branches. It can also be seen that the levels of the power flow transmissibility were less negative at peak frequencies. It implies that the power of transmitted waves in the dual-layer beam structure can only be little attenuated in the peak frequencies. As a result, it is

easier to have structure-borne sound problem at peak frequencies. Besides, it can be seen that the levels of the power flow transmissibility became more negative in the gap regions as the number of periodic elements increased from 12 to 18. It is because the transmitted structure-borne sound waves are strongly attenuated by the periodic beam elements in the gap regions.

Case III shown in in Fig. 5.3(c) has same number of beam element (N) as Case I shown in Fig. 5.3(a) and has same beam length (L_A) as Case II shown in Fig. 5.3(b). However, the band structure of the levels of the power flow transmissibility shown in Fig. 5.3(c) is different from that shown in Fig. 5.3(a) and Fig. 5.3(b). It means that the band structure is independent of the beam length or number of beam element. Besides, the band structure of the levels of the power flow transmissibility shown in Fig. 5.3(a) is similar to that shown in Fig. 5.3(b). It means that the band structure is dependent on the length of periodic element (L_0). Moreover, it was notable that within the regions near several peaks, the level of the power flow transmitted into the second layer of supporting structure through beam B could be even higher than the level of the power transmitted into the first layer, so that "cross-layered" noise transmission would be considerable in these conditions.

5.4 SUMMARY

In this chapter, a model based on the transfer matrix that considers the mono-coupling of flexural wave and the multi-coupling of flexural and longitudinal waves at each connection was developed to study the transmission of the structure-borne sound power flow through a periodic dual-layer beam structure. Using this model, numerical calculations were performed to analyze the structure-borne sound power transmitted through a finite periodic dual-layer beam into the supporting structure. The calculated results using the developed method and model .suggest that the power of the structure-borne sound transmitted through a dual-layer beam into the supporting building structure, but also on the attenuation caused by the periodic beam elements with coupling branches and the exciting position of source. The results also reveal that the model under mono-coupling condition to be similar to that under the multi-coupling in the relatively low frequency region. Further, the transmitted power was strongly attenuated in a number of frequency regions, and in several frequency regions the power was even transmitted into the second layer of the supporting structure to a considerable degree. The analysis indicated that this study is useful in understanding the structure-borne sound power flow transmission from the first layer into the second layer of the dual-layer beam structure.

Nomenclature of Chapter 3, 4 and 5

$[\mathbf{V}_n]$	velocity vector of the longitudinal-flexural waves in the dual-layer beam
$[\mathbf{F}_n]$	force vector of the longitudinal-flexural waves in the dual-layer beam
$[\mathbf{\Gamma}_0]$	transfer matrix of the uncoupled longitudinal and flexural waves propagation
$[\mathbf{S}_{VF}]$	transfer matrix for transforming wave components to velocity-force vector
$[\mathbf{P}_{w0}]$	transfer matrix of the wave components prapagating through the continous beam part
(a,b)	express "in the beam A and B"
$\overset{+}{i}$	express "right side of the ith beam connection with branch"
$\overset{-}{i}$	express "left side of the ith beam connection with branch"
ω_n	angular frequency of the excited wave in the beam structure
k_f	longitudinal wave number in a beam
k_l	flexural wave number in a beam
R_l	longitudinal wave impendence factor
R_f	flexural wave impendence factor
ρ	linear density of the beam
c_0	longitudinal wave speed
$\mathbf{I}_m$	m× m identity matrix
$[\mathbf{W}_C]$	wave-coupling matrix at the connection of the beam structure
$[\mathbf{Z}_C]$	coupling impendence matrix of the coupled waves at the connection of the beam structure
$\mathbf{Z}_{Cl}$	2×2 longitudinal coupling impendence matrix of branch
$\mathbf{Z}_{Cf}$	4×4 flexural coupling impendence matrix of branch
$\mathbf{M}_{Cl}$	longitudinal propagation matrix of the coupled waves in the branch
$\mathbf{M}_{Cf}$	flexural propagation matrix of the coupled waves in the branch
ϕ_{Cl}	longitudinal propagation factor in the branch
ϕ_{Cf}	flexural propagation factor in the branch
ς_{in}	normalized velocity vector of ith characteristic wave type
ξ_{in}	normalized force vector of ith characteristic wave type
s_i	magnitude of ith characteristic wave type
μ_i	propagation constant of ith characteristic wave type
$\mathbf{e}_d^{-j\mu}$	6×6 diagonal matrix of 6 propagation constants μ_i
$[\varsigma_{(+,-)}]$	6×6 velocity matrix of the positive or negative-going characteristic wave types
$[\xi_{(+,-)}]$	6×6 force matrix of the positive or negative-going characteristic wave types
$\mathbf{r}_L$	reflection matrix of the flexural-longitudinal waves at the left boundary
$\mathbf{r}_R$	reflection matrix of the flexural-longitudinal waves at the right boundary
$[\mathbf{Y}_{nn}]_{jL}$	direct mobility matrix of the left *j*-elements subsystem
$[\mathbf{Y}_{nn}]_{jR}$	direct mobility matrix of the right *N-j* elements subsystem

$[\mathbf{Y}_{nn}]_j$	input mobility matrix of the total periodic beam system at a_j, b_j
$[\mathbf{Y}_{nn}]_{Nj}$	mobility matrix at the boundary of the beam structure
$[\mathbf{V}_t]_N$	velocity vector at the boundary sides of the two-layer beam
L_0	element length of the periodic beam structure
$L_{A,B}$	whole length of the beam A and B
h_0	thickness of the beam A and B
d_0	width of the beam A and B
h_c	thickness of the branch beam
d_c	width of the branch beam
L_c	length of the branch beam
E_0	Young's modulus of the beam
B_s	Bending stiffness of the beam
h_T	side length of the square cross section of the supporting Timosheko beam
Y_{Tb}	the point mobility at the supporting point of Timosheko beam
$k_{I,II}$	complex waves numbers in the Timosheko beam
$L_{(pt)}$	level of power flow transmissibility

CHAPTER 6. POWER TRANSMISSION FROM TWO COHERENT MACHINES TO A DUAL-LAYER COUPLING FLOOR STRUCTURE

6.1 INTRODUCTION

Vibration isolators are commonly adopted by engineers to reduce the amount of structure-borne sound transmitted from building services equipment to the floor structure [49, 80, 81]. Using total sound power as a way to describe such structure-borne sound transmission appears more viable than the concept of transmitted forces which is commonly used by building engineers. This is because it has a single value and is independent of the amplitude and phase differences of the complex forces and velocities transmitted between the contacts and receiver [6]. Some studies of the transmission of structure-borne sound power into supporting structures from multi-point or -component sources have been conducted by Pinnington, Koh, and White [82-84] and [61]. The influence of multiple contact points and components of excitation, and of the motion of the structure-borne sound source, on power transmission has been studied by Gibbs and Petersson [10, 85]. This work has provided us with a practical approach to the estimation of structure-borne sound power emission by using the characteristics of the source and receiver structures.

Many complicated vibration-isolated systems have been analyzed as a combination of several simple systems of power flowing through multiple isolators into a flexible structure [11, 82], in which the interaction due to the transfer mobility between the various contact points of the structure is important to the total power transmission. To simplify the description of the latter, it has often been assumed that only the vertical transmitted forces contribute to the total emission [83]. The power transmissibility

method, using the concepts of effective floor mobility and total structure-borne sound power transmission, has been proposed by Mak and Su [86, 41-42] as a means by which to assess the performance of different methods of vibration isolation. Their approach is based on a derived mobility matrix using a source model of a rigid machine and a simply supported ideal plate.

The dynamic characteristics of the connecting structures in buildings play an essential role in structure-borne sound transmission, since many of them can be treated as coupling multi-layered structures with periodic connections [49] (for example, multi-storey buildings, multi-support beams, stiffened plates, and some layered composite constructions). To be able to predict the transmission of structure-borne sound through such coupling structures, it is essential to model the built-up structure to describe correctly the characteristics associated with the coupled wave propagation. This is the case when statistical descriptions are applied as well as when applying analytical descriptions, but it is quite difficult for those complex or irregular structures in the low frequency regime. The numerical technique is thus employed to validate the models for the built-up structure. The ideas underlying such numerical developments are related to finite element techniques with recent developments in computing ability [87]. Most numerical methods take advantage of finite element modeling of a representative part of the periodic coupling structure [88].

When considering the vibration control of coherent machines placed on coupling structures, the interaction of the structural vibrations caused by the forces needs to be taken into account. It is common to install several machines on different floors of a floor structure, such as two water pumps of the same type in two separate plant rooms. Inaccurate prediction of the performance of vibration isolation may cause excessive structure-borne sound power to be transmitted from the machines to the floor structure in such situations. This study therefore analyzes the effect of the interaction between

two coherent vibratory machine sources on a dual-layer plate structure. It is based on two rectangular machine models of even-mass distribution with four symmetrical supports, and the calculated mobility matrix of the supported, dual-layered, concrete floor.

6.2 COHERENT, VIBRATION-ISOLATED SYSTEM ON A DUAL-LAYERED FLOOR STRUCTURE

6.2.1 FINITE ELEMENT ANALYSIS FUNDAMENTALS

This research is based on a structural model of a dual-layered plate that is connected at intervals, with transverse beams on two sides. A diagram of this structure is shown in Fig. 6.1. The vibration induced by the transmitted structure-borne sound includes both flexural and longitudinal motion in the two horizontal plates; it is also periodically connected at both sides of each junction with the 10 connection beams.

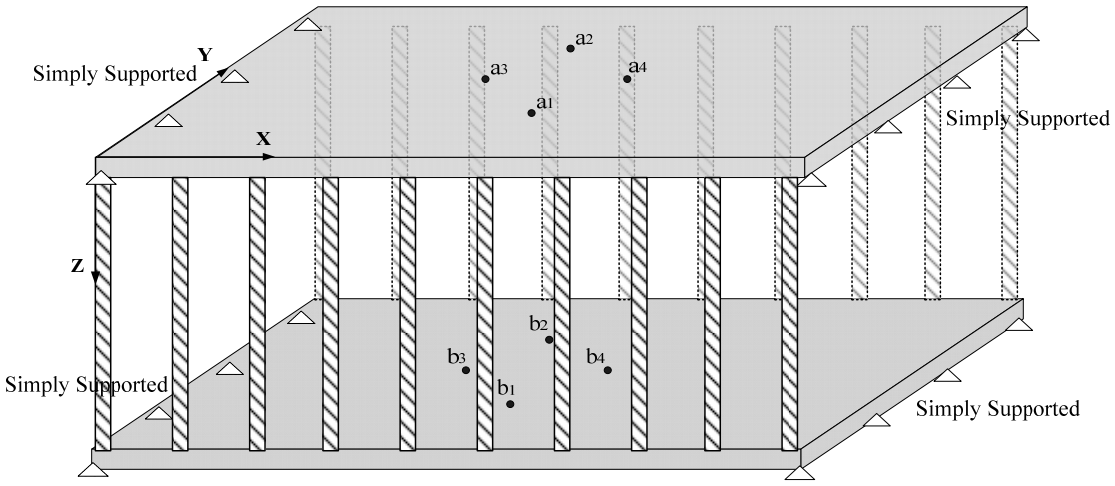

Fig. 6.1 Finite periodic coupling dual-layered structure and the supporting structure.

The points a1, a2, a3, and a4 are the four symmetric mounting points of a machine source located on the first layered plate; and b1, b2, b3, and b4 are the equivalent points for another machine source on the second such plate.

The spectral element method (Nelson, 2004) has been successfully applied for finite element simulation of beam-type structures in frequency domain and it is also adopted in this paper. The spectral element for a segment of the beam-type waveguide between two nodes can be defined for a section of a long beam extending to infinity. Considering a short section of length Δ of a uniform beam, the dynamic equation of its motion can be expressed as

$$\begin{bmatrix} \mathbf{D}_{LL} & \mathbf{D}_{LR} \\ \mathbf{D}_{RL} & \mathbf{D}_{RR} \end{bmatrix} \begin{bmatrix} \mathbf{u}_L \\ \mathbf{u}_R \end{bmatrix} = \begin{bmatrix} \mathbf{f}_L \\ \mathbf{f}_R \end{bmatrix} \tag{6.1}$$

where the subscripts *L* and *R* donate the left and right side of the section. The spectral finite element method applied for the beam-type waveguide is formulated using the equation for the dynamic matrix

$$\mathbf{D} = \mathbf{K} + j\omega\mathbf{C} - \omega^2 \mathbf{M} \tag{6.2}$$

where K, C, M are the stiffness, damping and mass matrices, which may be formed using commercial finite element packages. For the uniform beam model, the following relationships holds:

$$\mathbf{D}_{LL} = \mathbf{D}_{LL}^T, \quad \mathbf{D}_{RR} = \mathbf{D}_{RR}^T, \quad \mathbf{D}_{LR} = \mathbf{D}_{RL}^T \tag{6.3}$$

The transformed matrix for the whole element can be written as

$$\left[\tilde{\mathbf{D}}_{EE} - \tilde{\mathbf{D}}_{EI}\tilde{\mathbf{D}}_{II}^{-1}\tilde{\mathbf{D}}_{IE}\right]\mathbf{u}_E = \mathbf{f}_E \tag{6.4}$$

Herein it should be noted that the dynamically condensed element matrices become frequency dependent. The superscript ~ donates the section has internal nodes and is not condensed, and the subscript *E* or *I* represents that the degrees of freedom are associated with edge nodes or internal nodes of the section.

In FEA, the plate elements are able to withstand both longitudinal and bending strain. For flat, thin-walled shell elements, the in-plane and bending forces cause independent

deformations and the corresponding expressions for the respective displacements are given by

$$\delta(L_{in}) = \int h dx \int_{-\eta}^{\eta} \left(\delta\{\hat{\boldsymbol{\varepsilon}}^*\}^{\mathrm{T}} \mathbf{D}_p \{\hat{\boldsymbol{\varepsilon}}\} - \rho_1 \omega^2 (\delta \hat{u}_1^* \hat{u}_1 + \delta \hat{u}_2^* \hat{u}_2 \right) \mathrm{dy} = 0 \tag{6.5}$$

$$\{\hat{\boldsymbol{\varepsilon}}\} = \left[\frac{\partial \hat{u}_1}{\partial x}, \frac{\partial \hat{u}_2}{\partial y}, \frac{\partial \hat{u}_1}{\partial y} + \frac{\partial \hat{u}_2}{\partial x} \right]^{\mathrm{T}}$$

$$\delta(L_{out}) = \int h dx \int_{-\eta}^{\eta} \left(\frac{h^2}{12} \delta\{\hat{\boldsymbol{\chi}}^*\}^{\mathrm{T}} \mathbf{D}_p \{\hat{\boldsymbol{\chi}}\} - \rho_1 \omega^2 \delta \delta \hat{u}_3^* \hat{u}_3 \right) \mathrm{dy} = 0 \tag{6.6}$$

$$\{\hat{\boldsymbol{\chi}}\} = \left[\frac{\partial^2 \hat{u}_3}{\partial x^2}, \frac{\partial^2 \hat{u}_3}{\partial y^2}, 2\frac{\partial^2 \hat{u}_3}{\partial x \partial y} \right]^{\mathrm{T}},$$

where ρ_1 is the mass density; h the thickness; u_1, u_2, and u_3 the displacements in the x-, y-, and z-directions respectively of the temporal Fourier transforms; and the stiffness matrix D is expressed by

$$\mathbf{D}_p = \begin{bmatrix} E' & E_\nu & \\ E_\nu & E' & \\ & & G \end{bmatrix}^{\mathrm{T}} \tag{6.7}$$

$$E' = \frac{E}{1-\nu^2}, E_\nu = \frac{E}{2(1+\nu)}$$

where E denotes Young's modulus and ν the Poisson ratio. The functions and their derivatives of the displacements u_i are viewed as independent from their complex conjugates (all the equations in this chapter are based on the harmonic wave of separate frequency ω_n with time dependence suppressed), as follows. For the in-plane motion that assumes linear displacement functions and for the out of plane motion that assumes a combination of cubic Hermite polynomials, the displacement functions in the interior of an element are determined from the nodal displacements nearby. The displacement field of the cross-section of an element is in a local co-ordinate system given by

$$u_1(x, y) = j \mathbf{N}_{ip}(y) \{\hat{\mathbf{u}}_1(x)\}_e \tag{6.8}$$

$$u_2(x,y) = \mathbf{N}_{ip}(y)\{\hat{\mathbf{u}}_2(x)\}_e \tag{6.9}$$

$$u_3(x,y) = \mathbf{N}_b(y)\{\hat{\mathbf{u}}_3(x)\}_e \tag{6.10}$$

In the finite element method, the displacement field of the cross-section of a strip element is represented by simple polynomials according to standard procedures [89], of which the details were presented in Gavric's notable work [87]. The boundary condition of this model assumes that the two short edges of every plate in the y-direction are simply supported, and the two edges in the x-direction are vertically connected with the thin beams, of which the longitudinal and bending motions are coupled at the connection points on two sides. Then the finite element model can be introduced to the computing tool ANSYS for simulation.

6.2.2 STRUCTURE-BORNE SOUND POWER TRANSMISSION

Three cases of vibratory systems on different floor structures can be described for the purposes of studying structure-borne sound power transmission and the performance of vibration isolation. In the first case, a machine with four symmetrical mounting points a1-a4 is placed both without and with vibration isolators on a single rectangular concrete plate that is simply supported at all edges as shown in Fig. 6.2(a). In the second, an identical independent machine with four symmetrical mounting points a1-a4 is mounted on the first layer of the dual-layered plate structure; and in the third case, two coherent machines with four symmetrical points a1-a4 and b1-b4 (that is, exactly the same as the first and second cases) are mounted separately on two different layers as shown in Fig. 6.2(d), which considers the coupling of the floor structure. The two plates of the dual-layer floor structure are assumed to be same.

It is assumed that the machine is driven effectively by an internal force F_0 at the center of gravity. While the difference of force and velocity at various contact points is negligible, for simplification, the machine is thought to be an effective simple source.

The vibratory systems for the single machine on the receiver floor and the two coherent sources on a coupling receiver structure can be described by the electrical analogy, as shown in Figs. 6.2(c) and 6.2(e) respectively.

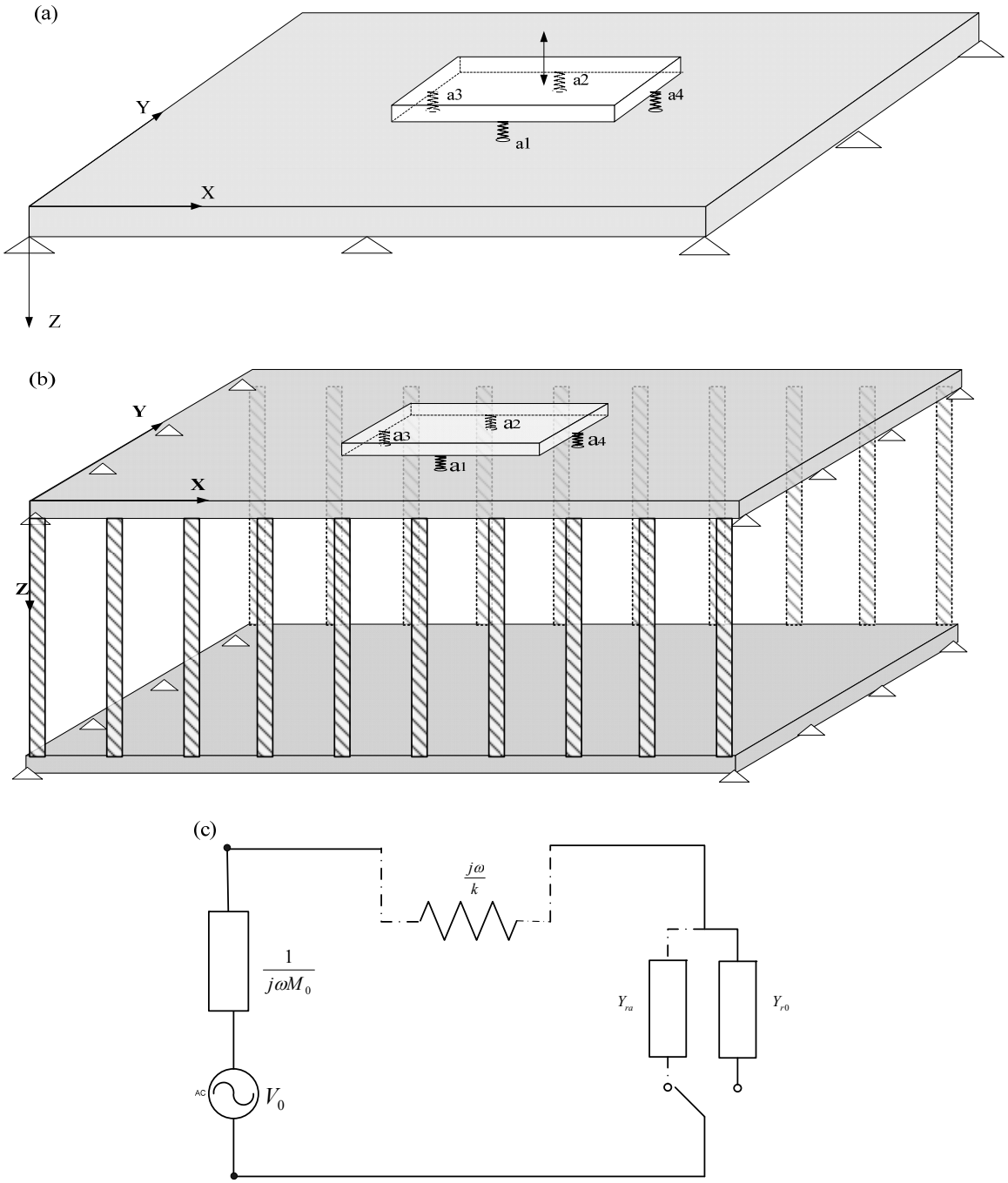

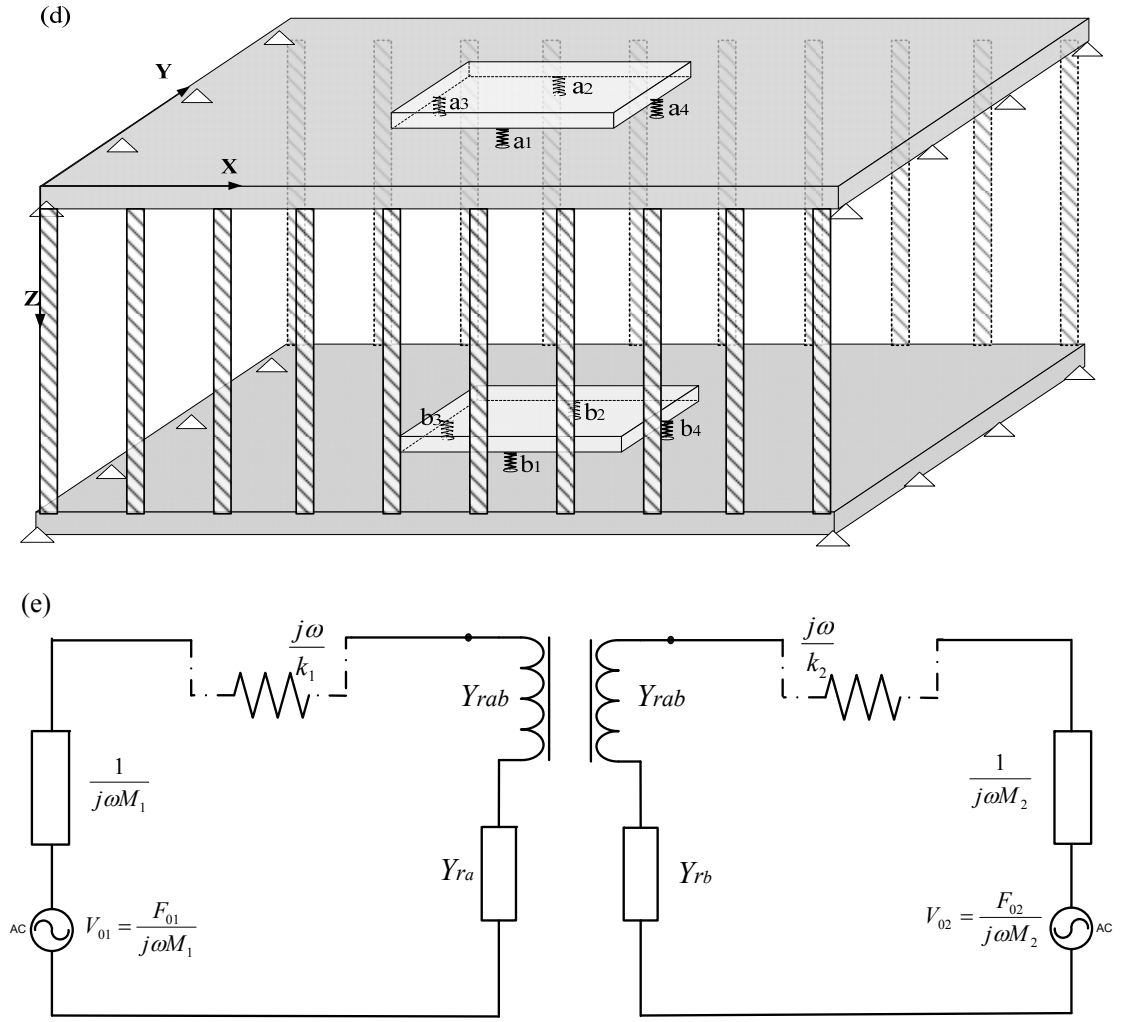

Fig. 6.2 (a) Vibration-isolated system of a single source machine mounted on a flexible floor; (b) On a coupling floor structure (c) equivalent circuit diagram of the simple vibratory system for a single source machine mounted on the coupling floor; (d) Two coherent source machines mounted on a coupling floor structure A; (e) equivalent circuit diagram of the simple vibratory system for two coherent source machines on a coupling floor structure.

A vibratory source is usually a multi-point machine, so here we apply a source machine model with four symmetrical mounting points as shown in Fig. 6.3. The model is a hollow rectangular machine asymmetrically placed on a flexible floor plate, with an even mass m_0, of which L_m is the length of its external square side, l_m the length of the internal square side, H_0 the hollow rectangular height, and $\mathrm{I}_{M0} = M_0 \dfrac{L_m^2 + l_m^2 + H_m^2}{12}$, which is the moment of inertia around the horizontal axial throughout the center of gravity.

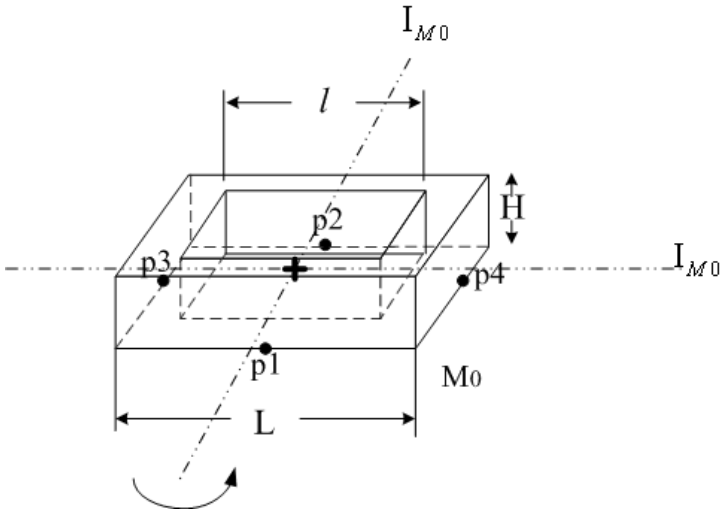

Fig. 6.3 Model of the rectangular source machine with 4 contact points.

The source machine is driven by a vibratory inherent force at the center of gravity, of which the free velocity vector $[V_{s0}]$ is expressed as

$$[V_{s0}] = \frac{F_0}{j\omega M_0}[1 \quad 1 \quad 1 \quad 1]^{\mathrm{T}} \tag{6.11}$$

Here, the components of the velocity vector express the values of the vibration velocity in the vertical degree at the different contact points. When the source is placed directly on a floor, the transmitted forces and total transmitted power to the floor through the four contact points can be calculated by

$$[F_{Tn}] = ([Y_s] + [Y_{rs}])^{-1}[V_{s0}] \tag{6.12}$$

$$L_{PT(ns)} = 10\log\frac{P_{T(ns)}}{\omega M_0 V_0^2}, \quad P_{T(ns)} = [F_{Tn}]^{*\mathrm{T}}\,\mathbf{Re}([Y_{rs}^{(1)}])[F_{Tn}] \tag{6.13}$$

where $[Y_{rs}]$ is the floor mobility matrix of the contact points as given by $[Y_{rs}] = \begin{bmatrix} Y_{rii} & Y_{rji} \\ Y_{rij} & Y_{rjj} \end{bmatrix}$, i, j=a1, a2, a3, a4, of which $Y_{r\mathrm{ii}}$ or $Y_{r\mathrm{ii}}$ are the point mobilities of the ith or jth mounting points on the floor, $Y_{r\mathrm{ij}} = Y_{r\mathrm{ji}}$ the transfer floor mobilities between the ith and jth mounting points, and $[Y_s]$ the source mobility matrix of the machine with four mounting points. The source mobility matrix of an even mass system

mounted at four midpoints of the square sides, as shown in Fig. 6.3, can be expressed as follows $\left[Y_{rs}^{(1)}\right]=\begin{bmatrix} F_{Tn} & Y_{aii} & \dots Y_{aji} \\ & Y_{aij} \dots & \dots Y_{ajj} \end{bmatrix}$

$$\left[Y_s\right]=\frac{1}{j\omega M_0}\left[Y_{a0}\right] \tag{6.14}$$

$$\left[Y_{a0}\right]=\begin{pmatrix} 1+\alpha_0 & 1-\alpha_0 & 1 & 1 \\ 1-\alpha_0 & 1+\alpha_0 & 1 & 1 \\ 1 & 1 & 1+\alpha_0 & 1-\alpha_0 \\ 1 & 1 & 1-\alpha_0 & 1+\alpha_0 \end{pmatrix},\ \alpha_0=\frac{M_0 L_m^2}{4\mathrm{I}_{M0}} \tag{6.15}$$

As the machine is mounted with four spring isolators, the transmitted forces and the normalized level of total power transmitted from machine to floor are given by

$$\left[F_{Ts}\right]=\left(\left[Y_s\right]+\frac{j\omega}{k_0}\left[I_4\right]+\left[Y_{rs}\right]\right)^{-1}\left[V_{s0}\right] \tag{6.16}$$

$$\overline{L}_{PT(s)}=10\log\frac{P_{T(s)}}{\omega M_0 V_0^2}\ \text{ and }\ P_{T(s)}=\left[F_{Ts}\right]^{*\mathrm{T}}\mathrm{Re}\left(\left[Y_{rs}\right]\right)\left[F_{Ts}\right] \tag{6.17}$$

where $[I_4]$ is a 4×4 identity matrix and k0 is the stiffness of the vibration isolator. Then the level of power transmissibility that is defined as

$$\gamma_s=10\log\left(\frac{P_{T(s)}}{P_{T(ns)}}\right) \tag{6.18}$$

is used to assess the vibration isolation for an independent multi-point machine mounted on a flexible floor structure.

The transmitted forces and normalized level of total power transmitted to the coupling dual-layered structure from two coherent machines (as shown in Fig. 6. 2(d)), without and with spring isolators respectively, are given by

$$\left[F_{Tn}^{(2)}\right]=\left(\begin{bmatrix} Y_{s1} & O \\ O & Y_{s2} \end{bmatrix}+\left[Y_{rs}^{(2)}\right]\right)^{-1}\begin{bmatrix} V_{s1} \\ V_{s2} \end{bmatrix} \tag{6.19}$$

$$P_{T(ns)}^{(2)}=\left[F_{Tn}^{(2)}\right]^{*\mathrm{T}}\mathrm{Re}\left(\left[Y_{rs}^{(2)}\right]\right)\left[F_{Tn}^{(2)}\right] \tag{6.20}$$

$$\overline{L}_{PT(ns)}^{(2)} = 10\log\frac{P_{T(ns)}^{(2)}}{\omega M_0 V_0^2} \tag{6.21}$$

$$\left[F_{Ts}^{(2)}\right] = \left(\begin{bmatrix} Y_{s1} & O \\ O & Y_{s2} \end{bmatrix} + j\omega\begin{bmatrix} I_4 k_1^{-1} & O \\ O & I_4 k_2^{-1} \end{bmatrix} + \left[Y_{rs}^{(2)}\right]\right)^{-1}\begin{bmatrix} V_{s1} \\ V_{s2} \end{bmatrix} \tag{6.22}$$

$$\overline{L}_{PT(s)}^{(2)} = 10\log\frac{P_{T(s)}^{(2)}}{\omega M_0 V_0^2}, \text{ and } \; P_{T(s)}^{(2)} = \left[F_{Ts}^{(2)}\right]^{*\mathrm{T}} \mathrm{Re}\left(\left[Y_{rs}^{(2)}\right]\right)\left[F_{Ts}^{(2)}\right] \tag{6.23}$$

where for the source machines M-1 and M-2, $[Y_{s1}]$ and $[Y_{s2}]$ are their source mobility matrices given in the same form as $[Y_s]$, and their free velocity vectors $[V_{s1}]$ and $[V_{s2}]$ are in the same form as $[V_{s0}]$. For the eight mounting points on two layers of the coupling plate structure, the whole floor mobility matrix $[Y_{rs}^{(2)}]$ takes the form $[Y_{rs}^{(2)}] = \begin{bmatrix} Y_{ra} & Y_{rab} \\ Y_{rab} & Y_{rb} \end{bmatrix}$, where $[Y_{ra}]$ and $[Y_{rb}]$ are the co-layer mobility matrices of the mounting points a1,…a4 on plate A, and b1,…b4 on plate B, whilst $[Y_{rab}] = [Y_{rba}]$ are the cross-layer coupling mobility matrices between the mounting points a1,…a4 and b1,…b4. The level of power transmissibility, which is defined as

$$\gamma_s^{(2)} = 10\,\mathbf{log}\left(\frac{P_{T(s)}^{(2)}}{P_{T(ns)}^{(2)}}\right) \tag{6.24}$$

can be calculated for the coherent machines to estimate the performance of the vibration isolation on a coupling floor structure.

6.3. ANALYSIS OF THE STRUCTURE-BORNE SOUND TRANSMISSION

6.3.1 CONDITIONS OF THE COMPUTATION FOR THE COUPLING PLATE STRUCTURE

The source machine M-1 is placed at the center of the floor plate, in which the positions of the four mounting points in the X-Y coordinate as shown in Fig. 6.1 are a1(3.0, 0.9), a2(3.0, 2.1), a3(2.4, 1.5), and a3(3.6, 1.5), with the meter units omitted. Similarly, in the case of the dual-layered plate, the mounting points in the same positions for machine M-2 are placed on the second layer, with the positions in X-Y coordinates being the same as those of points a1-a4 in the first plate.

The sources and spring isolators are assumed to be the same type, of which the mass is M_0= 1.0×10^3 kg and the stiffness k_0= 0.88×10^7 N/m with a small viscous damping factor (0.01). The physical parameters of the concrete floor are as follows; density ρ_c = 2.8×10^3 kg/m^3, Young's modulus $E_0 = 2.1\times10^{10}$ N/m^2, loss factor $\eta = 2\times10^{-2}$, and Poisson's ratio $\nu = 0.2$. The boundary of the square floor is simply supported, with sides of length $L_a = 6$m, $L_b = 3$m, and thickness d_0 = 0.24m. For the dual-layered plate structure, the connection branches are made from the same type of steel with a circular cross-section of diameter d_c = 8 cm, and branch length L_c = 3.0 m. The periodic elements were symmetrically distributed along the two long side edges of the plate structure, with the total number N=10 at each side at regular intervals of l_0 = 0.66m along the x-direction. The curves plotted in Fig. 6.7 show the predicted levels of the normalized transmitted power and power transmissibility versus the normalized frequency. The normalized frequency is given by $f_n = f / f_0$, with the natural frequency for an ideal mass-spring system defined as $f_0 = \frac{1}{2\pi}\sqrt{\frac{k}{M_0}} = 15$ Hz.

6.3.2 THE COMPUTED FLOOR MOBILITY AND VIBRATION MODES

In this section, the point and transfer mobility of a single point are investigated for the initial analysis of the multi-source coupling, and the effect of coupling structure on the floor mobility and vibration modes is illustrated.

When excited by a vertical force F_0 at point a1 of a single plate simply supported at every edge, the point mobility, defined as $Y_{a11} = v_{a1}/F_0$, is separately calculated by using the analytical equation as derived in Ref. [40]

$$Y_{a11} = \frac{4j\omega}{m'' L_a L_b} \sum_{n_1,n_2=1}^{\infty} \frac{\left(\sin n_1 x_1 \pi / L_a \sin n_2 y_1 \pi / L_b\right)^2}{\omega_n^2 - \omega^2} \tag{6.25}$$

$$\omega_n = \sqrt{\frac{B_0}{m''}}\left[\left(\frac{n_1\pi}{L_a}\right)^2 + \left(\frac{n_2\pi}{L_b}\right)^2\right]$$

$$B_0 = \frac{E_0}{1-\mu^2}\frac{h^3}{12}, \quad m'' = \rho_0 d_0$$

and the finite element simulation. The results calculated using the different approaches are compared in Fig. 6.4(a). It can be observed that for the simply supported single plate, the calculated mobility curve obtained using finite element simulation agrees very well with that produced by using the analytical equation. The finite element model is therefore reliable and can be used to study the vibration of the coupling dual-layered plate structure.

The curves of the point mobility of a1 and transfer mobility between a1 and b1 of the dual-layered plate structure are plotted in Fig. 6.4(b). Comparing the point mobility for the same excitation position a1, it can be seen that the cross-layered transfer mobility curves of the coupling structure are similar at most frequencies. Notably, it can be seen that at frequencies around 50-70 Hz, the level of transfer mobility for a1-b1 is

obviously larger than the point mobility for a1, which means the former has to be considered in the vibration systems of coherent sources on the coupling plate structure.

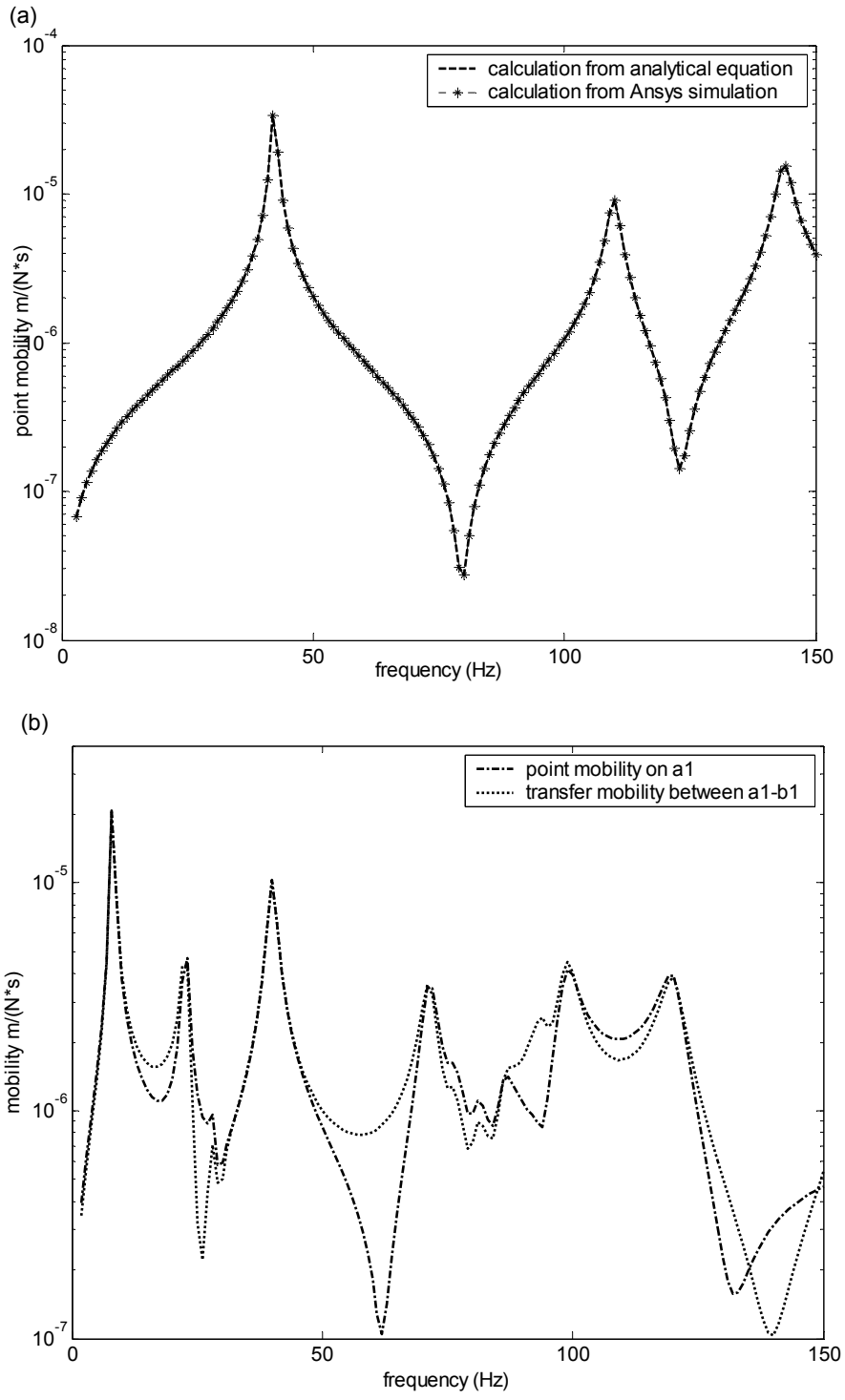

Fig. 6. 4 (a) The results of a1 point mobility from two approaches for a simply supported plate; (b) Comparison between point mobility Y_{a11} and transfer mobility Y_{a1b1} of the dual-layered plate structure.

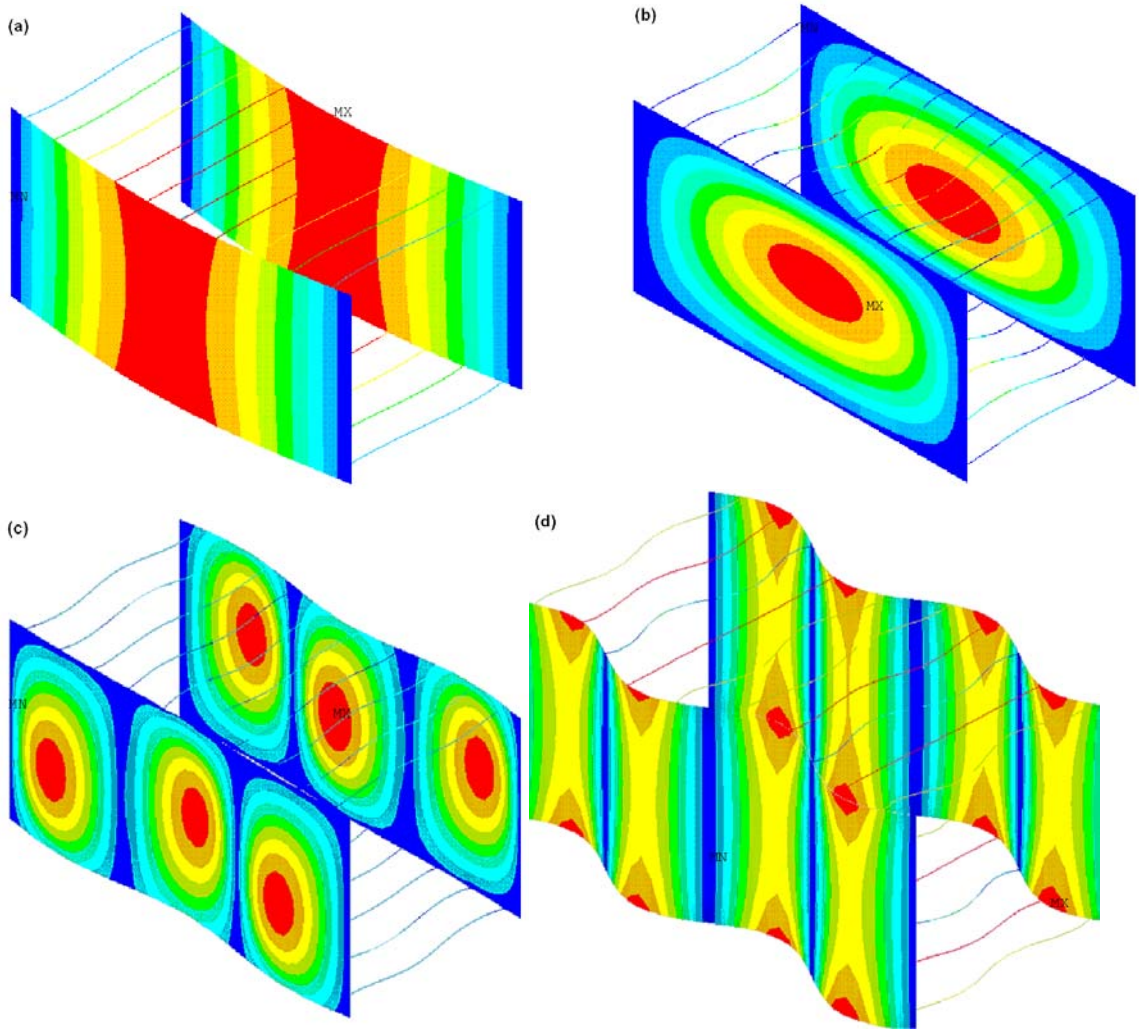

Fig. 6.5 The field of vibration modes of the coupling dual-layer plate. (a) 8Hz around the 0-1 resonant mode; (b) 40Hz around the 1-1 resonant mode; (c) 98Hz around the 3-1 resonant mode; (d) 127 Hz between the 4-0 and 4-1 mode.

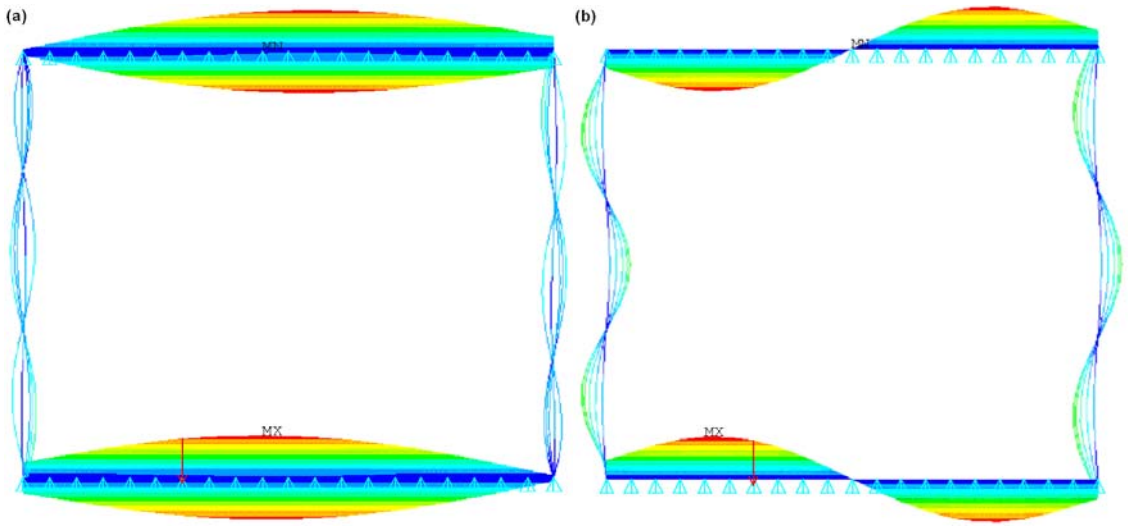

Fig. 6.6 The Y-Z plane field views of the vibration modes of the coupling dual-layer plate. (a) symmetric mode around 98Hz; (b) anti-symmetric mode around 120Hz.

Fig. 6.5 shows the vibration velocity distributions of a dual-layered plate excited by a vertical force on point a1, with four frequencies around four different vibration modes being selected. It can be observed that the coupling effect between the two layers of the dual-layered plate is significant. Moreover, it can be seen that the mounting points on the dark areas have an obvious effect on the coupling effect of the coherent sources on the coupling structure and therefore should be avoided. As shown in Fig. 6.6, these vibration modes of a dual-layered plate can be divided into two groups, namely symmetric and antisymmetric, based on the different phase relationships of the bending motions between layers A and B. The symmetric vibration modes are named here because the phase differences of the z-degree vibration motions between the two plates are zero. They are like mirror images around the symmetry axis in the Y-Z plane of the dual-layered structure. For the motions of the antisymmetric modes, the phase differences of the z-degree velocities between the two plates are π. To attenuate the structure-borne sound from the coherent sources more efficiently, two machines should be placed on the undertone areas of two plates so that the final transmitted power will not be significantly influenced by cross-layer coupling.

6.3.3 STRUCTURE-BORNE SOUND POWER TRANSMITION ON A SIMPLY SUPPORTED PLATE AND A COUPLING DUAL-LAYERED STRUCTURE

In this section, the effect of wave coupling on the transmission of structure-borne sound power is investigated by using the model developed above with different conditions for the supporting structure. In the 3 cases where all machines are directly mounted without isolators, the normalized levels of transmitted power, which reveal the relative strengths of the active structure-borne sound power transmitted into the floor structures corresponding to the kinetic energy of the free source, are plotted in Fig. 6.7(a) in the range of normalized frequencies $f_n = f / f_0$ from 0 to 10. In the three

cases where all machines are mounted with isolators, the power transmissibility for the vibratory systems are plotted in Fig. 6.7(b) in the same frequency range.

Fig. 6.7(a) shows that for the first and second cases, transmitted power at most frequencies is quite different because of the different floor mobilities. In the third case, the normalized transmitted power from the two coherent sources is larger than that from the independent source in most regions of normalized frequencies around 4 to 6 and >8, while the level for coherent sources on the coupling structure is lower than that for the independent source in the normalized frequencies of around 1.8 to 3.3. This result means that the effect of structure coupling for the coherent sources would enhance structure-borne sound transmission in these frequency regions f_n of around 4 to 6 and >8. At the normalized frequencies of around 1.8 to 3.3 for the coherent sources, the transmitted force acting on the mounting point of a single such source reduces the magnitude of the in-phase part of the vibrating velocity with the transmitted force at the mounting point of the other source. As a result, the real part of the effective point mobility for the coherent source decreases, so that the transmitted power is reduced at these frequencies. The working region of f_n around the enhanced area (that is, the increase in the normalized level of transmitted power) of the transmitted structure-borne sound power needs to be considered when predicting the performance of vibration isolation methods.

It can be seen from Fig. 6.7(b) that the overall trend of power transmissibility for the first case is similar to that for the second and third at most of the isolation regions (that is, normalized frequencies $>\sqrt{2}$) except for some of the peak regions. It is notable that the level of power transmissibility for the two coherent sources increases significantly at the region of normalized frequencies around 5.2 to 6.0, and is smaller than that for the independent sources at normalized frequencies of around 6.1 to 6.7. The values for the two coherent sources indicate that the isolator performs well at the latter set of

normalized frequencies but does not attenuate the structure-borne sound power effectively at normalized frequencies of around 5.2 to 6.0. The result from the resonances excited at the mounting points of the machines implies that the coherence between the sources at the mounting positions on the floor can significantly affect the total transmitted power at some frequencies. When predicting the performance of vibration isolation for coherent machine sources, therefore, the interaction between the different machines mounted on the coupling floor structure needs to be considered. The region of good isolation, for example around the normalized frequency of 6.6, could include the major working frequency region of the machines; the region of the poor isolation effect could be considerably distant from such an area.

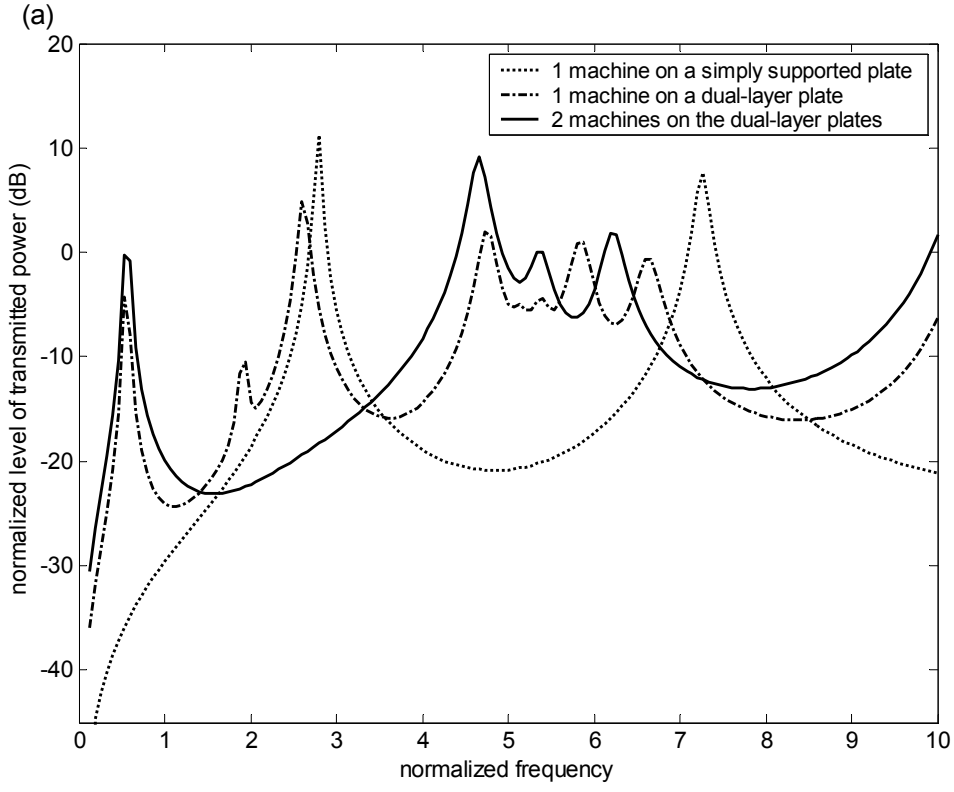

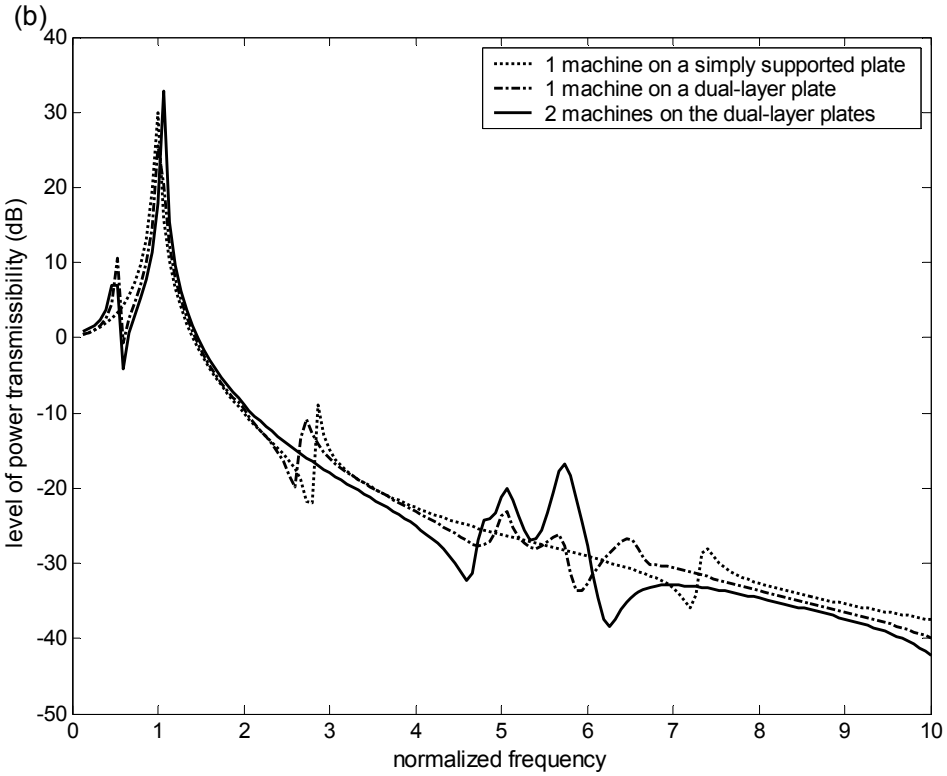

Fig. 6.7 (a) Normalized level of transmitted power for the vibratory systems without vibration isolators in the 3 cases; (b) Levels of structure-borne sound power transmissibility for the vibratory systems with vibration isolated in the 3 cases.

6.4. SUMMARY

In this chapter, a model for coherent vibration systems on a dual-layered plate structure has been developed to study structure-borne sound transmission in such a coupling structure within a building. The analysis indicates that this study has been useful in understanding the structure-borne sound power flow transmission from the first into the second layer of such a dual-layer beam structure.

In the common case, where a vibratory machine is mounted on a floor, the amount of power it transmits to a structure is significantly affected by the interaction of the contact points between it and the floor plate. A more accurate prediction for the performance of vibration isolation in a multi-layered building structure can only be obtained if the coupling between the two coherent sources is considered. The power transmissibility for the two sources will increase significantly at the normalized frequencies around some strong coupling modes and decrease considerably at other frequencies. The analysis has shown that the transmitted power from two coherent machines can be enhanced at some frequencies in the vibration isolation region.

To predict the performance of isolation more accurately, the power transmissibility method should therefore consider not only the influence of effective floor mobility and the interactions of the mounting points of the independent sources, but also the interactions of the mounting points of different sources on the coupling floor structure. Future work is needed to explore the selection of optimum mounting positions for coherent machines on a multiple-layered floor structure so that the total structure-borne sound power transmitted from the machines to the building can be minimized in a region of major working frequencies.

CHAPTER 7. CONCLUSION AND FUTURE WORK

This section includes conclusions on the whole work of this thesis and propose some suggestions for future work.

First of all, the fundamental source-receiver model of a vibration-isolated system is represented by using electrical analogy, and the complex model is applied to a multi-point source machine that is vibrating in three degrees of freedom and asymmetrically mounted on a flexible floor with isolators in vertical direction. The analytical solution is developed for the model of a multi-point source machine with uneven mass distribution that is isolated with an inertia block. For this improved model of vibration-isolated system, the level of power transmissibility, the level of vibration velocity transmissibility, the mounted vibration velocity level, and the mounted rotational velocity level of the vibratory machine are proposed in order to assess the performance of vibration isolation and the stability of isolated multi-point vibratory building services equipment. The results primarily indicate that the use of an inertia block does not mainly affect the performance of vibration isolation. Instead, it decreases the vibration velocity and rotational velocity of the isolated vibratory machine, so that it can increase the stability of the vibratory system, regardless of whether the machine has slightly or highly uneven mass distribution. It is also obtained for the machine with uneven mass distribution placed asymmetrically on the floor, what the ratio of the combined inertia of the additional inertia block should be corresponding to the extent of uneven mass distribution. The analysis reveals that, for the mounted vibratory machine, an inertia block with a larger mass can reduce the vibration and rotation of the isolated vibratory machine. As a result, it enhances the stability of the isolated vibratory system of machines with highly uneven mass distribution in 3 degrees of freedom. Therefore, in addition to proposing indices for assessing the

stability of the vibratory building services system, this work provides an insight into the selection of inertia blocks based on the mass distribution of an isolated vibratory machine.

Secondly, a new analytical method based on a multi-coupling wave transfer matrix has been developed to study the phenomena of the coupled flexural-longitudinal wave motions that propagate in a tri-coupling dual-layered periodic beam structure. A lightly damped semi-infinite structure that consists of two equally thin semi-infinite beams connected with resonant branches has been numerically analyzed. It is shown that the complex propagation constants govern the transmission of wave types in the structures, and the characteristics of pass and stop bands and the wave-coupling phenomena. It is found that there are six characteristic coupled wave types that propagate through such a structure, and these can be divided into symmetric and antisymmetric groups of flexural-longitudinal and predominantly near-field characteristic wave types. It is further revealed that the structure-borne sound energy from the synchronous longitudinal excitations at two beams mainly propagate through the periodic structure in the form of one or two types of symmetric characteristic coupled flexural-longitudinal waves. In contrast, the structure-borne sound energy from the synchronous rotational excitations mainly propagate along the structure in the form of one or two types of antisymmetric characteristic coupled flexural-longitudinal waves. This work gives an insight into the physical properties of wave motions and the vibrational energy contribution in such structures.

Thirdly, the dynamic characteristics of the longitudinal-flexural motions and energy transmission in a finite dual-layered beam structure are studied for better vibration control in such a structure. Based on the developed model using the analytical wave coupling transfer matrix method derived in last chapter, numerical calculation was performed to predict the behavior of the coupled wave motion excited by a longitudinal

force in a finite periodic structure. The numerical results based on the theoretical model compared with the experimental results. In the experiment, a lightly damped finite structure consisted of two equally thin beams with multiple resonant branches in the form of thin beams that were connected perpendicularly at regular intervals. The numerical results of the theoretical model generally agree well with the experimental results at the frequencies from 10 to 2000 Hz, which suggests that the developed transfer matrix method for the finite periodic structure model could be useful in most middle-low frequency regions. Further, the cross-layer energy transmission of the coupled waves in the finite periodically-connected dual-beam waveguide was then calculated and analyzed by using the developed theoretical model. The results reveal that the longitudinal energy transmitted in the cross-layer of finite periodic structure is enhanced not only at the longitudinal resonant modes but also the flexural resonant modes of the finite beam of connection branches due to the wave coupling of the structure. It is shown that the damping factor of the coupling connection influences most peaks of cross-layer transmitted energy of the coupled wave at the flexural resonant modes of connection branches, which indicates that the structure-borne sound control method could be applied on those similar beam structures.

Moreover, the model and method is developed to study the transmission of the structure-borne sound power flow through the finite dual-layered beam structure in a boundary supporting condition. Using the developed model for different coupling conditions, the calculation suggests that that the power flow transmission under mono-coupling condition to be similar to that under the multi-coupling condition mostly in the relatively low frequency. The structure-borne sound power flow transmitted throughout such a beam framework into the supporting structure would not just depend on the characteristics of source and receiver, but also on the attenuation determined by the coupling beam elements and the mounting position of source. In

several frequency regions, the power flow can be even transmitted into the second layer of the supporting structure to a considerable degree, which indicates the cross-layer power transmission need to be noted for the coupling beam structure.

Finally, the model for the coherent vibration-isolated systems on a dual-layered plate structure is developed, and it is used to study the structure-borne sound transmission and isolation for the coherent source machines in such a coupling multi-layered structure of building. For the more accurate estimation of the isolation performance, the power transmissibility method should consider not only the effect of effective floor mobility and the interactions of the mounting points of the independent sources, but also the interactions of different mounting points of coherent sources on the coupling floor structure. This study also indicates that new method is needed for the selection of the optimum mounting positions of coherent machines on a coupling multi-layered floor to achieve better isolation performance.

In future, further work will be conducted to develop a simplified model to effectively include moment actions at multiple contact points for complex vibration-isolated systems in multiple degrees of freedom. A method based on such model requires the available information about the characteristics of source machines and receiver structures in order to estimate the structure-borne sound power transmission and assess the performance of vibration isolation. The isolators such as spring is normally designed using the model of SDOF, with the source model based on the rigid-body source is just reasonable in relative low-frequency region. The advanced models of multi-degree isolators including moment actions together with stiffness-control and resonance-control sources will be considered in the future's work for higher frequency region. Moreover, the models for 3-dimensional coupling structures need to be further developed to efficiently analyze the structure-borne sound transmission with coupling effects in a multi-layered building structure. The model based on the equilibrium

equations of “self-consistent” method as developed in Ref. [90] will be used for the 3-dimensional structures or disorder structures.

REFERENCES OF THE Ph.D THESIS

[1] A. Fry, *Noise control in building services*. Sound Research Laboratories Ltd, Oxford: Pergamon Press; 1988.

[2] L.L. Beranek and I.L. Vér, *Noise and vibration control engineering : principles and applications*, New York : Wiley; 1992.

[3] B.J. Smith, R.J. Peters and S. Owen, *Acoustics and noise control*. 2nd ed, Addison Wesley Longman; 1996.

[4] C.M. Harris, *Shock and vibration handbook*, New York: McGraw-Hill; 1995.

[5] Popkov VI, Vibroacoustic, "diagnosis and the reduction of the vibration of shipboard machinery," *JPRS*, Arlington 1975, translation 64931,.

[6] J.M. Mondot and B.A.T. Petersson, "Characterization of structure-borne sound sources: the source descriptor and coupling function," *Journal of Sound and Vibration* 1987; **114**: 507-518.

[7] B.A.T. Petersson, J. Plunt, "On effective mobilities in the prediction of structure-borne sound transmission between a source structure and a receiving structure, part 1: Theoretical background and basic experimental studies," *Journal of Sound and Vibration* 1982; **82**(4): 517-529.

[8] B.A.T. Petersson, J. Plunt, "On effective mobilities in the prediction of structure-borne sound transmission between a source structure and a receiving structure, part 2: procedures for the estimation of mobilities," *Journal of Sound and Vibration* 1982; **82**(4): 531-540.

[9] T.T. Wolde and G.R. Gadefelt, Development of standard measurement methods for structure-borne sound emission, Noise Control Engineering Journal 1987; **28**: 5-14.

[10] B.A.T. Petersson and B.M. Gibbs, "Use of the source descriptor concept in studies of multipoint and multidirectional vibrational sources," *Journal of Sound and Vibration* 1993; **168** (1):157-176.

[11] B.A.T. Petersson, "Structural acoustic power transmission by point moment and force excitation, Part I: Beam-like and frame-like structures," *Journal of Sound and Vibration* 1993; **160**: 43-66.

[12] B.A.T. Petersson, "Structural acoustic power transmission by point moment and force excitation, Part II: Plate-like and frame-like structures," *Journal of Sound and Vibration* 1993; **160**: 67-91.

[13] R.A. Fulford and B.M. Gibbs, "Structure-borne sound power and source characterization in multi-point-connected systems, part 1: Case studied for assumed force distributions," *Journal of Sound and Vibration* 1997; **204**(4): 659-677.

[14] R.A. Fulford and B.M. Gibbs, "Structure-borne sound power and source characterization in multi-point-connected systems, part 2: About mobility functions and free velocities," *Journal of Sound and Vibration* 1999; **225**(2): 203-224.

[15] R.A. Fulford and B.M. Gibbs, "Structure-borne sound power and source characterization in multi-point-connected systems, part 3: ratio estimates," *Journal of Sound and Vibration* 1999, **225**(2): 239-282.

[16] A.T. Moorhouse, “A dimensionless mobility formulation for evaluation of force and moment excitation of structures,” *Journal of the Acoustical Society of America* 2002, **112**(3): 972-980.

[17] B.A.T. Petersson and B.M. Gibbs, “Towards a structure-borne sound source characterization,” *Applied Acoustics* 2000, **61**(3): 325-343.

[18] A.T. Moorhouse and B.M. Gibbs, “Prediction of the structure-borne noise emission of machines: development of a methodology,” *Journal of Sound and Vibration* 1993, **167**: 223–237.

[19] J.X. Su, A.T. Moorhouse and B.M. Gibbs, “Towards a practical characterisation for structure-borne sound sources based on mobility techniques,” *Journal of Sound and Vibration* 1995, **185**: 737-741.

[20] L. Ji, B. R. Mace and R. J. Pinnington, “A power mode approach to estimating vibrational power transmitted by multiple sources,” *Journal of Sound and Vibration* 2003; **265**(2): 387-399.

[21] A.T. Moorhouse, “On the characteristic power of structure-borne sound sources,” *Journal of Sound and Vibration* 2001; **248**(3): 441-459.

[22] B.M. Gibbs, N. Qi and Moorhouse AT, “A practical characterisation for vibro-acoustic sources in buildings,” *Acta Acustica united with Acustica* 2007, **93**: 84–93.

[23] International Standards Organization, "characterisation of sources of structure-borne sound with respect to sound radiation from connected structures--measurement of velocity at the contact points of machinery when resiliently mounted," *ISO-9611 Acoustics*; 1996.

[24] T. Tenwolde, “Reciprocity method for measurement of mechano-acoustical transfer-functions,” Journal of Sound and Vibration 1975; **42**: 49-55.

[25] B.K. Kim , J.G. Ih, "Insitu estimation of an acoustic source in an enclosure and prediction of interior noise by using the principle of vibroacoustic reciprocity ," *Journal of the Acoustical Society of America* 1993; **93**(5): 2726-2731.

[26] K. Wyckaert, F. Augusztinovicz, P. Sas, "Vibro-acoustical modal analysis: Reciprocity, model symmetry, and model validity," *Journal of the Acoustical Society of America* 1996; **100**(5): 3172-3181.

[27] S.H. Yap and B.M. Gibbs, “Structure-borne sound transmission from machines in building, part 1: indirect measurement of force at the machine-receiver interface of a single and multi-point connected system by a reciprocal method,” *Journal of Sound and Vibration* 1999; **222**(1): 85-98.

[28] S.H. Yap and B.M. Gibbs, “Structure-borne sound transmission from machines in buildings, part 2: Indirect measurement of force and moment at the machine-receiver interface of a single point connected system by a reciprocal method,” *Journal of Sound and Vibration* 1999; **222**(1): 99–113.

[29] B.A.T. Petersson, “On the use of giant magnetostrictive devices for moment excitation,” *Journal of Sound and Vibration* 1987; **116** (1): 191-194.

[30] M.A. Sanderson and C.R. Fredo, “Direct measurement of moment mobility Part 1: Theoretical study,” *Journal of Sound and Vibration* 1995; **179**(4): 669-684.

[31] M.A. Sanderson, “Direct measurement of moment mobility Part 2: An experimental study,” *Journal of Sound and Vibration* 1995; **179** (4): 685-696.

[32] J. X. Su and C. M. Mak, "Direct measurement of moment mobility and a moment excitation system," *Applied Acoustics* 2001; **63**(2): 139-151.

[33] J. X. Su and B.M. Gibbs, "Measurement of Point Moment Mobility in the Presence of Non-Zero Cross Mobility," *Applied Acoustics* 1998, 54 (1): 9-26.

[34] V. Marchand, J. Authesserre, J. Pouyet, et al. 1996 "Determination of the elastic constants of materials, in the form of plates, by a free vibration method," *Journal of Sound and Vibration* 1996; **194** (4): 497-512.

[35] K. Liu, "Modal parameter estimation use the state space method," *Journal of Sound and Vibration* 1996; **174**(4): 387-402.

[36] N. H. Farag and J. Pan, "Modal characteristics of in-plane vibration of rectangular plates," *Journal of the Acoustical Society of America* 1999; **105**: 3295-3310.

[37] B. Cauberghe, P. Guillaume and R. Pintelon, "Frequency-domain subspace identification using FRF data *from* arbitrary signals," *Journal of Sound and Vibration* 2006; **290**(3): 555-571.

[38] M. Späh, B. M. Gibbs, and H. M. Fischer, "Measurement of structure-borne sound power of mechanical installations in buildings," *11th International Congress on Sound and Vibration*, St. Petersburg 2004.

[39] R. Cookson and N. Qi, "A reception plate method of measurement of the free velocity of machines in buildings," *13th International Congress on Sound and Vibration*, Vienna 2006.

[40] L. Cremer, M. Heckl, and B.A.T. Petersson, *Structure-borne sound, 3rd edition*, Berlin: Springer-Verlag; 2005.

[41] C.M. Mak, and J.X. Su, "A study of the effect of floor mobility on structure-borne sound power transmission," *Building and Environment* 2003, **38**(3): 443-455.

[42] C.M. Mak, and J.X. Su, "A power transmissibility method for assessing the performance of vibration isolation of building services equipment," *Applied Acoustics* 2002, **63**(12): 1281-1299.

[43] J.C. Tao and C.M. Mak, "Effect of viscous damping on power transmissibility for the vibration isolation of building services equipment," *Applied Acoustics* 2006, **67(8)**: 733-742.

[44] Rivin EI, *Passive vibration isolation*, New York: ASME Press; 2003.

[45] A. Webster and W. Semke, "Frequency-Dependent Viscoelastic Structural Elements for Passive Broad-Band Vibration Control," *Journal of Vibration and Control* 2006; **11**(12): 1535–1552.

[46] C. Kittel, *Introduction to Solid State Physics*, New York: John Wiley & Sons; 1996.

[47] J.W. MILES, "Vibrations of beams on many supports," *Proceedings of the American Society of Civil engineers* 1956; **82**, EM1.

[48] M. Heckl, "Investigations on the vibrations of grillages and other simple beam structures," *Journal of the Acoustical Society of America* 1964; **36**: 1335-1343.

[49] C. H. Hodges and J. Woodhouse, "Vibration isolation from irregularity in a nearly periodic structure: Theory and measurements," *Journal of the Acoustical Society of America* 1983; **74**: 894-905.

[50] M. S. Kushwaha, Int. J. Mod, “Classical band structure of periodic elastic composites,” *International Journal of Modern Physics B* 1996; **10**: 977-1094.

[51] S. D. Lust, P. P. Friedmann and O. O. Bendiksen, "Free and forced response of multi- span beams and multi-bay trusses with localized modes," *Journal of Sound and Vibration* 1985; **180**: 313-332.

[52] D. J. Mead, “A general theory of harmonic wave propagation in linear periodic system with multiple coupling,” *Journal of Sound and Vibration* 1973; **27**: 235–260.

[53] D. J. Mead, “Wave propagation and natural modes in periodic systems: II. Multi-coupled systems, with and without damping,” *Journal of Sound and Vibration* 1975; **40**: 19–39.

[54] M. Heckl, “Structure-borne sound propagation on beams with many discontinuities,” Acustica 1995; **81**: 439-449.

[55] M.A. Heckl, “Coupled waves on a periodically supported Timoshenko beam,” *Journal of Sound and Vibration* 2002; **252**: 849-882.

[56] L. Friis and M. Ohlrich, “Coupling of flexural and longitudinal wave motion in a periodic structure with asymmetrically arranged transverse beams,” *Journal of the Acoustical Society of America* 2005; **118**: 3010-3020.

[57] L. Friis and M. Ohlrich, “Coupled flexural-longitudinal wave motion in a finite periodic structure with asymmetrically arranged transverse beams,” *Journal of the Acoustical Society of America* 2005; **118**: 3607-3618.

[58] B.J. Smith, R.J. Peters, S. Owen, *Acoustics and noise control*. *2nd ed.*, Addison Wesley Longman; 1996.

[59] J.X. Su, A.T. Moorhouse, and B.M. Gibbs, “Towards a practical characterization for structure-borne sound sources based on mobility techniques,” *Journal of Sound and Vibration* 1995, **185**(4): 731–741.

[60] J.H. Ginsberg, *Advanced Engineering Dynamics*, Cambridge: Cambridge University Press; 1995.

[61] Y.K. Koh and R.G. White, “Analysis and control of vibrational power transmission to machinery supporting structures subjected to a multi-excitation system, part I: driving point mobility matrix of beams and rectangular plates,” *Journal of Sound and Vibration* 1996; **196**(4): 469–493.

[62] S. Falati and M.S. Williams, “Vibration tests on a model post-tensioned concrete floor”, 1998, University of Oxford,

[63] J.D. Joannopoulos, R.D. Meade and J.N. Winn, *Photonic Crystal-Molding the Flow of Light*; Princeton, NJ: Princeton University Press; 1995.

[64] M. Ibanescu, Y. Fink, S. Fan, E.L. Thomas and J.D. Joannopoulos, "An All-Dielectric Coaxial Waveguide," *Science* 2000; **289**: 415-419.

[65] H. L. Müller, "Attenuation of bending waves caused by symmetrical and eccentric blocking masses," Dr.-Ing. Dissertation, Institut für Technische Akustik der Technischen Universität, Berlin; 1957.

[66] H. Umezawa, *Advanced Field Theory*, New York: AIP Press; 1995.

[67] R.H. Lyon, *Statistical Energy Analysis of Dynamical Systems*, Cambridge, MA: MIT Press; 1975.

[68] A.C. Nilsson, "A method for the prediction of noise and velocity levels in ship constructions," *Journal of Sound and Vibration* 1984; **94**: 411-429.

[69] R.S. Langley, "A dynamic stiffness technique for the vibration analysis of stiffened shell structures" *Journal of Sound and Vibration* 1992; **156**: 521-540.

[70] A. K. Roy and R. Plunkett, "Wave attenuation in periodic structures," *Journal of Sound and Vibration* 1986; **104**: 395–410.

[71] Y. Yong and Y. K. Lin, "Propagation of decaying waves in periodic and piecewise periodic structures of finite length," *Journal of Sound and Vibration* 1989; **129**: 99–118.

[72] L. Brillouin, *Wave Propagation in Periodic Structures*, New York: Dover; 1953.

[73] L. Meirovitch and R.C. Engels, "Response of periodic structures by the Z-transform method," *AIAA Journal* 1977; **15:** 167–174.

[74] G. Maidanik and J. Dickey, "Velocity distributions on unloaded finitely and regularly ribbed membranes," *Journal of Sound and Vibration* 1991; **149**: 43–70.

[75] D. J. Mead, "A new method of analyzing wave propagation in periodic structures: Applications to periodic Timoshenko beams and stiffened plates," *Journal of Sound and Vibration* 1986; **104**: 9–27.

[76] Y. Yun and C. M. Mak, "A study of coupled flexural-longitudinal wave motion in a periodic dual-beam structure with transverse connection," *Journal of the Acoustical Society of America* 2009; **126:** 114-121.

[77] P.G Luan and Y. Zhen, "Acoustic wave propagation in a one-dimensional layered system", *Physical Review E* 2001, **63**: 066611.

[78] D. J. Mead, "Coupled flexural-longitudinal wave motion in a periodic beam," *Journal of Sound and Vibration* 1983; **90**: 1-24.

[79] H.L. Sun, H.B. Chena, K. Zhanga and P.Q. Zhang, “Research on performance indices of vibration isolation system,” *Applied Acoustics* 2008; **69**(9): 789-795.

[80] F.S. Tse, I.E. Morse and R.T. Hinkle, *Mechanical Vibrations: Theory and Applications* 1979, Boston: Allyn & Bacon.

[81] S.S. Rao, *Mechanical Vibrations* , *3rd edition* 1995, MA: Addison-Wesley.

[82] R.J. Pinnington, R.G. White, “Power flow through machine isolators to resonant and non-resonant beams,” *Journal of Sound and Vibration* 1981; **75**(2): 179-197.

[83] R.J. Pinnington, “Vibrational power transmission to a seating of a vibration isolated motor,” *Journal of Sound and Vibration* 1987; **118**(3):515-530.

[84] Y.K. Koh and R.G. White, “Analysis and control of vibrational power transmission to machinery supporting structures subjected to a multi-excitation system, Part II: Vibrational power analysis and control schemes,” *Journal of Sound and Vibration* 1996; **196**: 495-508.

[85] B.M. Gibbs, B.A.T. Petersson, “Structure-borne sound source characterization. 1: multi-point coupling,” *14th International Congress on Acoustics*, Proceedings 1992; **1**-4: 1025-1026.

[86] C.M. Mak and J.X. Su, “A study of the effect of floor mobility on isolation efficiency of vibration isolators,” *Journal of Low Frequency Noise, Vibration and Active Control* 2001; **20**(1):1-13.

[87] L. Gavric, “Finite element computation of dispersion properties of thin walled waveguides,” 1994, *Journal of Sound and Vibration* **173** (1), 113–124.

[88] G. Solaroli, Z. Gu, A. Baz, and M. Ruzzene, "Wave Propagation in Periodic Stiffened Shells: Spectral Finite Element Modeling and Experiments," 2003, *Journal of Vibration and Control* **9**, 1057 – 1081.

[89] O. C. Zienkiewicz, *The Finite Element Method*, Maidenhead: McGraw-Hill 1977.

[90] B. Liang and J. C. Cheng, "Acoustic localization in weakly compressible elastic media containing random air bubbles" 2007, *Phys. Rev. E* **75**, 016605.

APPENDIX. DETAILS OF EXPERIMENT

P1. The equipments used for this experiment: (1) the finite periodical coupling dual-layered beam suspended on elastic strings so that it could ideally vibrate freely in all degrees; (2) the amplifier of driving signal (LING Dynamic PA300) that was fed with a white noise source; (3) the electro-dynamic vibration exciter (LING Dynamic System Type V403); (4) the force transducer (PCB ICP F-sensor) that is set to measure the exciting force; (5) the conditioner of the force transducer; (6) the accelerometers (B&K Type 4394) to measure the vibration of the beam structure ; (7) the signal conditioner of the accelerometers; (8) NI equipment (RIO-9233) for the multi-channel data acquisition (9) the NI platform (PXI-8187) using the LabView program for the control of measurement and the data analysis.

A photo is given to illustrate the details of the equipments and setting of the experiment that was conducted for the study of chapter 4. The material of the two equal beam layers A and B is aluminum alloy, for which the Young's modulus is $E_{1,2} = 5.05 \times 10^{10}$ N/m^2 and density $\rho_{1,2} = 3220$ kg/m^3 with an assumed loss factor $\eta_{1,2} = 0.01$. The dimensions of the two equal beams with a rectangular cross-section are periodic element length $L_0 = 50$ mm, so its total length is 3.0 m, thickness $h_0 = 6.0$ mm, and width $d_0 = 38.1$ mm. The material of the connection branch is steel, for which the Young's modulus is $E_3 = 1.15 \times 10^{11}$ N/m^2 with assumed loss factor $\eta_3 = 0.011$ and

density ρ_3 = 7690 kg/m.[3] The dimensions of the branch are thickness h_c = 1.54 mm, width d_c = 38.2 mm, and length of its vertical beam component L_c = 320 mm. The attaching part on two sides of the connection branch, which has the same cross-section but a short length l_s = 9.0 mm, is perpendicular to the vertical part of the branch. The attaching part of the connection branch is fixed on a horizontal beam layer by two steel screws with nuts of a diameter of 4 mm. The total number of periodic elements of this finite periodic structure is N = 6. In the experimental setting, the man-made dual-layer periodic beam structure was suspended by four elastic strings under the long tables so that it could ideally vibrate freely in all degrees (the model shown in Fig. 4.2). The structure was longitudinally excited at the left boundary of beam B by an electro-dynamic vibration exciter (LING Dynamic System Type V403). The vibration exciter was driven by an electrical current amplifier (LING Dynamic PA300) that was fed with the input signal from a white noise generator. A force transducer (PCB ICP F-sensor) was set to acquire the exciting force on the periodic beam structure, and the vibrational responses of the beam structure were measured by two accelerometers (B&K Type 4394). All of the acquired force and vibration signals were synchronously input into a NI module of 4-channel A-D signal transducer (NI RIO-9233). The data recording, processing and analysis were conducted with NI equipment (NI PXI-8187) using the LabVIEW program.